

ELECTRICAL AND BIOCHEMICAL PERFORMANCES OF A PLASMA JET AT
ATMOSPHERIC PRESSURE

A Dissertation

Submitted to the Graduate School
of the University of Notre Dame
in Partial Fulfillment of the Requirements
for the Degree of

Doctor of Philosophy

by

Ek Raj Adhikari

Sylwia Ptasinska, Advisor

Graduate Program in Physics

Notre Dame, Indiana

April, 2019

ELECTRICAL AND BIOCHEMICAL PERFORMANCES OF A PLASMA JET AT ATMOSPHERIC PRESSURE

Abstract

by

Ek Raj Adhikari

In the last couple of decades, cold atmospheric pressure plasmas have demonstrated the capabilities to be a promising tool for clinical medicine such as wound healing, sterilization, blood coagulation, dentistry, and cancer treatment. Although the preliminary results for the potential use of these sources in clinical medicine are highly encouraging, a detailed understanding of the potential clinical applications has yet to be achieved. The primary goal of this research is to understand the physical and biochemical mechanisms underlying the plasma-biological molecules interactions in a well-controlled system.

This dissertation starts with a study of the correlation between the plasma parameters (e.g., flow rate, voltage) and DNA damage level induced due to plasma irradiation. The DNA damage level is attributable to the amount of reactive species in an APPJ. A significant increase in DNA damage level was observed for the closer treatment distance, longer irradiation time and higher flow rate of the feed gas. The investigation of

the interactions between plasma components and air components (e.g., oxygen, water vapor) showed that the plasma power remained the same or decreased when the mixture of gases was used as the plasma jet environment or the feed gas, respectively, but in both cases, DNA damage is increased.

There is also a need for techniques to detect, identify, and quantify the intermediate, short-lived plasma species, which can trigger a cascade of biochemical reactions. To measure the total yield of reactive species formed during plasma irradiation, an acidified ferrous sulfate solution was employed. The yield of Fe^{3+} ions from Fe^{2+} is attributable to the amount of reactive species formed in the sample due to plasma irradiation. The results indicated that the number of reactive species formed was related to frequency and voltage increases.

These results reveal the mechanism of plasma propagation in an ambient atmosphere along with plasma species interactions with surrounding air components, liquid samples, and biomolecules. This information could be a gateway to understand the mechanism of change in physical properties of plasma itself as well as its chemical and biological effects in various applications under atmospheric conditions.

This is for my parents, Chhabi Lal Adhikari and Kharika Adhikari.

CONTENTS

Figures.....	v
Tables.....	x
Acknowledgments.....	xi
Chapter 1: Introduction.....	1
1.1 Introduction to plasma.....	1
1.2 Atmospheric pressure plasma jet (APPJ).....	2
1.3 Estimation of reactive species.....	9
1.4 Outline of the dissertation.....	10
Chapter 2: Correlation of APPJ variables with DNA damage.....	11
2.1 Introduction.....	11
2.2 Experimental setup and methods.....	13
2.3 Results and discussion.....	15
2.3.1 Characterization of the plasma source.....	15
2.3.2 Effects on DNA.....	18
2.4 Conclusions.....	25
Chapter 3: Plasma interactions with air components.....	27
3.1 Introduction.....	27
3.2 Experimental setup and methods.....	30
3.2.1 Fixed jet environment and varied feed gas.....	31
3.2.2 Fixed feed gas and varied jet environment.....	31
3.3 Results and discussion.....	34
3.3.1 APPJ current, voltage and power.....	34
3.3.2 DNA damage.....	38
3.3.3 Mass spectrometry.....	43
3.4 Conclusions.....	47
Chapter 4: In situ characterization of an APPJ.....	49
4.1 Introduction.....	49
4.2 Materials and methods.....	52
4.3 Results and discussion.....	58
4.4 Conclusions.....	69

Chapter 5: Role of hydrogen peroxide to generate reactive species in an APPJ	71
5.1 Introduction.....	71
5.2 Materials and methods	73
5.3 Results and discussion	76
5.4 Conclusions.....	82
Chapter 6: Summary and future work.....	84
6.1 Summary	84
6.2 Future work.....	87
6.2.1 Modification of experimental setup.....	88
6.2.2 Target dependence of plasma propagation	89
Appendix A: Agarose gel electrophoresis of DNA	92
Appendix B: Supplementary materials	94
Bibliography	100

FIGURES

- Figure 1.1: A photograph of a typical APPJ (taken using Nikon D3100 camera, f5.6, ISO 3200, t = 1 s). Dotted squares indicate the boundaries of electrodes.4
- Figure 1.2: Diagram of plasma species propagation in a plasma jet (a) discharges initiated followed by electron avalanche (b) After electron avalanche, formation of plasma with electrons, ions, and excited species (c) electrons accelerate towards the positive electrode and creating more ionization and excitation (d) excited species and ions formed plasma head, forming plasma bullets in the plasma jet.5
- Figure 1.3: DBD process for the pulsed voltage (a) first electron avalanche during rising edge of applied voltage (b) no ionization while the amplitude of applied voltage is remained maximum (c) second electron avalanche during falling edge of applied voltage (d) all electric field becomes zero and no ionization again.....6
- Figure 1.4: The images of a helium APPJ launching to an open atmosphere. The images are taken with a 5 ns exposure time and various delay time.8
- Figure 2.1: A schematic diagram of the APPJ source.14
- Figure 2.2: (a) Photographs of plasma jets at various flow rates (taken using a Nikon D3100 camera, f 1.8, ISO 3200, t =20 s). Variation of plasma jet length as functions of (b) voltages applied at a helium flow rate of 2 slm, and (c) flow rates at a voltage of 10.6 kV, note the red dashed line indicates a linear dependence between the jet length and the flow rate.16
- Figure 2.3: (a) Voltage waveform at a voltage of 10.6 kV. (b) Current waveform for various flow rates, and (c) plasma power obtained under conditions in (b) at the voltage shown in (a).17

Figure 2.4: (a) Average plasma power for various flow rates of helium at a voltage of 10.6 kV. Fractions of SSBs, DSBs, and undamaged DNA induced (b) at different flow rates of helium at 15 s of plasma irradiation and at a distance of 2.5 cm below the orifice, note that the time “0” indicates the control sample, (c) at various durations of plasma irradiation at a flow rate of 2 slm and at a distance of 2.5 cm below the orifice, and (d) at various distances below the orifice at plasma irradiation of 15 s and a helium flow rate of 2 slm. These fractions were detected at a voltage of 10.6 kV and in samples with DNA concentration of 6.67 ng/μL. .20

Figure 2.5: (a) Total damage to DNA normalized to the initial amount of damaged DNA molecules in a sample with a concentration of 3.33 ng/μL. (b) Fractions of SSBs, DSBs, and undamaged DNA induced by the APPJ in samples with various DNA concentrations at helium flow rate of 2 slm, distance of 2.5 cm below the orifice, voltage of 10.6 kV, and the duration of plasma irradiation of 15 s.22

Figure 2.6: (a) Average plasma power at various voltages applied at a helium flow rate of 2 slm. (b) Fractions of SSBs, DSBs, and undamaged DNA induced by the APPJ within 15 s of irradiation at helium flow rate of 2 slm and distance of 2.5 cm below the orifice for various voltages applied in samples with DNA concentration of 6.67 ng/μL.24

Figure 3.1: (a) Schematic diagram and (b) photograph of the experimental setup.29

Figure 3.2: (a) Voltage waveform for a voltage of 8 kV and frequency of 500 Hz (b) Current waveform for 4 slm helium in a capillary and 5 slm nitrogen in the chamber at the voltage shown in (a).35

Figure 3.3: Plasma current waveforms for various fractions of (a) oxygen and (b) water vapor in the fixed feed gas and varied jet environment, and (c) oxygen and (d) water vapor in the fixed jet environment and varied feed gas experimental conditions for the rising edge of the voltage applied in Figure 3.2(a).37

Figure 3.4: Fractions of total damaged DNA (green triangles) in the sample after 15 s of plasma irradiation and plasma power (red circles) for the various fractions of (a) water vapor and (b) oxygen in the fixed feed gas and varied jet environment, and (c) water vapor and (d) oxygen in the fixed jet environment and varied feed gas experimental conditions.39

Figure 3.5: Mass spectra for plasma on and off when the pure helium was used as a feed gas and the chamber was filled with pure nitrogen, and open atmosphere.43

Figure 3.6: Mass spectra for the experimental conditions mentioned in the section 3.2 of the main text at the maximum content of oxygen or water vapor when the plasma was ignited.44

Figure 4.1: Schematic of the experimental setup.53

Figure 4.2: (a) Temperature variation of the solution during plasma exposure for three trials under three different experimental conditions; (b) Absorbance as a function of exposure time for three initial concentrations of Fe^{2+} in the solution. The plasma was ignited at a voltage of 10 kV, frequency of 1 kHz, flow rate of 2 slm, and treatment distance of 10 mm, and (c) Fe^{3+} yield rate estimated from the absorbance in (b) for the various initial concentrations of Fe^{2+} in the solution. ...56

Figure 4.3: General forms of the differential equations for six chemical reactions with the rate constants (k) taken from [96] for each individual species numbered in red from 1 (i.e., electron, e) to 11 (i.e., hydroxide, OH^-). Note, y' is the rate of yield of particular species (specified by suffix) and y is the amount of species in the solution at the particular time.57

Figure 4.4: (a) *In situ* measurement of absorbance of the Fricke solution during plasma exposure with a helium flow of 2 slm, frequency of 1 kHz, and treatment distance of 10 mm at various applied voltages for three independent trials; (b) slope of the curves in (a) as a function of voltage applied for three independent trials and their average; (c) comparison of the Fe^{3+} yield rates in situ and post-exposure measurements (i.e., *ex situ*); and (d) Fe^{3+} yield rate during plasma exposure at a voltage of 10 kV, frequency of 1 kHz, and flow rate of 2 slm as a function of treatment distance.59

Figure 4.5: Schlieren photograph of a helium gas channel in the atmosphere at a flow rate of 2 slm.61

Figure 4.6: (a) Rate of evaporation of the solution, and (b) Fe^{3+} yield rates as a function of flow rate within plasma exposure of 400 s at a voltage of 10 kV, frequency of 1 kHz, and treatment distance of 10 mm.61

Figure 4.7: (a) Fe^{3+} yield rate as a function of pulse frequency at a voltage of 10 kV, flow rate of 2 slm, and treatment distance of 10 mm; and (b) Fe^{3+} yield per pulse as a function of the frequency estimated from (a).62

Figure 4.8: (a) Number of species as a function of reaction time obtained by solving the corresponding differential equations for each reactant; (b) enlarged image of (a) in the time range from 1×10^{-4} to 2×10^{-3} s equivalent to the time periods/frequencies used in this study.63

Figure 4.9: Normalized Fe^{3+} yields as a function of frequency used in experimental study and the calculated yield after the first pulse assuming that electrons and OH^\bullet are delivered from the APPJ to the solution.64

Figure 4.10: Normalized Fe^{3+} yields as a function of frequency used in experimental study and the calculated yield after one pulse assuming that (a) only electrons are delivered from the APPJ to the solution (b) electrons and OH^\bullet with some initial amount of H_2O_2 are delivered from the APPJ to the solution (c) electrons and OH^\bullet with some initial amount of H_2O_2 and HO_2^\bullet are delivered from the APPJ to the solution (d) electrons and OH^\bullet with some initial amount of H_2O_2 and HO_2^\bullet are delivered from the APPJ to the solution and some Fe^{3+} amount present in the solution generated from the previous pulse. All initial values for electrons, OH^\bullet , H_2O_2 , HO_2^\bullet and Fe^{3+} are reported in reference [95].	65
Figure 4.11: Normalized Fe^{3+} yield per pulse for a typical pulse at every 1000th pulse. Dotted curves are the yield per pulse for a particular pulse number while the data points are the average values of 10000 pulses. The arrow indicates the increasing order of pulse number.	67
Figure 4.12: Normalized Fe^{3+} yields after different number of pulses as a function of frequency used in experimental study. Dotted curves are the yields for a particular pulse number, while circle data points are the average values of 10000 pulses as in Figure 4.11. The arrow indicates the increasing order of pulse number.	67
Figure 4.13: Total DNA damage induced within 15 s of plasma irradiation as a function of pulse voltage at a frequency of 1 kHz, flow rate of 2 slm, and treatment distance of 10 mm.	68
Figure 4.14: Normalized Fe^{3+} yield and DNA damage level within 15 s of plasma exposure as functions of (a) voltage, (b) treatment distance, and (c) flow rate of the feed gas (DNA damage level data in (b) and (c) were taken from Chapter 2 Figures 2.4(d) and (b) respectively).	68
Figure 5.1: Schematic of the experimental setup.	74
Figure 5.2: (a) The yield rate of Fe^{3+} due to plasma irradiation as a function of the fraction of water vapor in the feed gas. Water vapor was fed into the feed gas with only water (H_2O , red circles) or hydrogen peroxide with water (H_2O_2 , green triangles); (b) difference in the yield rates of Fe^{3+} for conditions in (a) as a function of the fraction of water in the feed gas; (c) yield rate of Fe^{3+} as a function of the fraction of hydrogen peroxide in the feed gas for plasma OFF (purple squares) and plasma ON (green triangles) conditions; (d) difference in the yield rates of Fe^{3+} for conditions in (c) as a function of the fraction of hydrogen peroxide in the feed gas.	78
Figure 5.3: The average plasma power for various fractions of (a) water vapor and (b) hydrogen peroxide vapor in the feed gas.	80
Figure 5.4. Fractions of DNA damage in the sample after 15 s of plasma irradiation as a function of the fraction of (a) water in the feed gas, and (b) hydrogen peroxide in the feed gas.	81

Figure 6.1: Schematic of the experimental set up to monitor the propagation of plasma bullets and reactive species in a controlled environment.	89
Figure A.1: Typical photographs taken for the various experimental conditions using a D3100 Nikon camera (exposure time 0.5 s, f/5.6, iso6400) (a) Jet striking the edge of the glass well; (b) and (c) Jet striking the center of the sample in two different trials. The green part represents the sample well.	95
Figure A.2: Photographs of the plasma jet and plasma discharged between the electrodes obtained under different experimental conditions using a Canon EOS Rebel T6i (exposure time: 2 s, f/5.6, ISO: 100, focal length: 18 mm). (a) 4 slm helium feed gas and 5 slm nitrogen in the chamber, (b) 16% humidity in the feed gas, (c) 0.25% oxygen in the feed gas, (d) 56% oxygen in the chamber, and (e) 62% humidity in the chamber.	95
Figure A.3: (a) Voltage waveform at a voltage of 10.6 kV; (b) Current waveforms for the feed gas at room temperature and heated gas at temperature of 149 °C.	96
Figure A.4: Fe ³⁺ yield rate during plasma exposure at a voltage of 10 kV, frequency of 1 kHz, and a flow rate of 2 slm as a function oxygen content in the feed gas.....	97
Figure A.5: (a) Applied voltage waveform. Plasma current waveforms for various fractions for (a) hydrogen peroxide with water (b) only water for the voltage applied in (a).	98
Figure A.6: Total DNA damage fractions due to the plasma irradiation as a function of irradiation time for the pure helium, and the mixture of water vapor or hydrogen peroxide vapor in helium, note that the time “0” indicates the control sample. ...	99

TABLES

Table 3.1: Area under the mass peaks for the experimental conditions mentioned in section 3.2 with the maximum content of oxygen or water vapor.	46
Table 6.1: The speed of plasma bullets for various experimental conditions.	90

ACKNOWLEDGMENTS

I believe one of the best decision I ever made is choosing the University of Notre Dame for my graduate school. For these 6 years or so, I have always been surrounded by great people.

First of all, I would like greatly thank my advisor, Dr. Sylwia Ptasinka, for providing me the exceptional environment and support to pursue my research interest and goals. We spent a lot of time discussing atmospheric pressure plasma research. It is my great fortune that I got a great scientist with a courteous, resourceful, and persistent personality as an advisor. I would also like to express my gratitude to Dr. Vladimir Samara who was always willing to answer questions on science, methods, hardware, software, and occasionally music, movie, culture, and food, depending on whatever I needed. I would like to thank Dr. James Kapaldo and Dr. Xu Han for being always there to discuss anything that I called for. I would also like to thank Notre Dame Radiation Laboratory for economic support for all my research work as well as to sustain my life. I am also grateful to Notre Dame Graduate School Professional Development Office and Graduate Student Union for supporting me to travel to attend many conferences.

I would like to thank my current group members, Pitambar Sapkota, Amal Sebastian, Dr. Surja Ghale, Dr. Souyma Banerjee, Daniel Lipa and former members Dr. Zhou Li, Dr. Michal S. Ryszka, Dr. Weixin Huang, Dr. Subha Sadhu, Dr. Xueqiang

Zhang, Dr. Krishna P. Arjunan, Dr. M. Michele Dawley, Dr. Denis A. Sokolov, Dr. Aleksandar R. Milosavljevic, Elizabeth Briley, Andrew Jensen, Evan Panken, and Elek Wellman for their genuine support, suggestions, encouragement, and help on my research projects and their great friendship. I would also like to thank all of my classmates (class enrolled in 2013) for supporting me in academic and socialization aspects.

This work would not be possible without the great help of technical support from the machine shop, glass shop, and electronics shop. A special thanks go to Kiva Ford, Joe Admave, Daniel Williams, and former staffs Roberto Moreno, John Budnick, and Kurt Belting.

I would like to thank my parents, Chhabi Lal Adhikari and Kharika Adhikari, for their loving support without doubting on my capacity to achieve my goal. I want to thank my brothers, Devi P. Adhikari, Toya N. Adhikari, and sisters, Tara Dhakal, Radha Paudel, and Saraswati Paudel for their support, love and being great siblings. I would like to thank my wife Shova Paudel for her love, encouragement, kindness, and for being with me in all ups and downs in this entire journey.

CHAPTER 1: INTRODUCTION

1.1 Introduction to plasma

Plasma is usually considered as a fourth state of matter which contains an approximately equal amount of unbound positive and negative charges; therefore plasma is electrically quasi-neutral even though it consists of charge species. Plasma also contains neutral species (e.g., atoms, molecules, radicals) along with electromagnetic radiation (photons). The commonly known natural plasmas in the Earth are lightning, fire, polar auroras, etc. There are many types of man-made plasma sources which are built according to the need of the people, e.g., welding, neon sign, fluorescent light, etc. Plasmas are classified into two groups on the basis of their temperature and equilibrium conditions: (1) thermal (or equilibrium) plasma and (2) non-thermal (non-equilibrium) plasma [1]. Thermal plasmas are characterized by high level of ionization, and all species achieve thermal equilibrium at high temperature ($\sim 10^4$ K) whereas, non-thermal plasma, also referred as cold plasma, are characterized by weak ionization, and the electron and heavy species (e.g., ions, neutrals) are not in thermal equilibrium. The gas temperature (i.e., temperature of heavy species) in cold plasma is equivalent to room temperature or little above (~ 25 to 40 °C). The electron density is typically less than 10^{19} m⁻³ [2]. The

non-thermal plasmas can be generated in low pressure as well as in the atmospheric pressure. There are various methods to generate atmospheric pressure plasmas, such as microwave discharge, radio frequency (RF) discharge, dielectric barrier discharge (DBD), and direct current (DC) discharge. All of these sources have their unique features that are suitable for certain applications. A commonly used atmospheric pressure plasma source is an atmospheric pressure plasma jet (APPJ) which I investigated in my study.

1.2 Atmospheric pressure plasma jet (APPJ)

Atmospheric pressure plasma jets (APPJs) are highly reactive, and non-equilibrium plasmas which are close to room temperature and able to treat heat sensitive surfaces. There are several approaches to generate plasma jet in a lab according to the need of the researchers. The different approaches include electrodes shape, feed gas (or gas mixture), applied voltage waveform, and frequencies that are used to ignite plasma [3]. Due to these variations in the currently used APPJs, the comparison of all results or achievement so far is still challenging. A photograph of a typical APPJ source that I used in my study is shown in Figure 1.1. This typical type of APPJ source consists of a dielectric tube, two electrodes, feed gas, and a power supply. An inert gas (usually He, Ar or Xe) flows through that dielectric tube and a high voltage (HV) pulse is applied to either top or bottom electrode. The plasma is ignited between two electrodes and propagates in a guided path provided by the feed gas forming a few centimeter long plasma jet into the atmosphere. The commonly used principle to ignite the plasma in an APPJ source is DBD. In DBD, one or both electrodes are covered by a dielectric. When the electric field is applied between two electrodes, electrons in the space start to

accelerate. Those accelerating electrons experience a number of elastic and inelastic collisions with gas molecules. When any accelerating electrons attain the energy higher than the ionization energy of a gas molecule and collide with that gas molecule, first ionization event happens. The electrons from that ionization event are further accelerated and create more ionization events, and eventually, electron avalanche will occur. Once the electron avalanche occurs, there are electrons, ions, excited species (ions or neutrals), and electromagnetic radiation (photons) in the system eventually creating the plasma. The excited species lose their energy and release photons, and these photons are captured by ground state molecules or other excited molecules. There is also frequent collisions between plasma species. These collisions may lead to the Penning ionization which is one of the critical processes responsible for plasma propagation. Penning ionization occurs when the flowing gas comprises a majority of atoms or molecules that have the high first excitation state, e.g., He (19.8 eV), with an admixture of gaseous atoms or molecules with ionization energies lower than the first excitation state, e.g., N₂ (15.58 eV) [4].

When the ionization occurs in the plasma jet, it creates an electric field in the jet which accelerates the electrons towards/away from the electrodes. When electrons accelerate, more ionization and excitation of molecules is possible. In this way, an ionization front propagates in the feed gas channel, as shown in Figure 1.2.

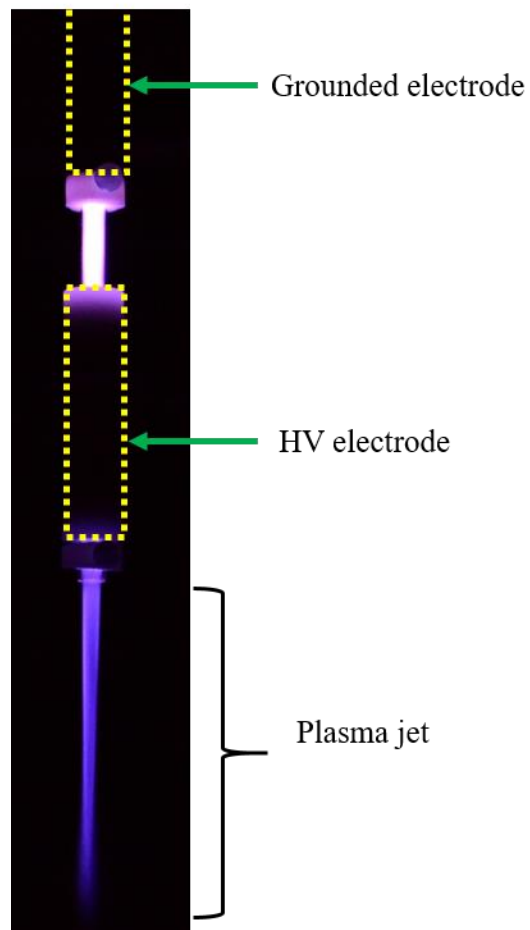


Figure 1.1: A photograph of a typical APPJ (taken using Nikon D3100 camera, $f/5.6$, ISO 3200, $t = 1$ s). Dotted squares indicate the boundaries of electrodes.

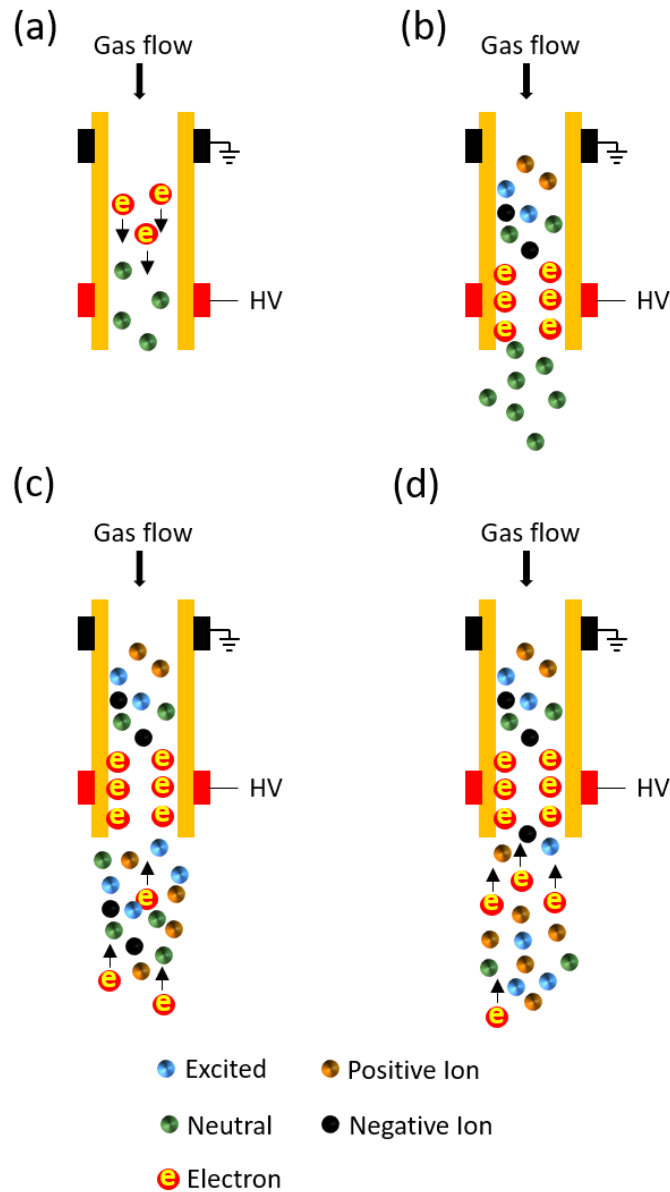


Figure 1.2: Diagram of plasma species propagation in a plasma jet (a) discharges initiated followed by electron avalanche (b) After electron avalanche, formation of plasma with electrons, ions, and excited species (c) electrons accelerate towards the positive electrode and creating more ionization and excitation (d) excited species and ions formed plasma head, forming plasma bullets in the plasma jet.

I used a DC pulsed voltage to ignite the plasma in our lab. A typical DBD process due to DC pulsed voltage is shown in Figure 1.3.

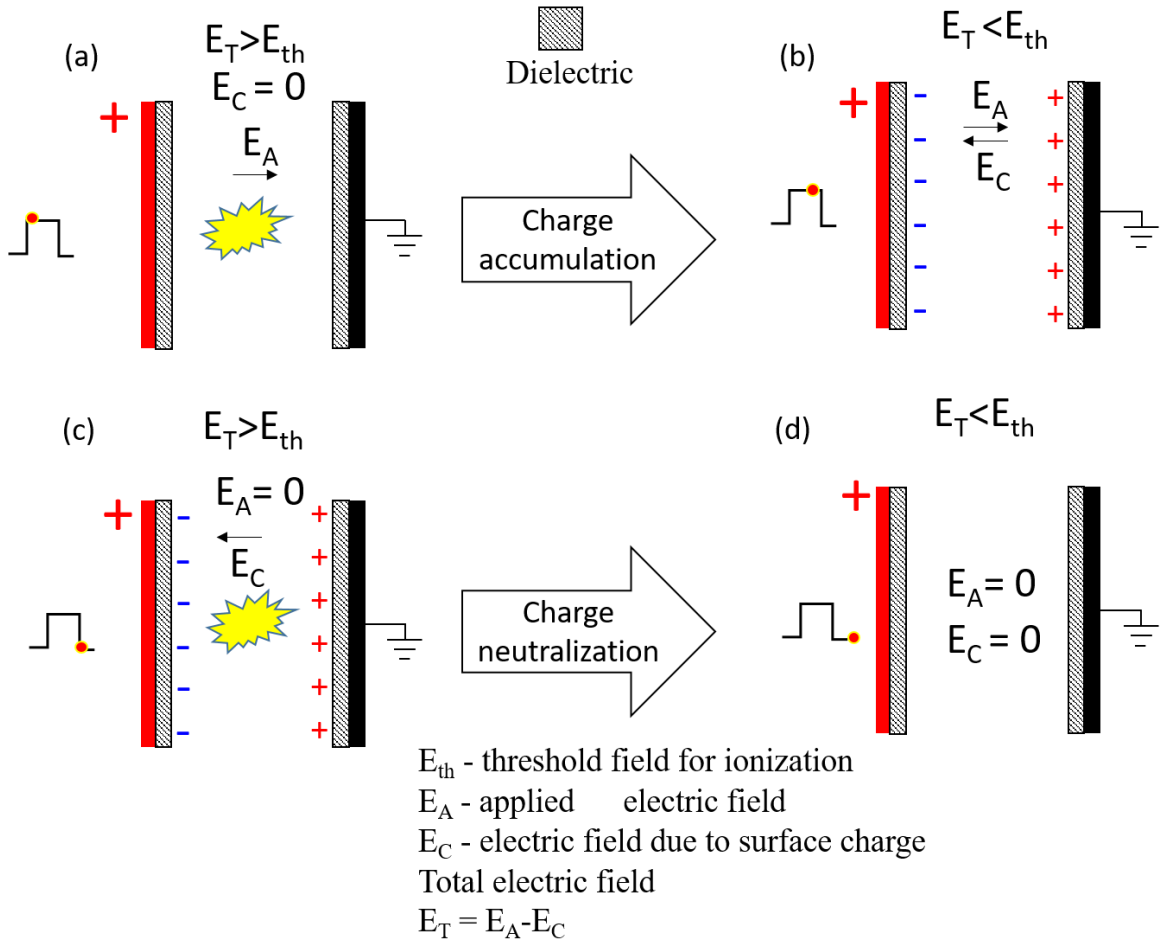


Figure 1.3: DBD process for the pulsed voltage (a) first electron avalanche during the rising edge of applied voltage (b) no ionization while the applied voltage is remained maximum (c) second electron avalanche during the falling edge of applied voltage (d) all electric field becomes zero and no ionization again.

When the applied voltage becomes maximum (at rising edge), first electron avalanche happens (Figure 1.3(a)). During the plasma propagation after that first electron avalanche, the electrons and positive ions will continue to accelerate towards the positive and negative electrodes where they attached on the dielectric walls (Figure 1.3(b)), causing a reduction of the electric field. Then the total electric field is not enough to continue the ionization process, and the plasma generation stops as long as there is a high voltage pulse. When the high voltage pulse ends (at falling edge), applied electric field becomes zero, however the electrons and ions on the surface of the dielectric create an electric field in the opposite direction to the initially applied field; they then become detached from the dielectric and accelerate in the opposite direction creating another electron avalanche (Figure 1.3(c)). After this second electron avalanche, electrons and ions recombine, and no field exists between two electrodes, and no further ionization happens (Figure 1.3 (d)). This process repeats for every pulse of the applied voltage. This plasma on and off processes will not allow for a sufficient time for plasma to achieve the thermal equilibrium and the temperature of the heavy species in the plasma jet remains equivalent to the room temperature. In the APPJ source that I used in my study, the electron avalanche happens between the electrodes and propagates out from the dielectric capillary along the direction of total electric field. The propagation of the plasma bullet is shown in Figure 1.4. An intensified charge coupled device (ICCD) camera (PI-MAX, Princeton Instrument, Trenton, NJ, USA) was used to take images of the helium APPJ using a short exposure time (~ 5 ns) and different delay time. The plasma was ignited using 10 kV voltage, 1 kHz frequency, and 2 slm (standard liter per minute) helium flow rate. In Figure 1.4, it is observed that the plasma bullet travels around 3 cm within 0.3 μ s,

i.e., around 100 km/s. This speed of the plasma bullet is not comparable with the moving speed of any atoms or molecules; however, it indicates the fast propagation of ionizing events as explained before.

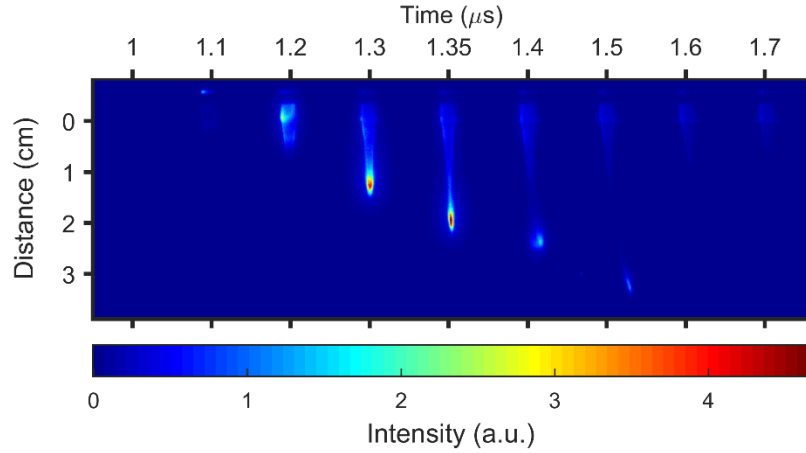


Figure 1.4: The images of a helium APPJ launching to an open atmosphere. The images are taken with a 5 ns exposure time and various delay time.

Since the plasma jet is in open atmospheric environment, it interacts with the air components and forms many reactive oxygen and nitrogen species (RONS) in the plasma jet [5]. The plasma jet environment highly influences the amount and type of reactive species in the plasma. The fluctuation in atmospheric conditions such as room temperature, and humidity, effects plasma jet environment which eventually influences the amount and type of reactive species in the plasma jet. Therefore, it is very challenging to reproduce plasma performance while operating in various places and time. Further, the plasma jet consists of very short-lived reactive species which can initiate a cascade of chemical reaction in the sample. I designed two separate experimental set ups to control

the plasma jet environment as well as the feed gas and to measure the total reactive species provided in plasma jet or originated in the sample during plasma irradiation.

1.3 Estimation of reactive species

It is well-known that there are many reactive species and these reactive species are important for the clinical application of an APPJ. Therefore, it is essential to know the type and amount of the reactive species precisely to upgrade the performance of an APPJ in clinical medicine. So far, there are several techniques in practice to identify and quantify the various reactive species in the plasma jet. Some of the notable methods in practice to characterize a plasma jet are ultra-fast imaging, laser-induced fluorescence (LIF), scattering techniques, optical emission spectroscopy, optical absorption spectroscopy, etc. Some of the other non-optical techniques are mass spectrometry, flow visualization, electron paramagnetic resonance spectroscopy (EPR), etc. [6]. These techniques have their own benefits according to species that needed to be identified and quantified. Briefly, the fast imaging technique is used to detect and monitor plasma bullets with pico- to nanosecond precision and study the streamer dynamics in APPJs. A gated and triggered ICCD camera is used to image the dynamic processes in plasmas. LIF is used to get information about the densities of the ground or excited states atomic and molecular species. OES has a limitation of detecting only excited species because it measures the radiation emitted by the excited atoms or molecules in the plasma. Nevertheless, a lot of information can be gained from OES, the absolute and relative line intensities, the line widths, the appearance of certain lines attributed to forbidden states or the emission continuum radiation. However, I have focused on some unique techniques to

characterize a plasma jet using a molecular probe (e.g., DNA), *in situ* characterization using chemical dosimeter (e.g., Fricke solution) along with the widely used technique ultra-fast imaging, flow visualization, and mass spectrometry.

1.4 Outline of the dissertation

Chapter 2 describes the construction and characterization of a helium APPJ source that I used for all of my experiments. This also includes the electrical characterization as well as the correlation of a helium APPJ variables and plasma-induced DNA damage level using DNA as a molecular probe. Then, I used that APPJ to study the interaction between the plasma components and air component which is explained in Chapter 3. To get more insight about the intermediate and short-lived reactive species in plasma jet, I developed an *in situ* absorption spectroscopy experiment employing Fricke solution as a sample which is described in Chapter 4. Then, I used that *in situ* absorption spectroscopy experimental set up to investigate the contribution of the H₂O₂ in increasing the reactive species in the plasma jet which description is included in Chapter 5. Finally, I summarize and conclude the dissertation in Chapter 6 and also discuss possible future work for further investigation of APPJs.

CHAPTER 2:
CORRELATION OF APPJ VARIABLES WITH DNA DAMAGE¹

2.1 Introduction

Atmospheric pressure plasma (APP) sources are being developed as a new tool in plasma medicine that combines plasma physics, life sciences, and clinical medicine [7]. The interest in using APPs in medicine is growing, because of their ability to produce a mixture of biologically reactive species, such as reactive oxygen species (ROS) and reactive nitrogen species (RNS), when plasma is exposed to ambient air [5], [8]. Until now, APPs have been used to manipulate cells to control their adhesion [9], for tissue ablation in surgery [10], [11], tissue sterilization [12]–[16], blood coagulation [16], wound healing [17], [18], and induction of apoptosis in cancer cells [19]–[26]. These and other biotechnological applications were reported in review papers [27]–[33]. To obtain a better understanding of these processes, it is vital to understand the effects of plasma on cells and their subcellular components. Among the biomolecules in cells, DNA is

¹ The results in this Chapter are published in the following peer-reviewed journal.

E. R. Adhikari and S. Ptasinska, “Correlation between helium atmospheric pressure plasma jet (APPJ) variables and plasma induced DNA damage,” *Eur. Phys. J. D*, vol. 70, no. 9, p. 180, 2016.

essential, as altered DNA can cause cells to function abnormally or die [34], [35]. It is desirable to maximize DNA damage in targeted cells, such as microbes and malignant cells, but to minimize it in neighboring cells [35], [36]. Thus, qualitative and quantitative knowledge of the effects of APPs on DNA offers an opportunity to increase the biological applications of these types of plasmas.

Several types of atmospheric pressure plasma jet (APPJ) sources have been used to study isolated, as well as cellular, DNA [34]–[44]. These sources use pure gas or an admixture of gases as feed gases [5]. Han *et al.* [34], Ptasinska *et al.* [38], Stypczynska *et al.* [40], and Bahnev *et al.* [42] used helium gas to investigate the effects of APPJ on plasmid DNA, while Alkawareek *et al.* [36], O’Connell *et al.* [35], Yan *et al.* [39], Niemi *et al.* [37] and Kim *et al.* [41] used helium with a small amount of oxygen as a feed gas. Kurita *et al.* [43], [44] used an argon APPJ to induce DNA damage, and the damage was quantified using molecular beacons [43] and single-molecule observations [44]. These previous studies have provided a plethora of exciting observations; in addition, they have attempted to establish a correlation between APPJ variables and DNA damage. However, various components of plasma (e.g., reactive species, ultraviolet light, electrons, and ions) can induce damage in DNA, which can be enhanced or reduced by varying the parameters of the APPJ source. For instance, adding a small amount of oxygen to a feed gas enhances DNA damage, due to the increased production of radicals. The results of all previous studies on DNA using APPJs were summarized in Arjunan *et al.*’s recent review [5].

The overall goal of this study was to contribute further to plasma medicine research by determining the correlation between experimental parameters, including flow

rate, voltage applied, and DNA concentration in a sample and the DNA damage, all of which are essential in understanding the effects of APPJs on cellular systems.

2.2 Experimental setup and methods

The schematic diagram of the experimental set-up was similar to that in [34], [45]. Briefly, the APPJ source consisted of two 50-mm brass electrodes, grounded and powered electrodes, separated by 30 mm and located on the outside of a fused silica capillary, as shown in Figure 2.1. The fused silica capillary had an orifice diameter of 5 mm. To ignite the plasma, a square pulse of 100 μ s with a frequency of 1.5 kHz was generated by a pulse waveform generator (80 MHz Function/Arbitrary Waveform Generator, 33250 A, Agilent Tech., Santa Clara, CA, USA) coupled to an HV transformer connected to the powered (HV) electrode. The helium (HE UHP300, Airgas Inc., Radnor, PA, USA) flow rate through a capillary was adjusted with a flow controller (MASS-VIEW flow regulator, MV-394-He, Bronkhorst High-tech. B.V., Ruurlo, The Netherlands). The voltage applied and plasma current were measured at the powered and grounded electrodes using a high voltage probe (P6015A, Tektronix, Inc., Beaverton, OR, USA) and an induction coil (Pearson Current Monitor Model 2877, Pearson Electronics, Inc., Palo Alto, CA, USA), respectively. The amplitude and shape of the waveforms of voltage and current were recorded using an oscilloscope (TDS2004B, Tektronix, Inc., Beaverton, OR, USA, sampling rate: 100 MHz, average: 128). The plasma was ignited between the two electrodes, and a visible plasma jet of a few centimeters was projected through the fused silica capillary into the open atmosphere.

Temperatures along the jet were measured at various distances and flow rates using a mercury thermometer and were below 30 °C.

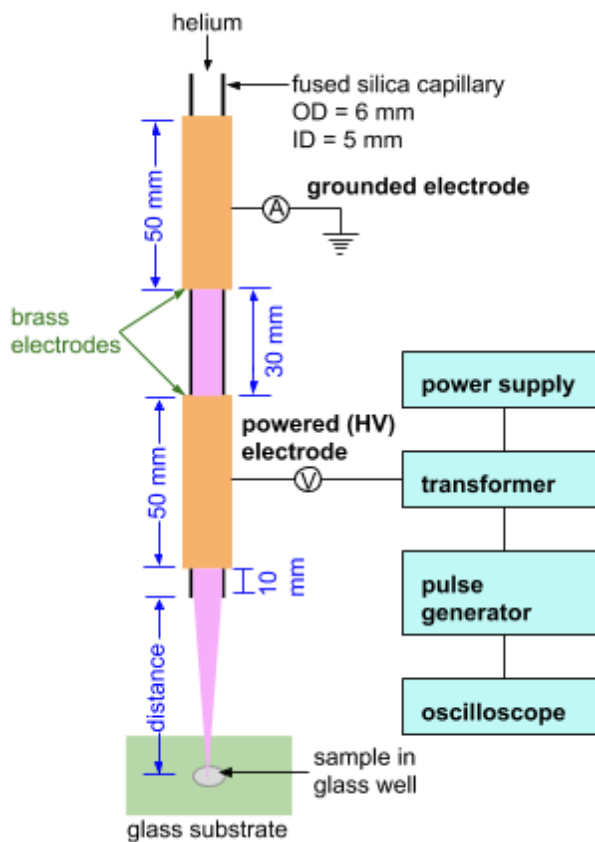


Figure 2.1: A schematic diagram of the APPJ source.

pUC18 plasmid DNA (ThermoFisher Scientific, Waltham, MA USA) with 2686 base pairs extracted from *Escherichia coli* (*E. coli*) was used as the sample. The stock DNA solution with A260/A280 ratio of 1.70 ± 0.03 measured using a NanoDrop™ 2000c spectrophotometer (ThermoFisher Scientific, Waltham, MA USA) was kept in a buffer (10 mM Tris (pH 7.6) and 1 mM EDTA) at -20 °C. The samples were diluted with deionized water (pH 6.0 ± 0.1) to the concentration desired and 15 μ L of the sample was irradiated in a glass well with a diameter of 4.2 mm and depth of 1.4 mm. The irradiated

sample was collected with a pipette and the glass well was washed three times with 5 μL PBS (Phosphate Buffered Saline) to collect the remaining DNA. I used the gel electrophoresis method (0.8 % agarose gel pre-stained by SYBR green dye, running time 3 h at 70 V) to quantify the DNA damage induced by plasma irradiation. The details of that method are provided in Appendix A. A mean value of the DNA fraction for each type of damage was calculated from at least three samples irradiated under the same experimental conditions, and the error bars represent the standard deviation from the mean. The mean value and error bars in average power were also calculated from at least three oscilloscope recordings.

2.3 Results and discussion

2.3.1 Characterization of the plasma source

Photographs of the APPJ for various flow rates are shown in Figure 2.2(a), while the average jet length (visible plasma region) for the various voltages and flow rates are shown in Figures 2.2(b) and 2.2(c), respectively. With an applied voltage of 10.6 kV, three distinguished regions were observed for the jet length as a function of the flow rate. As marked by a red curve in Figure 2.2(c), the jet length increased linearly up to 4 slm (standard liter per minute). This increase indicated the elongation of a flowing gas channel, which provides the path for the propagation of plasma bullets and ionization waves into the atmosphere [46], [47].

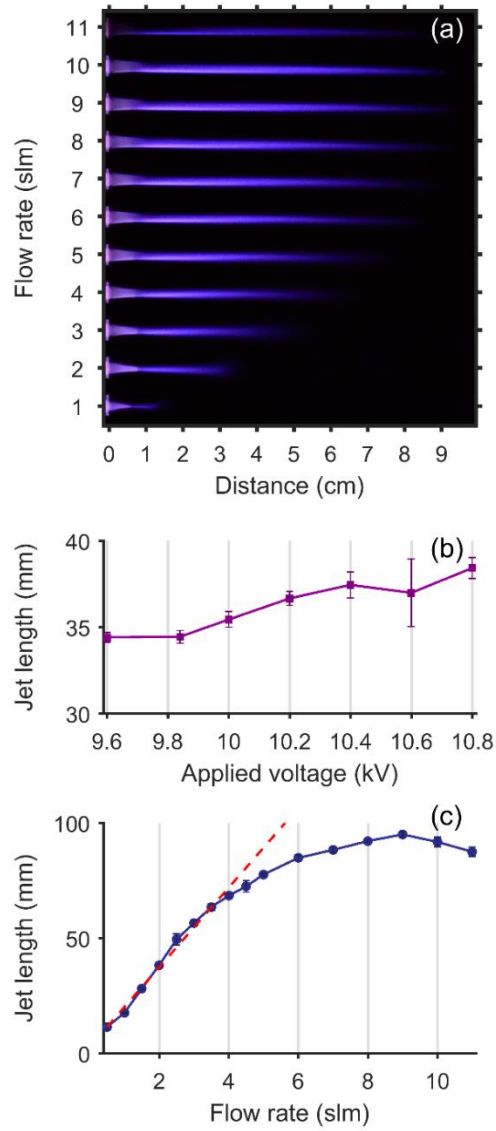


Figure 2.2: (a) Photographs of plasma jets at various flow rates (taken using a Nikon D3100 camera, f 1.8, ISO 3200, $t=20$ s). Variation of plasma jet length as functions of (b) voltages applied at a helium flow rate of 2 slm, and (c) flow rates at a voltage of 10.6 kV, note the red dashed line indicates a linear dependence between the jet length and the flow rate.

Above 4 slm, the jet length continued to increase until attained its maximum value of about 100 mm at the flow rate of 9 slm. Furthermore, the jet became shorter and unstable, most likely because of the transition from laminar to turbulent flow, as was observed for another APPJ source [48].

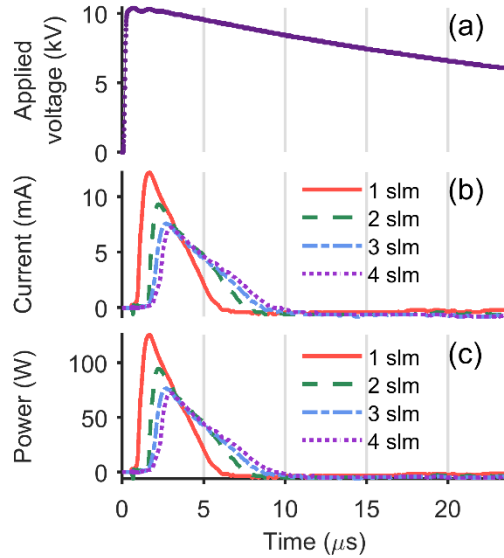


Figure 2.3: (a) Voltage waveform at a voltage of 10.6 kV. (b) Current waveform for various flow rates, and (c) plasma power obtained under conditions in (b) at the voltage shown in (a).

However, the jet's instability above a helium flow rate of 9 slm is not visible in the figure, because of the long exposure time (20 s) on the camera. These observations indicated that the length of the gas channel plays a crucial role in determining jet length. The length of the gas channel remained constant for a particular flow rate; therefore, the additional energy derived from an increment in voltage applied (i.e., input power) can only drive the plasma species' presence slightly beyond the helium gas channel. Indeed, by varying the voltage from 9.6 to 10.6 kV, I observed that the jet length increased

slightly with an increase in voltage (Figure 2.2(b)). It is interesting to note that the shape of the current waveforms changed for different flow rates, as shown in Figure 2.3(b) at a voltage of 10.6 kV (Figure 2.3(a)). The instantaneous power for the conditions presented in Figure 2.3(b) was calculated by multiplying the voltage and current; power as a function of time is shown in Figure 2.3(c). In addition, the average power of the plasma was calculated by averaging the instantaneous power over a cycle (Equation 2.1).

$$\bar{P} = \frac{1}{T} \int_0^T P(t) dt = \frac{1}{T} \int_0^T V(t) I(t) dt . \quad (2.1)$$

The peak maxima of current, and hence, the power waveforms, became smaller and the phase of both waveforms shifted with increased flow rates, while the average power decreased slightly with increased flow rates, as shown in Figure 2.4(a).

2.3.2 Effects on DNA

To monitor the effects of external factors (e.g., sample handling, gas flow), the following control samples were prepared: (1) stock control: DNA stock solution, (2) substrate control: the sample was placed on the substrate and collected from the well without irradiation, and (3) flow control: the sample was treated with the feeding gas for 60 s and collected from the well. The DNA in all control samples showed about 10% damage with no DSBs observed. Initially, the sample was irradiated for different durations at a distance of 2.5 cm from the and with a fixed flow rate of 2 slm. For irradiation between 15 and 60 s, the fractions of single strand breaks (SSBs), double strand breaks (DSBs), and undamaged DNA changed from 9% to 84%, 0% to 16%, and 91% to 0%, respectively, as shown in Figure 2.4(c). It is interesting to note that more than 50% of intact DNA experienced SSBs or DSBs within the first 15 s of irradiation. A

similar result was reported in other studies using a helium APPJ [34], [38] and an APPJ with a small amount of oxygen in helium [35], [36]. However, some other research groups have reported slower degradation of DNA using different plasma sources and detection methods [39], [43], [44]. In addition, I observed that, after 60 s of irradiation, almost all previously intact DNA molecules were affected by the formation of SSBs or DSBs; with longer irradiation time, DNA molecules broke into small fragments, which appeared as smeared zones in the agarose gel images. The fraction of DSBs reached approximately 16% within an irradiation time of 60 s, which was higher than that reported in other studies using helium APPJs [34], [38].

To investigate the DNA damage due to changes in other variables (e.g., flow rate, distance, DNA concentration), I irradiated samples only for 15 s and varied these variables. A previous study demonstrated that the amount and distribution of plasma species (e.g., N_2 , N_2^+ , OH^\bullet , O) changed with a particular flow rate [49]. Specifically, it was reported that an increment in ROS production (e.g., OH^\bullet , O) led to increased yields of DNA damage [35], [37], [50]. Figure 2.4(b) represents the fraction of types of DNA damage detected in samples irradiated within 15 s as a function of flow rates, which varied from 1 to 4 slm for samples at a distance of 2.5 cm. At a lower flow rate (1 – 1.5 slm), when the jet was relatively shorter, and thus not in contact with the sample, the fraction of DNA degradation was low (<20%), but at a higher flow rate (2 – 4 slm), the fractions of SSBs and undamaged DNA changed from 19% to 73% and 81% to 19%, respectively, while the fraction of DSBs remained relatively constant (<8%). In addition, because the distribution of species in APPJs depends on the distance from the orifice [38], [49], it was important to investigate DNA damage at different distances. Figure 2.4(d) represents the DNA damage as a function

of distances from 1 to 4 cm at a helium flow rate of 2 slm and irradiation time of 15 s. In the visible plasma region (up to 2.5 cm from the orifice), I observed a significant fraction of DNA damage (>60%), while for the region in which the plasma jet was not in contact with the sample (3-4 cm from the orifice) the DNA degradation was relatively small (<15%). This is consistent with a result reported previously by Han *et al.* [34], who used a plasma source similar to mine.

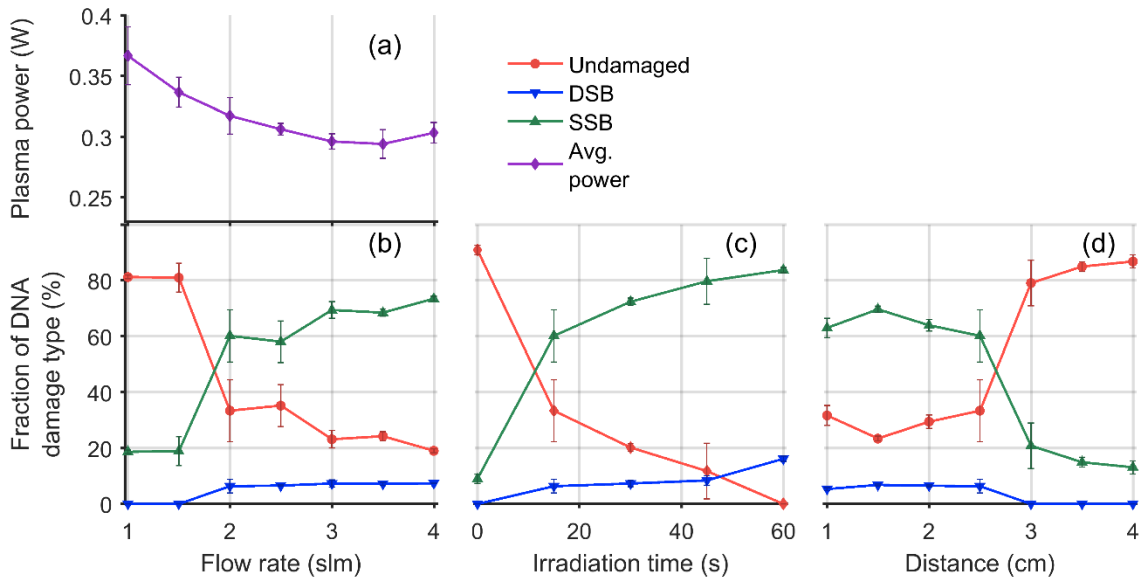


Figure 2.4: (a) Average plasma power for various flow rates of helium at a voltage of 10.6 kV. Fractions of SSBs, DSBs, and undamaged DNA induced (b) at different flow rates of helium at 15 s of plasma irradiation and at a distance of 2.5 cm below the orifice, note that the time “0” indicates the control sample, (c) at various durations of plasma irradiation at a flow rate of 2 slm and at a distance of 2.5 cm below the orifice, and (d) at various distances below the orifice at plasma irradiation of 15 s and a helium flow rate of 2 slm. These fractions were detected at a voltage of 10.6 kV and in samples with DNA concentration of 6.67 ng/ μ L.

However, Bahnev *et al.* [42] reported a different result with variation in distances. They studied the spatial distribution of DNA damage using a helium APPJ driven by a radio frequency sinusoidal voltage, and reported that the damage level was highest (~60%) at the tip of the visible plasma region and decreased in any axial or radial directions from the tip of the jet, such that they observed DNA damage even at a distance of 25 cm from the orifice. In contrast, in my experiment, I observed a sharp decrease in the yield of DNA damage at the tip of the jet. This raises an interesting question about the nature of plasma propagation with both alternating or single pulses of applied voltages, and also with different pulse frequencies. Some recent research has investigated the propagation of plasma into the atmosphere for differently shaped pulses and frequencies of voltage applied. For example, a comparative study of a plasma source driven by a pulsed dc and a sine wave reported that the pulsed-dc-generated plasma had a higher discharge current, plume length, plasma generation efficiency, and bullet velocity than did the sine-wave-excited plasma [51]. Although a pulsed-dc-generated plasma source similar to in this work should ignite plasma more efficiently, the DNA damage caused by a sine-wave-generated plasma source [42] was significantly higher, beyond the visible region of plasma. I also observed that the volume of the sample decreased significantly during irradiation (from 15 to ~10 μL with an irradiation time of 60 s), which indicated that the concentration of the sample also changed. Figure 2.5(b) shows the fraction of DNA damage for different concentrations of DNA in a sample irradiated within 15 s at a distance of 2.5 cm and a flow rate of 2 slm. The total degradation of DNA, including SSBs and DSBs, decreased by 30% (from 87% to 57%) when the concentration was tripled (from 3.33 to 10 $\text{ng}/\mu\text{L}$). Under

similar conditions of plasma irradiation (e.g., voltage applied, flow rate), the amount of reactive species delivered to the sample may be considered constant.

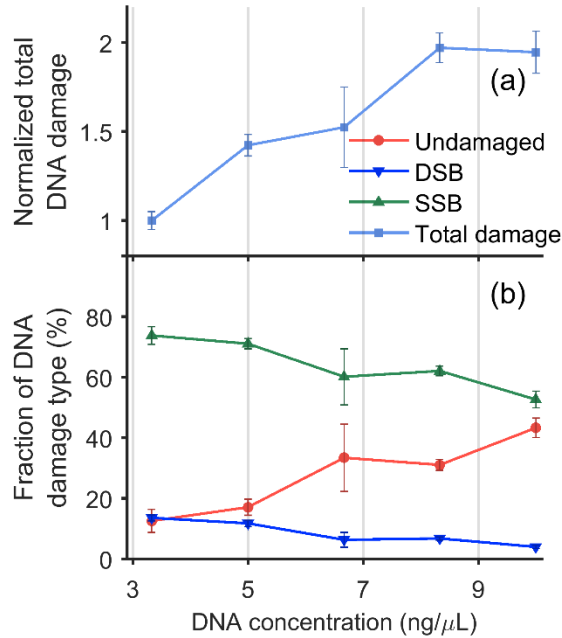


Figure 2.5: (a) Total damage to DNA normalized to the initial amount of damaged DNA molecules in a sample with a concentration of $3.33 \text{ ng}/\mu\text{L}$. (b) Fractions of SSBs, DSBs, and undamaged DNA induced by the APPJ in samples with various DNA concentrations at helium flow rate of 2 slm, distance of 2.5 cm below the orifice, voltage of 10.6 kV, and the duration of plasma irradiation of 15 s.

Therefore, a number of events at which plasma species interacted with DNA molecules increased with higher DNA concentrations in the sample, as shown in Figure 2.5(a). This figure shows the total damage to DNA, including both SSBs and DSBs, normalized to the initial amount of damaged DNA molecules in a sample with a concentration of $3.33 \text{ ng}/\mu\text{L}$. Initially, there was a linear correlation between the total damage and DNA concentration, but at the doubled concentration the saturation was achieved. At higher concentrations, DNA itself may act as a radioprotector [52] or create

physical shielding, reducing the accessibility of free radicals to other DNA molecules. In addition, the formation of DSBs increased as DNA concentration decreased (Figure 2.5(b)), suggesting that more than one event (i.e., the number of plasma species interacting with DNA) induced this type of damage.

A previous study using a plasma source similar to in this work reported that discharge current, energy transferred to gas, bullet velocity, and the number of the main reactive species in the jet (e.g., N_2 , N_2^+ , OH^* , O) increased with an increase in the voltage [53]. Therefore, the voltage applied could also influence the yield of DNA damage. To confirm this hypothesis, we measured average plasma power and DNA damage as a function of voltages in the range of 10.0 – 10.8 kV, at which the APPJ could be ignited and was relatively stable. The power of the plasma increased slightly with an increase in voltage applied, which is shown in Figure 2.6(a). This indicates that the average plasma power can be controlled by adjusting the voltage. In addition, we observed that the total DNA damage was almost constant for voltages from 10 to 10.2 kV, and increased about 10% due to the SSB formation when the voltage increased from 10.4 to 10.8 kV. The variation in the yields of DNA damage at various voltages is shown in Figure 2.6(b). It is interesting to note here that the jet length (Figure 2.2(c)) and the total DNA damage (Figure 2.4(b)) increased rapidly with an increase in flow rate from 1 to 4 slm; however, the average plasma power decreased from 0.37 to 0.30 W (Figure 2.4(a)) over the same range. Moreover, the average plasma power, jet length, and total DNA damage increased approximately 30%, 10%, and 10%, respectively, when the voltage increased from 10.0 to 10.8 kV. These increments were nominal in comparison to the effects observed at higher flow rates.

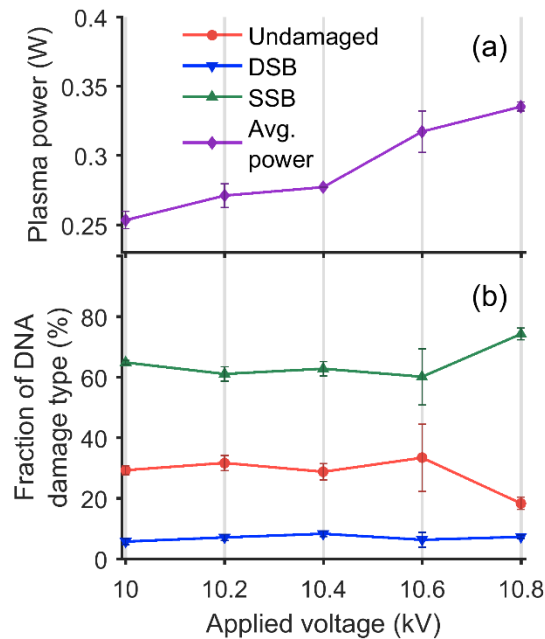


Figure 2.6: (a) Average plasma power at various voltages applied at a helium flow rate of 2 slm. (b) Fractions of SSBs, DSBs, and undamaged DNA induced by the APPJ within 15 s of irradiation at helium flow rate of 2 slm and distance of 2.5 cm below the orifice for various voltages applied in samples with DNA concentration of 6.67 ng/ μ L.

From these observations, I concluded that the average plasma power in the range of voltages applied in my experiment had a minor influence on the total DNA damage, but the jet length was correlated positively with those levels of damage. Because the plasma jet contains biologically reactive species [5], [8] that play key roles in DNA damage [35], [37], [50], I suggest that the spatial distribution of reactive species in a visible portion of plasma, which can be varied by changing the flow rate, is crucial in determining the total DNA damage. This conclusion is supported further by the yields of

DNA damage as a function of distance between the orifice and sample (Figure 2.4(d)), which demonstrated a higher level of DNA damage near the orifice.

2.4 Conclusions

A helium APP source with a dielectric capillary and two tubular electrodes was characterized by monitoring the current and voltage waveforms. The plasma source was used to induce strand breaks in aqueous plasmid DNA. I quantified the fractions of SSBs and DSBs in DNA induced by plasma irradiation, and assessed its correlation with flow rate, voltage applied, and sample concentration. An increase in flow rate increased the jet length, resulting in a large increase in DNA damage. The damage in the DNA was significantly higher when the sample was in contact with the visible plasma region. Moreover, the increase in jet length may have induced changes in the distribution of plasma species in the visible plasma region, and increased the number of these species delivered to the sample, which may eventually induce more DNA damage. This has importance for biological systems, in which DNA damage causes abnormal functioning of cells or cell death [34], [35]. In contrast to the observed high levels of DNA damage at higher flow rates, increases in voltage caused only a slight increase in jet length, and resulted in a nominal increase in DNA damage. In addition, in a sample with a lower DNA concentration, the number of plasma species interactions with DNA molecules was much higher, which led to greater damage. It has been reported previously that plasma reactive species, such as neutral radicals, contribute most to the damage in DNA molecules [38]. To acquire a detailed understanding of the mechanism of strand breaks in aqueous DNA samples due to plasma irradiation, further investigation of the species

generated in a liquid environment is required. More importantly, a way to control and tune these species in the plasma jet is needed to achieve the effects desired, not only in DNA, but also in other biological systems.

CHAPTER 3: PLASMA INTERACTIONS WITH AIR COMPONENTS²

3.1 Introduction

Atmospheric pressure plasma sources have captured the attention of many researchers because of their potential use in clinical medicine, such as wound healing, blood coagulation, dermatology, and cancer treatment [5], [54]–[57]. Although the preliminary results for the potential use of these sources in clinical medicine are highly encouraging [58], a detailed understanding of the potential clinical applications has yet to be achieved. To understand the clinical potential of plasma better, the biological effects of plasma in preclinical models have been investigated at the cellular [55] and molecular [5] levels. These studies have revealed that DNA is highly susceptible to the plasma components and any alteration in DNA can cause the cells to function abnormally or die. Thus, it is essential to study DNA's response to the plasma components to explore the mechanism of their interactions with a cellular system. To investigate the interactions

² The results in this Chapter are published in the following peer-reviewed journal.

E. R. Adhikari, V. Samara, and S. Ptasinska, "Influence of O₂ or H₂O in a plasma jet and its environment on plasma electrical and biochemical performances," *J. Phys. D: Appl. Phys.*, vol. 51, no. 18, p. 185202, 2018.

between plasma components and DNA molecules, several studies have been performed using various types of plasma sources and different types of feed gases. In addition, some previous studies also have reported that the amount and distribution of plasma species (e.g., N_2 , N_2^+ , OH^* , O) changed when oxygen or water vapor was added to the plasma jet [59]–[64], while other studies have demonstrated that atmospheric pressure plasma sources that have a fraction of oxygen or water vapor in the feed gas result in more DNA damage [36], [41], bacteria inactivation [59], [65], [66], sterilization [67], [68], and induction of apoptosis in cancer cells [21], [69]. Further, some studies [70]–[73] have been performed using a shielding gas (gas curtain) around the plasma jet, and reported that shielding gas could be used to control the reactive species in the plasma jet. Among the various plasma species, reactive oxygen species (ROS) play a crucial role in increasing the level of DNA damage [35], [37], [50]. Interestingly, the addition of a moderate amount of oxygen or water vapor to the feed gas and plasma jet environment may increase ROS production in the plasma [62]. Previous studies have provided abundant information that has been summarized in review papers [5], [74], [75], and an excellent attempt has been made to establish a correlation between variables in APPJ sources and DNA damage. However, those experiments were performed at different places around the globe, where the temperature, humidity, ambient pressure, and feed gas impurity vary. Thus, it is difficult to reproduce and compare their results. To investigate the influence of air components on plasma effectiveness systematically, I performed two types of experiments while APPJ was inserted in a glass chamber. In one, the feed gas varied, while the plasma jet environment was kept constant (i.e., fixed jet environment

and varied feed gas), and in the other, the plasma jet environment varied while the feed gas remained constant (i.e., fixed feed gas and varied jet environment).

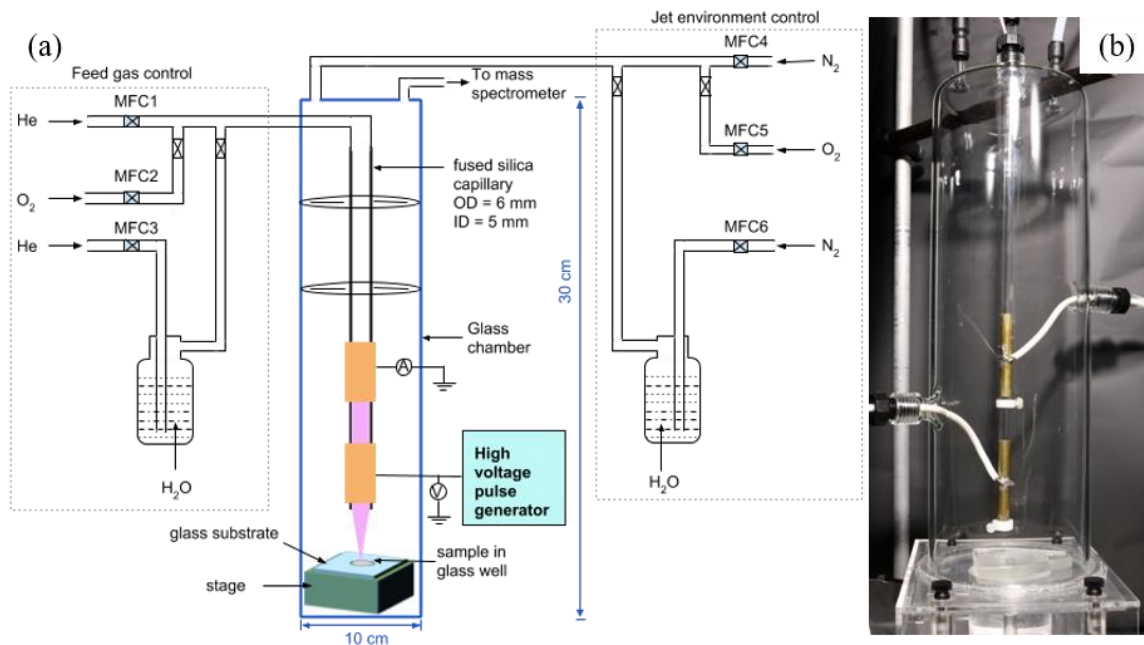


Figure 3.1: (a) Schematic diagram and (b) photograph of the experimental setup.

This research focused on studying the interactions between the APPJ and DNA in a controlled environment. The goal of the study overall was to determine the correlation between the fraction of oxygen or water vapor in the plasma jet environment as well as in the feed gas and DNA damage level. I selected DNA molecules for this study not only because of their biological importance, but also because they can be used as a molecular probe to detect changes in the physical and chemical properties of the APPJ. As previous work has shown, the plasma components can induce damage in DNA [38], and it already has been used successfully as a detector to identify the jet boundary of the plasma [42]. Therefore, DNA molecules can provide information about the APPJ that may lead to the

development of a method to compare various plasma jets. Similar methods are used already in radiation chemistry, in which other biomolecular compounds, e.g., alanine is the molecule used most commonly [76]–[78], are dosimeters for ionizing radiation.

In addition, I performed mass spectrometric analysis of the relative changes in the intensities of gas phase compounds attributable to changes in both experiments, i.e., fixed jet environment and varied feed gas, and fixed feed gas and varied jet environment.

3.2 Experimental setup and methods

A helium APPJ similar to that used in references [34], [45], [79] was enclosed in a cylindrical glass chamber with a diameter of 10 cm and a height of 30 cm; a schematic is shown in Figure 3.1. The plasma was ignited using a square pulse of 8 kV with a frequency of 500 Hz and a 50% duty cycle (to maintain plasma discharges, which occur only at rising and falling edges, in a fixed interval) generated by a homemade high voltage (HV) pulse waveform generator based on a MOSFET switcher by Behlke (HTS 151-03-GSM, Behlke Power Electronics GmbH, Kronberg, Germany). A high-voltage probe (P6015A, Tektronix, Inc., Beaverton, OR, USA) and an induction coil (Pearson Current Monitor Model 2877, Pearson Electronics, Inc., Palo Alto, CA, USA) were used to monitor the voltage and plasma current applied, respectively. The amplitude, together with the shape of the waveforms of voltage and current, were recorded using a digital oscilloscope (NI USB-5133, National Instruments, Austin, TX, USA). The flow rates and fractions of gases in the chamber and a fused silica capillary were controlled separately using different mass flow controllers (MFCs). The flow rates of oxygen and nitrogen were adjusted using two identical flow controllers, MFC4 and MFC5 (MV-304,

Bronkhorst High-Tech B.V., Ruurlo, The Netherlands), and the helium flow through the capillary was adjusted using another flow controller MFC1 (MV-394-He, Bronkhorst High-Tech B.V., Ruurlo, The Netherlands). The experiment was performed under the following two working conditions.

3.2.1 Fixed jet environment and varied feed gas

The flow rate of pure nitrogen (NI UHP300, Airgas Inc., Radnor, PA, USA) to the chamber was maintained at 5 slm using MFC4, while MFC5 and MFC6 (MV-304, Bronkhorst High-Tech B.V., Ruurlo, The Netherlands) were closed throughout the experiment. The total helium (HE UHP300, Airgas Inc., Radnor, PA, USA) flow rate in the capillary was maintained at 4 slm using MFC1. Initially, the fraction of oxygen (OX UHP300, Airgas Inc., Radnor, PA, USA) in the feed gas was varied from 0 to 10 standard cubic centimeter per minute (sccm) using MFC2 (MC-10SCCM-D/5M, Alicat Scientific, Inc., Tucson, AZ, USA) and keeping MFC3 closed. In the other experiment, MFC2 was closed, and the amount of humidity desired in the feed gas was maintained by passing a fraction of helium gas through the water bottle. The small flow of helium through the water bottle was controlled using another flow controller, MFC3 (Mass Flow Controllers, MKS Instruments, Andover, MA, USA) that was powered and adjusted by a Type 247 4 channel readout (MKS Instruments, Andover, MA, USA).

3.2.2 Fixed feed gas and varied jet environment

The flow rate of pure helium in the capillary was maintained at 4 slm using MFC1, while MFC2 and MFC3 were closed throughout the experiment. Initially, MFC6 was closed, and the total flow rate of nitrogen and oxygen in the chamber was maintained

at 5 slm by adjusting MFC4 and MFC5. The fraction of the oxygen in the chamber varied from 0% to 56%, which was the maximum fraction of oxygen that could be achieved for my experimental setup because of the presence of the helium APPJ in the chamber. In the other experiment, MCF5 was closed, and the amount of humidity desired in the chamber was maintained by passing a fraction of nitrogen through the water bottle. The flow rate of nitrogen through the water bottle was controlled using another flow controller, MFC6. The maximum humidity that can be achieved in the chamber using my experimental setup was 61% because of the flow of helium into the APPJ chamber. The humidity in the feed gas, as well as in the chamber, was monitored by a humidity sensor (HDC1000EVM, Texas Instruments Inc., Dallas, TX, USA).

The samples were prepared as in these previous works [34], [79]. Briefly, pUC18 plasmid DNA (ThermoFisher Scientific, Waltham, MA, USA) with 2686 base pairs was diluted to a concentration of 6.67 ng/uL, and 30 μ L of the sample was placed in a glass well with a diameter of 4.1 mm and depth of 2.8 mm. The glass substrate was inserted in the chamber 16 mm below the nozzle, to assure the direct contact of the APPJ with a DNA sample. The plasma length in the open atmosphere was investigated previously [79] and was about 70 mm for the flow rate of 4 slm in an open atmosphere. The glass substrate was kept for 120 s to fill the chamber completely with the fraction of gases desired before the plasma was ignited. The sample was irradiated for 15 s, and the irradiated sample was collected with a pipette. The glass well was rinsed three times with 5 μ L PBS (Phosphate Buffered Saline) to collect the remaining DNA. I used gel electrophoresis to quantify the DNA damage induced by plasma irradiation; the details of the method are provided in [34]. All data points in this work represent the mean of at

least three trials under the same experimental conditions, and the error bars represent the standard deviations.

First, several control samples were prepared to monitor the effects of external factors on plasmid DNA (e.g., sample handling, gas flow), as explained in previous works [34], [79]. Briefly, stock control was used from DNA stock solution, and the substrate control was prepared by placing the sample on the substrate in the chamber for 135 s, and was collected from the well without irradiation. The flow control was prepared similarly as a substrate control sample in the chamber together with the feeding gas treatment for 135 s, after which it was collected from the well. The DNA in all control samples showed less than 5% damage. Then, the sample was irradiated with helium APPJ in which the chamber was filled with pure nitrogen. I found that approximately 30% of the DNA molecules were transformed into SSB and DSB within the 15 s of irradiation. It is interesting to note that more than 90% of the damaged DNA experienced SSBs, while only less than 10% experienced DSBs. These results were similar to those in other studies that have used a helium APPJ [34], [38], [79] and an APPJ with a small amount of oxygen in the helium [35], [36]. To confirm that there was direct contact between a visible portion of the plasma jet and the sample, several photographs were taken with digital camera of each irradiated sample during irradiation shown in Appendix B (Figures A.1 and A.2). As 30% of the DNA sample experienced damage within 15 s of plasma irradiation under these experimental conditions, all other samples were irradiated within this time to observe any influence on DNA damage attributable to the addition of a fraction of oxygen or water vapor, either in the plasma jet environment or the feed gas.

To analyze the gas composition in the chamber, I used a VetaSpec MBx mass spectrometer (Extrel CMS, LLC, Pittsburgh, PA, USA) which had an inlet connected to the chamber. VetaSpec MBx is a quadrupole mass spectrometer (QMS) with a three-stage discrete pumping system. The pressure at the inlet was ~ 0.5 mbar, and the vacuum chamber had a base pressure of $\sim 10^{-8}$ mbar. Ionization occurred via the internal QMS filament with a fixed electron energy of 70 eV. Other research groups [80]–[82] have used a similar technique to measure neutral species, and positive and negative ions that originate in APPJs.

3.3 Results and discussion

3.3.1 APPJ current, voltage, and power

High voltage square pulses were applied to ignite the plasma, as shown in Figure 3.2(a). Figure 3.2(b) represents a typical current waveform for the rising and falling edges of the voltage pulse applied. Current waveforms for a given voltage with various fractions of oxygen and water vapor in the chamber and the feed gas are shown in Figure 3.3. I noticed that there was a significant change in the intensities and phases of current waveforms when a fraction of oxygen (Figure 3.3(c)) or water vapor (Figure 3.3(d)) was introduced to the feed gas, but there was only a minor change in the current waveforms when a fraction of oxygen (Figure 3.3(a)) or water vapor (Figure 3.3(b)) was introduced to the chamber filled with nitrogen. This indicated that the ignition process of plasma depends significantly on the feed gas. Further, the intensities and phases of the current waveforms depended strongly on the fraction of oxygen and water vapor in the feed gas.

With an increase in the fraction of oxygen or water vapor in the feed gas, the current intensity increased first, attaining a maximum value of 90 mA for 0.125% of oxygen and 102 mA for 3% of humidity. A further increase in the fraction of gases added quenched the current intensities, while in both cases, the phases of the waveforms shifted toward zero as more gases were added to the APPJ.

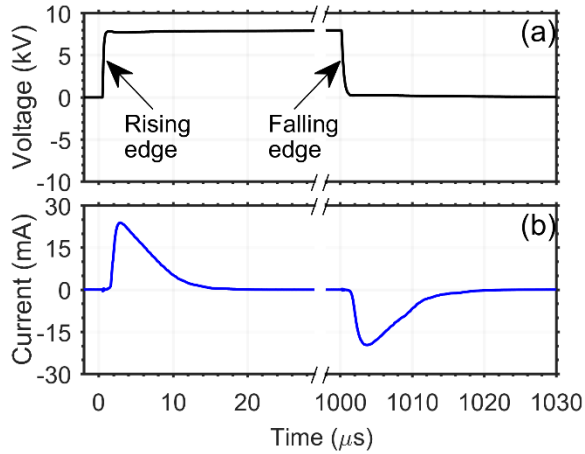


Figure 3.2: (a) Voltage waveform for a voltage of 8 kV and frequency of 500 Hz (b) Current waveform for 4 slm helium in a capillary and 5 slm nitrogen in the chamber at the voltage shown in (a).

Three major factors, feed gas temperature, ionizing energy, and electronegativity of gas molecules, affected the shape of a current waveform, but ionizing energy and electronegativity were two competing factors. After an excessive number of oxygen or water molecules was added to the feed gas, the collision between electrons and oxygen or water molecules increased the average temperature of the feed gas slightly. This increase resulted in a decrease in the density of the gas, which increased the reduced electric field further. That increase in the reduced electric field caused acceleration of electrons that affected the phase and current intensity. The effect of feed gas temperature on the phase

and the current intensity is explained in Appendix B (Figure A.3). Because the ionization energies of both oxygen (12.07 eV) and water (12.65 eV) molecules are lower than that of the helium (24.59 eV) atom [83], the electron avalanche occurs earlier when there is a small fraction of oxygen or water vapor in the feed gas than in the case of pure helium. Further, both oxygen and water molecules are electronegative molecules, and both have a significant electron attachment cross-section in the low electron energy range with a maximum at 6-9 eV [84]. If there is an excessive number of oxygen and water molecules in the feed gas, some electrons are captured by oxygen and water molecules from the plasma, which results in the decrease in current intensity. This indicates that there is a significant change in the plasma core attributable to the addition of oxygen or water vapor in the feed gas, while there is only a minor change in the plasma core attributable to the addition of oxygen or water vapor in the jet environment. The addition of a fraction of oxygen or water vapor may change the chemistry in the plasma core and hence, influence the production of reactive species in the plasma core region. In a previous study, Nikiforov et al. [61] used an AC discharged argon APPJ with a fraction of water vapor and reported that the maximum emission of OH^{*} in the plasma jet was observed when the water content in the argon was 350 ppm. Another study that used a helium μ -APPJ reported that the largest amount of OH^{*} and O was observed in the jet with 6000 ppm water vapor in the feed gas [64], and Winter et al. [63] reported that the density of H₂O₂ and OH^{*} in the plasma jet depended on the feed gas humidity level. This indicates that there is a significant change in the amount of ROS in the plasma jet after oxygen or water vapor is added to the feed gas. Some studies [70]–[73] that used shielding gas

around the plasma jet have reported that reactive oxygen and nitrogen species can be tuned in the plasma jet using various mixtures of gases as a shielding gas.

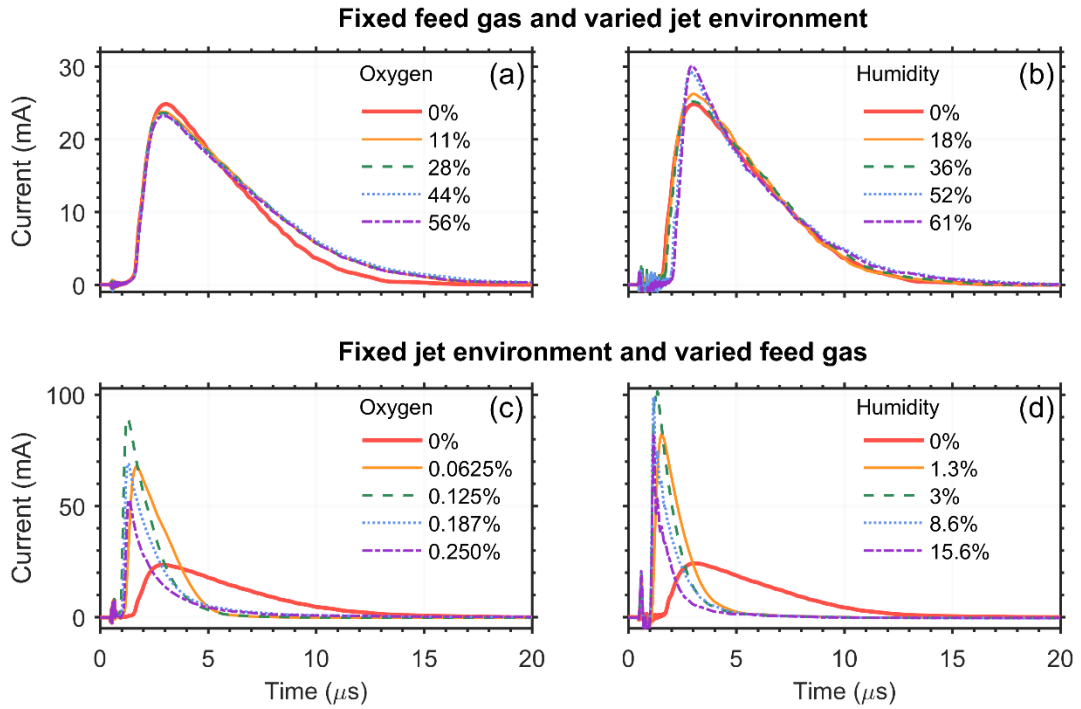


Figure 3.3: Plasma current waveforms for various fractions of (a) oxygen and (b) water vapor in the fixed feed gas and varied jet environment, and (c) oxygen and (d) water vapor in the fixed jet environment and varied feed gas experimental conditions for the rising edge of the voltage applied in Figure 3.2(a).

It is important to stress that addition of gas to the feed gas or changes in the environment affect chemical composition of plasma species, as well as electrical properties, e.g., discharge mode. Two recent review papers summarize the current knowledge on discharge mode, propagation of plasma in the gas flow, formation of reactive species in the plasma, interaction of plasma species with liquid media, and biological materials for various types of atmospheric pressure plasmas [6], [85]. However, these studies have not characterized the APPJ using a molecular probe (e.g.,

DNA) after adding oxygen or water vapor to the APPJ environment. Using mass spectrometry, a qualitative comparison of the production of reactive species in the plasma jet environment for different conditions will be discussed on the basis of both the level of damage induced in aqueous DNA because of plasma irradiation and the production of ionic plasma species. Further, the instantaneous power for the conditions presented in Figure 3.3 was calculated by multiplying the voltage and current, and the average deflected power of the plasma was calculated by averaging the instantaneous power over a cycle using Equation 2.1 (Chapter 2). As the intensities and phases of the current waveforms change when a fraction of oxygen or water vapor is added to the feed gas, the average power decreased significantly with an increase in the fraction of oxygen (Figures 3.3(d) and 3.4(d)) or water vapor (Figures. 3.3(c) and 3.4(c)). There was a minor change in the intensities and phases of the current waveforms with an increase in the fractions of oxygen or water vapor in the jet environment, and hence, the average power remained constant, as shown in Figures 3.3(b) and 3.4(b), and Figures 3.3(a) and 3.4(a).

3.3.2 DNA damage

In the experiment with a fixed jet environment and varied feed gas, the chamber was filled with pure nitrogen gas and the plasma was ignited with a mixture of helium in which the fraction of oxygen or water vapor varied. The level of DNA damage in the sample measured after the plasma irradiation is shown in Figures. 3.4(d) and 3.4(c) as a function of the fraction of oxygen or water vapor in the feed gas, respectively. With a small amount of water vapor in the feed gas (up to 1.3% of humidity), it was observed

that the total DNA damage level increased from 30% to 45%. When humidity in the feed gas was higher than 1.3%, the total DNA damage level remained constant.

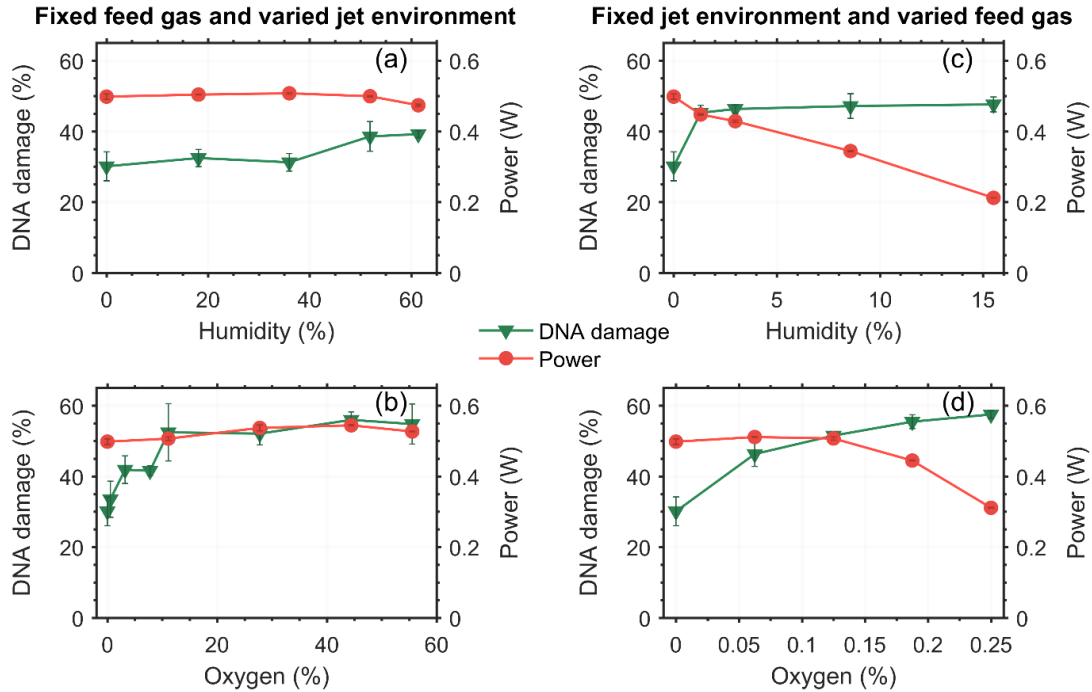


Figure 3.4: Fractions of total damaged DNA (green triangles) in the sample after 15 s of plasma irradiation and plasma power (red circles) for the various fractions of (a) water vapor and (b) oxygen in the fixed feed gas and varied jet environment, and (c) water vapor and (d) oxygen in the fixed jet environment and varied feed gas experimental conditions.

The result was similar when a fraction of oxygen was added to the feed gas, in that the total DNA damage level increased from 30% to 46% when a small fraction of oxygen (0.062% of oxygen in the total flow) was added and increased further, from 46% to 57%, when the amount of oxygen in the feed gas increased from 0.062% to 0.25%. Despite the relatively constant DNA damage for greater amounts of water vapor and oxygen in the feed gas, it is important to note that the plasma power decreased under

these conditions. Although it was not surprising to find a decreased plasma power, as I described in Section 3.1, it was very surprising that there still was a very high percentage of damaged DNA. If I compare the initial level of DNA damage by the pure helium APPJ, which was 30% at a power of 0.5 W, to that when the maximum amount of water (16%) or oxygen (0.25%) was added to the feed gas, the power decreased more than twice, but the DNA damage level increased to 50%. This finding indicates the importance of characterizing APPJ, not only from the point of view of its electrical properties, as many works have reported the plasma current or power, but of its chemical characteristics. Moreover, it also stresses the need to develop chemical dosimeters to compare different APPJ sources better to standardize their effectiveness in medical applications. As mentioned before, DNA can be a good indicator of chemical changes in the APPJ as it is susceptible to a variety of plasma species [38].

In the experiment with fixed feed gas and varied jet environment, plasma was ignited with pure helium gas and the chamber was filled with various fractions of oxygen or water vapor. There was a minor change in the total DNA damage level, from 30% to 38%, when the humidity in the chamber was increased from 0% to 61% Figure 3.4(a). Under these conditions, the plasma power remained nearly constant, indicating that the water environment had a negligible influence on the electrical characteristics of the plasma core. However, I observed a slight influence of water on the chemistry of APPJ; specifically, I can expect that reactive species will form at the plasma jet boundary. Similarly, I detected no changes in the plasma power in the case of the oxygen admixture, while there was a significant increase in the total DNA damage level, from 30% to 52%, when the amount of oxygen in the chamber increased from 0% to 11%. The total DNA

damage level remained nearly constant with further increases in the oxygen content in the chamber, up to 56% (Figure 3.4(b)). These results again indicated that changes in electrical characteristics can be decoupled from changes in the chemical properties of APPJ induced by adding a fraction of oxygen or water vapor to the plasma jet environment as well as to the feed gas, particularly, in the latter case, in which no changes in plasma power were found, while in the former case, I saw an inverse correlation in which the power decreased when oxygen or water was added, while the DNA damage level increased simultaneously.

This higher level of DNA damage indicates that there might be an increase in the ROS level in the plasma after oxygen or water vapor is added to the feed gas, as well as to the jet environment, as ROS play a crucial role in inducing DNA damage [35], [37], [50]. Some investigations have reported the effects of adding oxygen or water vapor to the feed gas. For example, Gorbanev et al. [62] studied the generation of ROS (e.g., OH[•], O₂^{•-}, O₃, H₂O₂) in plasma-treated liquid samples. They reported that the concentration of H₂O₂ increased in the plasma with an increase in feed gas humidity, in which the OH[•] radical could come either from the humidity in the jet environment or the feed gas, and a small amount of O₃/¹O₂/O can form from water molecules, but the bulk of them would come from molecular oxygen added to the feed gas. Recent work by Yan et al. [86] investigated effects of plasma-stimulated solutions on cancer cells, particularly cell-dependent response due to reactive oxygen species in the specific H₂O₂-containing environment. Yue et al. [73] used three methods of adding O₂ to increase the O atom concentration in an APPJ. Their results showed a significant increase in the O concentration, attaining a maximum at 1.5% of O₂ added to the feed gas. This situation

corresponds to my case in which I fixed the jet environment and varied O₂ percentage in the feed gas. My results also showed an increase in the DNA damage level, which could correlate to the increase of O in the APPJ. It is interesting to notice that in the 0% to 0.25% range of added O₂ to the feed gas, I observed a twice higher increase in the DNA damage level, whereas the concentration of O in Yue et al.'s study increased about 10 times in the same range. This smaller increase in DNA damage can suggest possible interactions of atomic O with the water in which DNA was diluted. Moreover, when O₂ was used as a shielding gas, which in my study, can correspond to the case of the fixed feed gas and varied jet environment, Yue et al. [73] reported no significant effect on the O concentration. However, the authors stressed the fact that their studies focused on detection of atomic O only, and other reactive species, such as OH, can be also formed. This could likewise be in my case, because when I add O₂ to the environment, I observed the increase in DNA damage level. Therefore, by comparing the trends in changes of O concentration and DNA damage as a function of O₂ percentage in the environment, most likely, other reactive species rather than atomic O contribute to DNA damage. Therefore, I suggest that the higher level of DNA damage observed in my experiments is attributable to the formation of additional ROS in the plasma after oxygen or water vapor is added to the feed gas and the plasma jet environment. As I observed in the plasma current, there was a significant change in the plasma core when a fraction of oxygen or water vapor was added to the feed gas, which may induce the production of more reactive species in the APPJ. Some of these might be short-lived, but some may have a sufficiently long life that allows them to reach the sample, and hence, increase the DNA damage level, while

adding oxygen or water vapor to the jet environment may produce more reactive species in the APPJ boundary without affecting the plasma core.

3.3.3 Mass spectrometry

To analyze the possible changes in chemical species formed in both experiments, i.e., fixed feed gas and varied jet environment, or fixed jet environment and varied feed gas, I used a mass spectrometer in which the gas inlet was attached to the glass chamber as shown in Figure 3.1. The mass spectra were recorded for the following conditions: when the maximum amount of water (16% humidity) or oxygen (0.25%) was added to the feed gas and when 56% of oxygen or 62% of humidity was added to the jet environment. These spectra are presented in Figures 3.5 and 3.6.

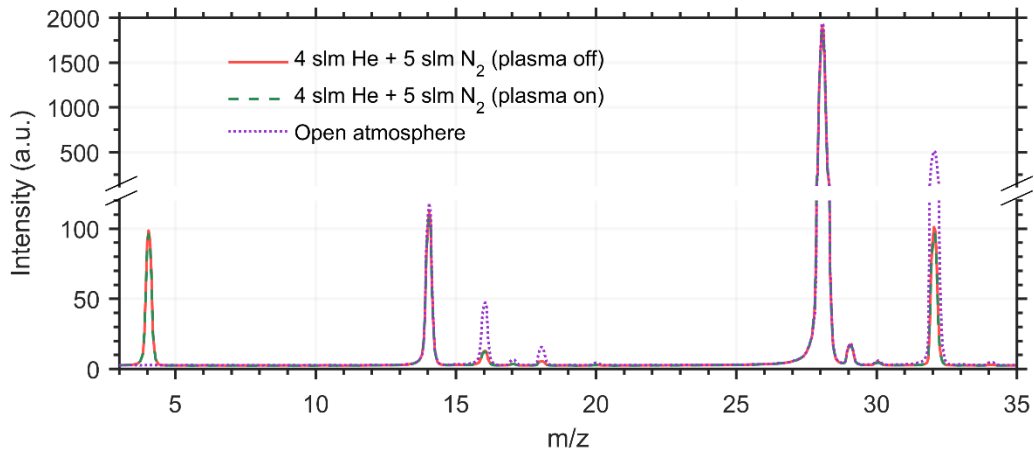


Figure 3.5: Mass spectra for plasma on and off when the pure helium was used as a feed gas and the chamber was filled with pure nitrogen, and open atmosphere.

For comparison, the mass spectra for a pure helium APPJ launched to the chamber filled with pure nitrogen and that for an open atmosphere also are presented in Figure 3.5. The intensities of ionic species (m/z 32, 28, 18, 17, 16, 14, and 4, corresponding to O_2 , N_2 , H_2O , OH , O , N , and He , respectively) obtained from integrating areas under the mass peaks in these spectra for plasma on (in which the APPJ was ignited) and plasma off (in which gas composition of the environment and feed gas were fixed, but without plasma ignition) are listed in Table 3.1.

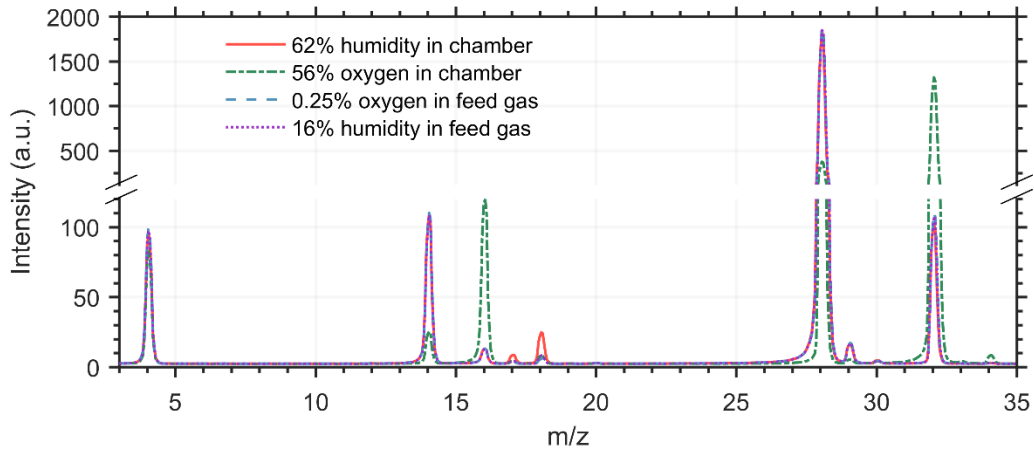


Figure 3.6: Mass spectra for the experimental conditions mentioned in the section 3.2 of the main text at the maximum content of oxygen or water vapor when the plasma was ignited.

First, I compared the intensities of ionic species with plasma on and off, which showed lower intensities ($\sim 2\%$) of N_2 and He in the former case, indicating that these gas components were consumed during plasma ignition in all experimental conditions. Similarly, lower intensities were observed for all other species present with 62% humidity and pure N_2 when the plasma was on. However, I observed an $\sim 8\%$ increase (16% humidity in the feed gas) and 40% (56% oxygen in the chamber) in the intensities

of both m/z 18 and m/z 17 in comparison to those with plasma off. Next, I compared the intensities of mass peaks for different conditions when the plasma was on. For example, in the case of 62% humidity in the chamber, I observed increases for m/z 18, 17, 32, 16, and 14, which were expected because water was added to the chamber. This increase correlated with an increase in DNA damage, as shown in Figure 3.4(a). Interestingly, m/z 14 increased, indicating that more nitrogen atomic species were preserved, which also may be a species that contributed to DNA damage. Intensities for m/z 28 and 4 dropped slightly, and I also observed a slight decrease in plasma power under these conditions (Figure 3.4(a)) in comparison to plasma launched in pure N_2 . Under other conditions, the introduction of H_2O or O_2 to the APPJ or to the chamber was accompanied by an increase in species coming from both gases, which thus caused more DNA damage, as well as a simultaneous decrease in N_2 , and He or N species, the main components necessary to sustain APPJ, thus indicating a power decrease.

TABLE 3.1:

AREA UNDER THE MASS PEAKS FOR THE EXPERIMENTAL CONDITIONS MENTIONED IN SECTION 3.2 WITH THE
MAXIMUM CONTENT OF OXYGEN OR WATER VAPOR

m/z	Area under mass peaks (intensity \times mass)									
	Fixed jet environment and varied feed gas						Fixed feed gas and varied jet environment			
	pure helium (plasma on)	pure helium (plasma off)	15.6% humidity (plasma on)	15.6% humidity (plasma off)	0.25% oxygen (plasma on)	0.25% oxygen (plasma off)	62% humidity (plasma on)	62% humidity (plasma off)	56% oxygen (plasma on)	56% oxygen (plasma off)
32	25.3	26.3	27.5	28.0	28.3	29.1	26.6	27.5	342.6	344.6
28	491.5	501.4	485.3	488.6	477.4	486.3	481.5	491.4	96.3	99.8
18	0.8	0.7	1.5	1.4	0.9	0.9	5.7	6.0	1.4	1.0
17	0.2	0.2	0.4	0.4	0.2	0.3	1.6	1.7	0.4	0.3
16	2.9	3.1	2.7	2.7	2.8	2.9	3.2	3.4	32.5	32.5
14	27.9	28.6	27.2	27.7	26.8	26.8	28.1	28.5	6.0	6.2
4	23.3	23.8	23.4	23.6	23.9	24.5	23.0	23.5	19.8	20.6

3.4 Conclusions

A stable environment around the plasma jet was maintained, and the effect on DNA damage level of various fractions of oxygen or water vapor in the plasma jet environment was observed. When a fraction of oxygen or water vapor was added to the jet environment, plasma components—specifically electrons and UV light—coming from the plasma core interacted with oxygen and water vapor in the plasma jet environment and may have produced additional ROS that increased the DNA damage level. The addition of a fraction of oxygen or water vapor in the feed gas also increased DNA damage. Reactive species with a sufficiently long lifetime that formed in the plasma core reached the sample and increased the level of DNA damage. When the fraction of oxygen or water vapor in the feed gas increased, DNA damage increased significantly initially, but there was only a minor increase in the damage level with further increases in oxygen or water vapor in the feed gas. From these observations, it is clear that reactive species that contribute to induce damage in DNA form in the plasma core as well as in the plasma jet. The production of these reactive species depends on the plasma jet environment as well as that of the feed gas. Further, the addition of oxygen or water vapor in the feed gas changed the phases and intensities of the plasma current significantly and also resulted in decreased plasma power. However, the power remained constant when oxygen or water vapor was added to the plasma jet environment. This indicates that there is no positive correlation between the plasma power and DNA damage level attributable to adding oxygen or water vapor to the plasma jet environment and feed gas. Thus, it is essential to characterize an APPJ from the point of view of

chemical, rather than electrical, properties. Moreover, the analysis of areas under the mass peaks in mass spectra showed that introducing water vapor to the chamber increased the intensities of molecular oxygen, water, hydroxyl radicals, atomic oxygen, and atomic nitrogen, while adding oxygen increased the intensities of molecular oxygen, hydroxyl radicals, and atomic oxygen. Further, adding oxygen or water vapor to the feed gas increased the intensities of molecular oxygen, water, and hydroxyl radicals, and there was a correlation between the increased intensities of ionic species and the level of DNA damage. Hence, an optimal level of oxygen or water vapor in the APPJ is necessary to optimize plasma performance in clinical applications. A quantitative measure of DNA damage level attributable to various APPJs under similar experimental conditions could be a parameter used to optimize the performance of APPJs in biological systems. A systematic method to quantify the reactive species formed in the plasma core, jet, and the plasma-liquid interface is required to make conclusive comparisons between various APPJ sources.

CHAPTER 4: IN SITU CHARACTERIZATION OF AN APPJ³

4.1 Introduction

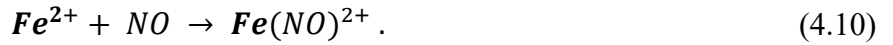
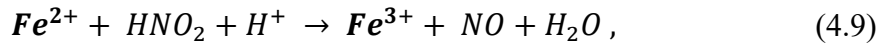
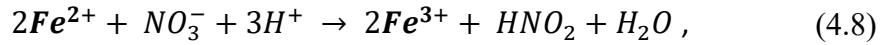
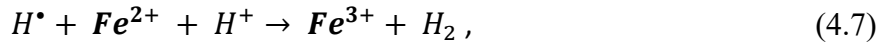
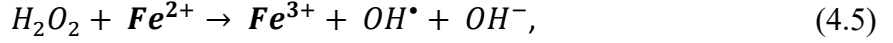
The potential to use atmospheric pressure plasma jets (APPJs) in clinical applications, such as wound healing, sterilization, blood coagulation, dentistry, and cancer treatment, is rapidly growing [54], [57], [87]–[89]. Due to the complex natures of the processes and components of both living cells and plasma, a detailed description of the exact mechanisms of plasma interactions with cellular components remains quite challenging, although some essential reaction pathways have been proposed for specific cellular targets, such as DNA [5]. Most plasma biochemical effects have been investigated using post-exposure methods; for example, cell survival rates after plasma exposure [5], [54], [55] provide information about the final effects but no information on possible intermediate reaction steps. Knowledge of these steps is necessary for obtaining a comprehensive picture of processes initiated by plasma. Therefore, the detection of intermediate, short-lived reactive species induced by plasma, which can trigger a cascade

³ The results in this Chapter are published in the following peer-reviewed journal.

E. R. Adhikari, V. Samara, and S. Ptasinska, “Total yield of reactive species originating from an atmospheric pressure plasma jet in real time,” *Biol. Chem.*, vol. 400, no. 1, pp. 93–100, 2019.

of biochemical reactions, is important to identify and quantify. To date, many different experimental methods have been employed to determine the types and amounts of plasma reactive species formed in the biological target. The most common ones can be classified as chemical dosimetry, in which the concentration of radicals is measured after the exposure of a specific compound (e.g., dye, molecular beacon, or isolated DNA) to the plasma [63], [90]–[93]. Furthermore, it is necessary to develop a variety of *in situ* techniques to measure the reactive species delivered and formed in the target during plasma irradiation as opposed to any post-exposure techniques, which fail in the detection of intermediate, short-lived reactive species. One solution is to use real-time fluorescence/absorption spectroscopy of chemical dosimeters exposed to plasma. For example, in a previous study, [91], the authors used a fluorescence technique to quantify the amount of OH[•] formed in an aqueous solution due to low frequency APPJ interactions. In contrast to this previous work, in which the authors quantified only one plasma component, my study focuses on the investigation of the overall formation of plasma reactive species. I employed an acidified ferrous sulfate solution, which is commonly used as a chemical dosimeter (also called a Fricke solution or dosimeter) to measure the total yield of reactive species formed during plasma exposure. Briefly, Fricke dosimetry is based on the oxidation of ferrous (Fe²⁺) to ferric (Fe³⁺) ions [94]. The concentration of Fe³⁺ ions is obtained from UV absorption spectra at 296 nm. In general, the irradiation of the Fricke solution causes the oxidation of Fe²⁺ to Fe³⁺ through direct or intermediate pathways, some of the significant reactions are shown in reactions (4.1) to (4.10).





Among these reactions, reaction (4.7) is possible only in the absence of oxygen, so it can be neglected in an environment accessible to oxygen (i.e., open atmosphere) [95], [96]. Furthermore, the rates for reactions (4.8) to (4.10) are slow and are significant only at a relatively high concentration of sulfuric acid [97]. Although all plasma components are crucial in the plasma-liquid interface chemistry [98], it is important to note that none of the nitrogen reactive species are involved in reactions (4.1) to (4.6); therefore, the Fe^{3+} yield generated from the acidified Fe^{2+} solution measures only the total reactive oxygen species and electrons formed or delivered due to plasma exposure. Thus, I focused only on the collective measurement of these plasma reactive species, although reactive oxygen and nitrogen species are equally important in the clinical applications of APPJs. I measured the total yield of Fe^{3+} ions in real time, attributable to

the collective effects of plasma reactive species as a function of APPJ parameters (e.g., pulse voltage and frequency applied, helium flow rate, and treatment distance). In addition, the Fe^{3+} yields were compared to those obtained from calculations and to DNA damage levels under similar experimental conditions.

The objective of this work was to establish a correlation between the total Fe^{3+} yield and plasma jet variables using the Fricke solution. The long-term goal of this project is to contribute to quantitative estimates of the reactive species formed in and due to APPJs in real time.

4.2 Materials and methods

Figure 4.1 shows a schematic diagram of the experimental setup constructed and developed to measure the absorbance of the Fricke solution during plasma exposure. The APPJ source used in this research was a DC-pulsed dielectric barrier discharge in helium gas. The helium gas flowed through a cylindrical fused silica capillary, and voltage was applied to one of the cylindrical brass electrodes around the capillary. The details of the plasma source assembly and discharge processes were reported previously [99], [100]. Briefly, the plasma discharge was ignited using square pulses of 6 to 10 kV at frequencies of 0.25 to 5 kHz, and a 50% duty cycle was generated by a homemade HV pulse waveform generator based on a MOSFET switcher (HTS 151-03-GSM, Behlke Power Electronics GmbH, Kronberg, Germany). A high voltage probe (P6015A, Tektronix, Inc., Beaverton, OR, USA) and an induction coil (Pearson Current Monitor Model 2877, Pearson Electronics, Inc., Palo Alto, CA, USA) were used to monitor the voltage applied and the plasma current, respectively. The amplitude, as well as the shape of the

waveforms of the voltage and current, were recorded using a digital oscilloscope (NI USB-5133, National Instruments, Austin, TX, USA).

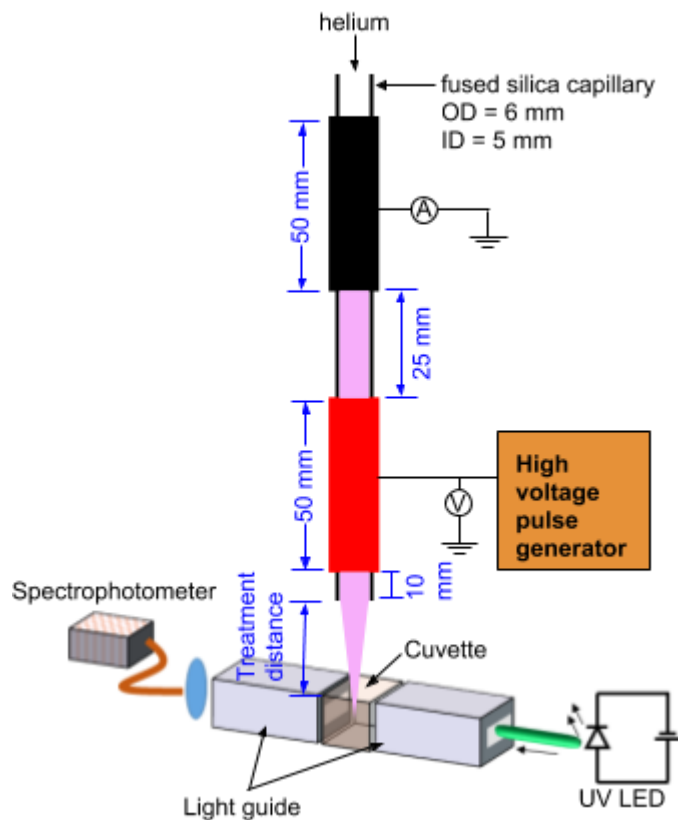


Figure 4.1: Schematic of the experimental setup.

The helium flow rate (HE UHP300, Airgas Inc., Radnor, PA, USA) in the capillary was monitored using a mass flow controller (MV-394-HE, Bronkhorst High-Tech B.V., Ruurlo, The Netherlands). The average plasma power increases at higher voltages. For example, it varies from about 0.5 to 1.5 W in the range of 6-12 V at a frequency of 1 kHz, and a flow rate of 2 slm. The light source was a UV LED (LED300W, Thorlabs, Inc., Newton, NJ, USA) with an emission maximum at 296 nm. First, the Fe^{3+} extinction coefficient was estimated using an acidified ferric sulfate

solution (ammonium iron (III) sulfate dodecahydrate from Sigma-Aldrich, St. Louis, MO, USA) in 0.4 M H₂SO₄ at 296 nm, which was measured to be 2132 mol L⁻¹ cm⁻¹. The extinction coefficient of the Fe²⁺ solution at 296 nm was approximately zero—that is, the absorption of Fe²⁺ at 296 nm was much lower than that of Fe³⁺ and, thus, could be neglected. To obtain a uniform solution, a magnetic stirrer (HI190M-1, Hanna Instruments, Woonsocket, RI, USA) was used throughout the experiment. The complete setup with the cuvette (10x10x10 mm³) was set on a magnetic stirrer, and a small magnet (2x2x5 mm³) was placed in the cuvette. The light transmitted through the sample was recorded by a spectrophotometer (HR4000, Ocean Optics, Inc., Largo, FL, USA). The light absorbed by the air along the optical path can inflate the sample's actual absorbance. To avoid such variations in the absorbance along the optical path caused by air mixing with the helium flow, it was necessary to shield the optical path from the flow (“light guides” in Figure 4.1). The LED, the spectrometer, and the magnetic stirrer were turned on at least 20 minutes before the actual measurement to warm up and stabilize. In the case of the *ex situ* study, I measured the absorbance of solutions using a spectrophotometer (Infiniti M200, Tecan Trading AG, Zurich, Switzerland).

A cuvette with an acidified ferrous sulfate solution (1 millimolar (mM) iron (II) sulfate heptahydrated from Sigma-Aldrich, St. Louis, MO, USA in 0.4 M H₂SO₄ (Fisher Scientific, Waltham, MA USA)), also known as Fricke solution, was positioned on a magnetic stirrer beneath the plasma jet, 10 mm from the outlet of the glass capillary, as shown in Figure 4.1. The Fe³⁺ concentration was estimated from the absorbance according to Beer-Lambert law:

$$A = \epsilon LC \tag{4.11}$$

where A is absorbance measured, ε is the extinction coefficient, L is the path length, and C the concentration.

Here, the extinction coefficient is temperature dependent, which also affects the absorbance and, hence, the estimated concentration of Fe^{3+} in the sample. The extinction coefficient of Fe^{3+} depends on temperature, as follows [101]:

$$\varepsilon_T = (1 + 0.007 * (T - 22^\circ\text{C})) * \varepsilon_{22C} \quad (4.12)$$

where $\varepsilon_{22C} = 2132 \text{ mol L}^{-1} \text{ cm}^{-1}$, the extinction coefficient at 296 nm at 22°C.

Three major factors, i.e., gas flow, magnetic stirring, and plasma irradiation, affected the solution's temperature. The room temperature ranged from 21°C to 23°C during these experiments. The gas flow decreased the temperature of the sample slightly, while the magnetic stirrer and plasma irradiation increased it. The fluctuation in the solution's temperature overall ranged from 20°C to 30°C under various experimental conditions with 400 s of plasma exposure (Figure 4.2(a)). To maintain a stable electrical discharge in the plasma jet, the temperature probe (Fiber optic temperature sensor, TS3, Optocon AG, Dresden, Germany) was removed from the sample after the temperature was measured. An extinction coefficient of 22°C (ε_{22C}) was used to estimate the Fe^{3+} concentration throughout the experiment, which may have introduced an uncertainty of up to 3% in the estimate. I observed that the initial volume of the sample (1 mL) decreased by approximately 10% after 400 s of plasma exposure. To observe the effect of evaporation on light absorption, an experiment was performed with three initial concentrations of the solution. I found that only a 10% increase or decrease in the absorbance occurred whereas the initial concentration of Fe^{2+} was doubled or halved (Figures 4.2(b) and (c)).

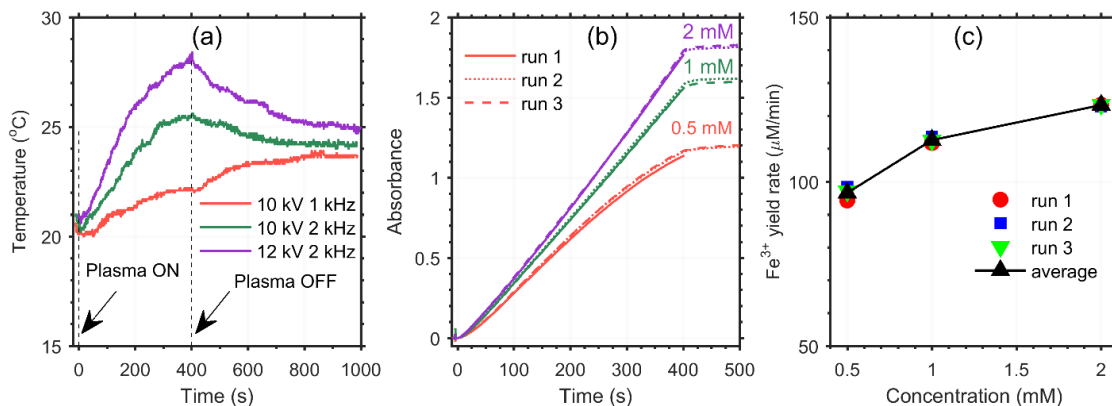


Figure 4.2: (a) Temperature variation of the solution during plasma exposure for three trials under three different experimental conditions; (b) Absorbance as a function of exposure time for three initial concentrations of Fe²⁺ in the solution. The plasma was ignited at a voltage of 10 kV, frequency of 1 kHz, flow rate of 2 slm, and treatment distance of 10 mm, and (c) Fe³⁺ yield rate estimated from the absorbance in (b) for the various initial concentrations of Fe²⁺ in the solution.

This indicates that the rate at which Fe³⁺ is generated depends in small part on the initial concentration of Fe²⁺ in the sample. However, the evaporation of the sample inflates the Fe³⁺ yield. To minimize the effects of evaporation and temperature, I used the initial portion of the dataset (50–300 s) to estimate the Fe³⁺ rate of generation when evaporation and temperature were not dominant factors. Note that, all experimental data represent the mean of at least three independent trials under the same experimental conditions, and the error bars represent the standard deviations.

To estimate the Fe³⁺ yield in a very short time (equivalent to the pulse period used in this study), I computed a corresponding differential equation for each reactant involved in reactions (4.1) to (4.6) [102] and used the rate constants of these reactions found in [96]. The general forms of the differential equations for these six chemical reactions are displayed in Figure 4.3. The differential equations corresponding to individual reactants

are zero-dimensional rate equations. I assumed that the plasma jet delivered only electrons and OH^{*} molecules to the sample. The number of electrons and OH^{*} molecules delivered to the sample per pulse was estimated to be 3.68×10^{11} and 1.61×10^{11} , respectively, based on previously reported results [95].

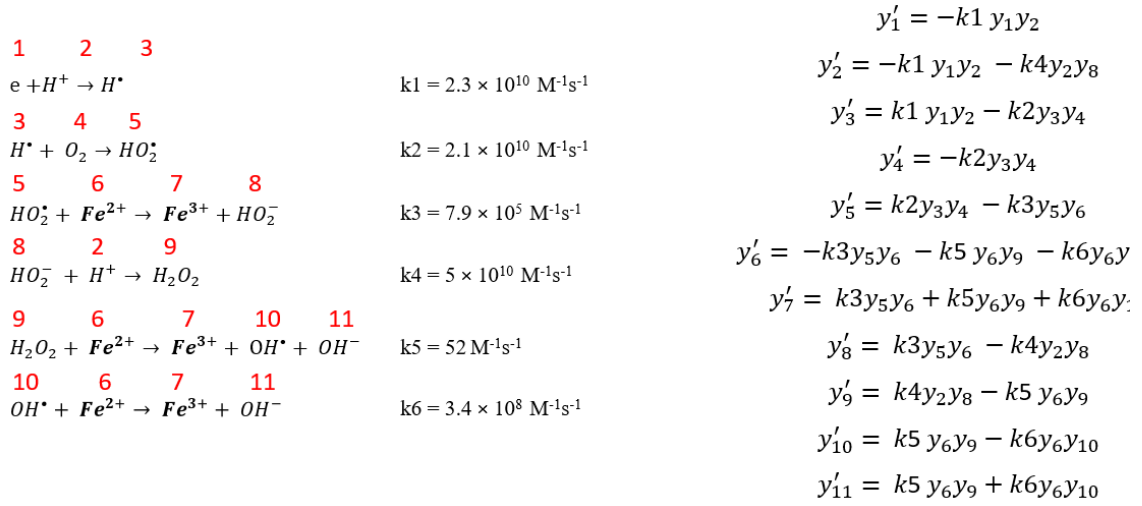


Figure 4.3: General forms of the differential equations for six chemical reactions with the rate constants (k) taken from [96] for each individual species numbered in red from 1 (i.e., electron, e) to 11 (i.e., hydroxide, OH⁻). Note, y' is the rate of yield of particular species (specified by suffix) and y is the amount of species in the solution at the particular time.

To calculate the number of species formed after the first pulse, the initial numbers of H⁺ and Fe²⁺ were estimated to be 4.82×10^{20} and 6.03×10^{17} , respectively, based on their concentration in the solution. The number of O₂ molecules was estimated to be 1.51×10^{17} , based on the amount of oxygen absorbed by the air-saturated sample. The numbers of HO₂^{*}, H₂O₂, H^{*}, Fe³⁺, HO₂⁻, and OH⁻ were assumed to be zero before plasma exposure. For the next and subsequent pulses, the initial values were set as the total yield during the previous pulse, and the numbers of electrons and OH^{*} per pulse were added to the sample at the beginning of each pulse.

4.3 Results and discussion

First, I studied the variation in absorbance within 400 s of plasma exposure for several pulse voltages at a frequency of 1 kHz, as shown in Figure 4.4(a). This figure indicates the increase in absorbance with exposure time, which also increases for higher pulse voltages. The Fe^{3+} yield rate was obtained from the slopes of changes in absorbance [94] shown in Figures 4.4(a) and (b). As seen in Figure 4.4(c), the Fe^{3+} yield rate increased three times (from about 50 to 140 $\mu\text{M}/\text{min}$) when the voltage increased from 6 to 12 kV. I observed similar results in the Fe^{3+} yield rates as functions of voltage applied in the case of post-exposure (*ex situ*) absorbance measurements (Figure 4.4(c)). From this comparison, I observed that, at a lower pulse voltage, the *in situ* and *ex situ* data of the Fe^{3+} yield rates matched; however, when a higher voltage was applied, the yield rate was slightly lower for *ex situ*. This minor decrease in the yield rate may be the result of a decrease in the temperature of the Fricke solution after plasma exposure. I also continued to collect data after the APPJ was turned off to observe the possible effect over time on the Fe^{3+} yield. A minor increase in the absorbance occurred after the APPJ was turned off, which is largely attributable to the ongoing reactions with a low rate constant in the solution. Previous studies have reported that slight changes in a flow rate and a treatment distance can influence the plasma-liquid interaction and distribution of reactive species in APPJs [49], [103]. Thus, to observe the effects of these two APPJ factors on the Fe^{3+} yield, I varied the helium gas flow rate and the treatment distance, which indicates the distance between the solution and a glass capillary of the APPJ source (Figure 4.1). In this study, I fixed a voltage of 10 kV and an exposure time of 400 s. These experimental parameters were chosen based on the data in Figure 4.4(a). Under these conditions, an

absorbance of 1.6 was achieved, which is still below the detection limit (i.e., absorbance below 2) on the spectrophotometer.

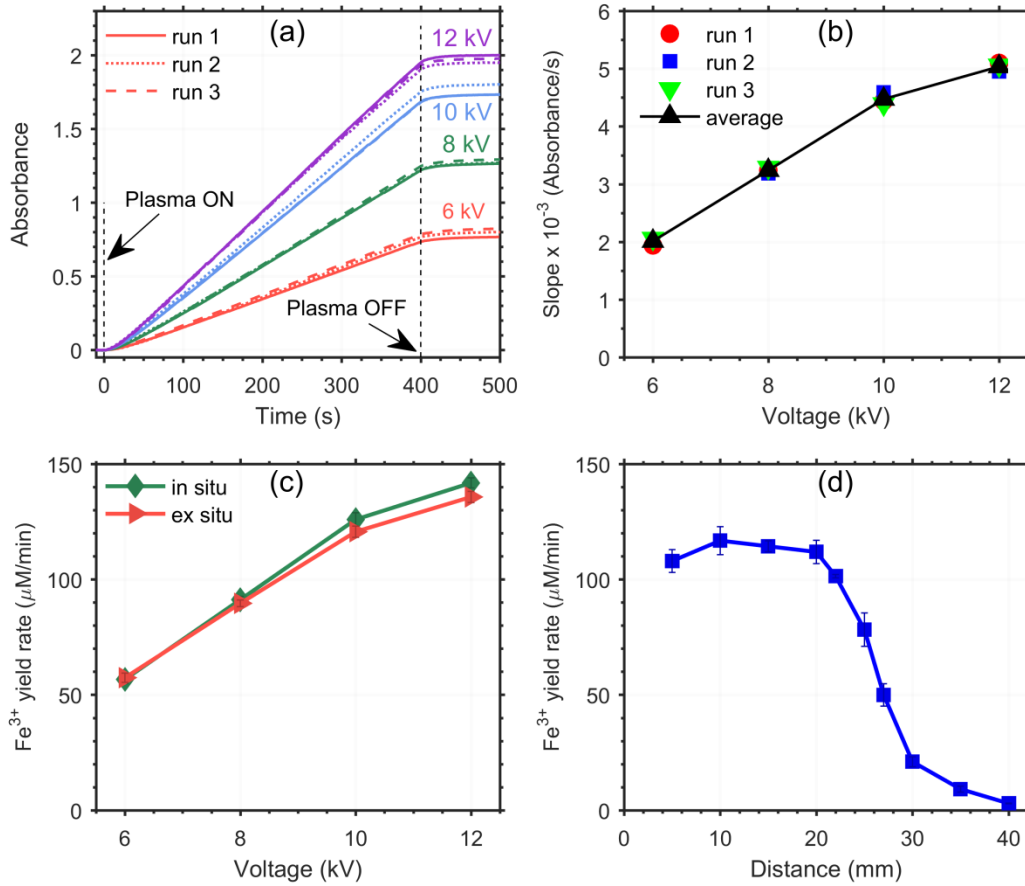


Figure 4.4: (a) *In situ* measurement of absorbance of the Fricke solution during plasma exposure with a helium flow of 2 slm, frequency of 1 kHz, and treatment distance of 10 mm at various applied voltages for three independent trials; (b) slope of the curves in (a) as a function of voltage applied for three independent trials and their average; (c) comparison of the Fe³⁺ yield rates *in situ* and post-exposure measurements (i.e., *ex situ*); and (d) Fe³⁺ yield rate during plasma exposure at a voltage of 10 kV, frequency of 1 kHz, and flow rate of 2 slm as a function of treatment distance.

From a treatment distance dependence (Figure 4.4(d)), I found that increasing the distance from 5 to 20 mm had a minor effect on the Fe^{3+} yield rate (from 110 to 112 $\mu\text{M}/\text{min}$). In this region, I could clearly see that the APPJ was in direct contact with the solution. However, at greater distances, the yield decreased gradually up to 21 $\mu\text{M}/\text{min}$ at 30 mm, as shown in Figure 4.4(d). This drop can be explained by the fact that the APPJ was in no further contact with the target. To confirm how far helium propagates in the atmosphere, I recorded schlieren images. From the images, I found that the helium gas channel extended up to 30 mm as shown in Figure 4.5. In my previous work [79], I analyzed jet images taken with a digital camera and reported that the plasma jet extended up to similar distances (approximately 35 mm). However, the length of the APPJ fluctuates, and this fluctuation is responsible for the minor Fe^{3+} yield at distances greater than 30 mm. Thus, the majority of plasma species propagate in the helium gas channel, although some of the plasma components with a sufficiently long lifetime can propagate slightly farther in the atmosphere. I then investigated the Fe^{3+} yield as a function of the flow rate in the range of 1 to 5 standard liters per minute (slm) at a treatment distance of 10 mm. I observed a slight increase in the yield (from 110 to 137 $\mu\text{M}/\text{min}$) when the flow rate increased, but one has to keep in mind that the evaporation rate also increased significantly when the flow rate increased as shown in Figure 4.6(a). This evaporation of the sample inflated the Fe^{3+} yield; thus, the Fe^{3+} yield had to be corrected based on the evaporation rate. After the volume correction, I observed a minor change in the Fe^{3+} yield of only of a few $\mu\text{M}/\text{min}$ when the flow rate was increased from 1 to 5 slm as shown in Figure 4.6(b). Thus, there was a minor increase in the rate of reactive species formation within the range of the helium flow rate studied.

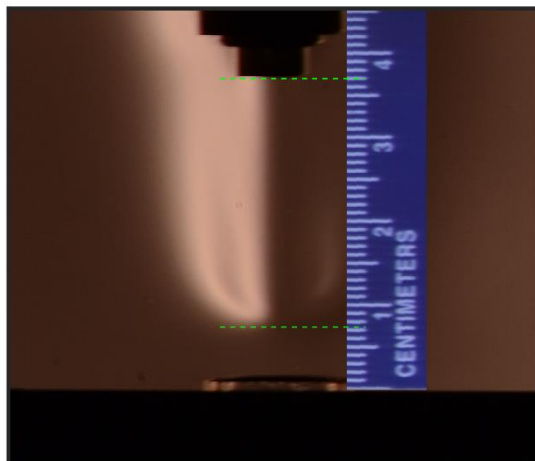


Figure 4.5: Schlieren photograph of a helium gas channel in the atmosphere at a flow rate of 2 slm.

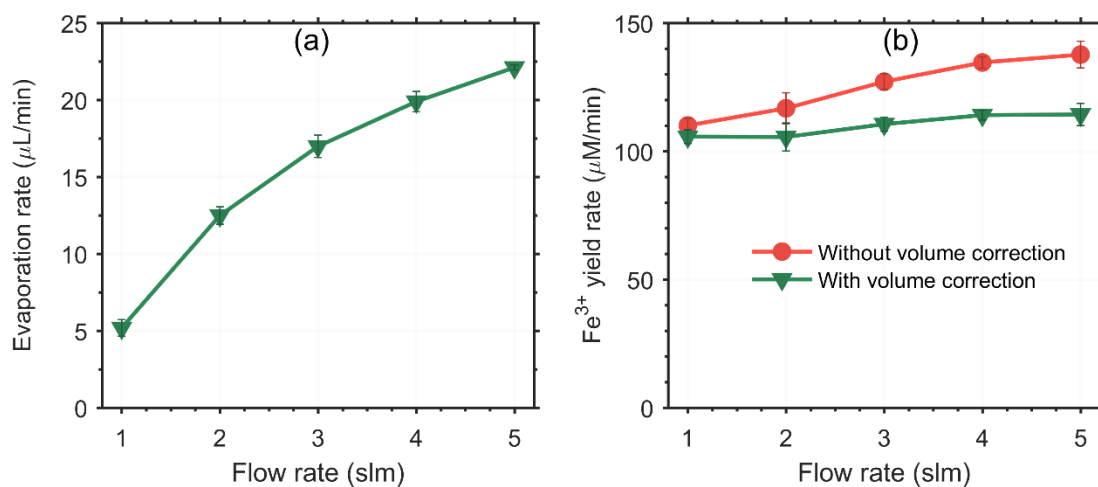


Figure 4.6: (a) Rate of evaporation of the solution, and (b) Fe^{3+} yield rates as a function of flow rate within plasma exposure of 400 s at a voltage of 10 kV, frequency of 1 kHz, and treatment distance of 10 mm.

Furthermore, I investigated the Fe^{3+} yield as a function of pulse frequency between 0.25 and 5 kHz, as shown in Figure 4.7(a). As expected, the Fe^{3+} yield increased significantly in this frequency range because, with higher frequencies and fixed exposure times, more interactions occur between plasma components and the solution. Surprisingly, the Fe^{3+} yield per pulse decreased as the frequency increased, as shown in Figure 4.7(b). I believe that this can be explained by a different time period between pulses, during which the previously mentioned reactions can still proceed.

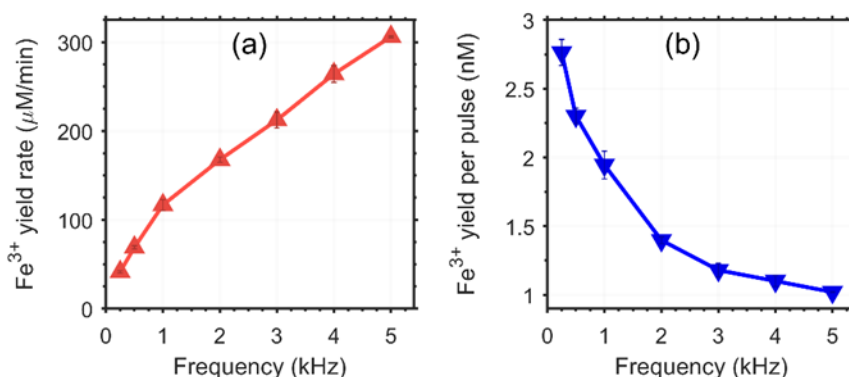


Figure 4.7: (a) Fe^{3+} yield rate as a function of pulse frequency at a voltage of 10 kV, flow rate of 2 slm, and treatment distance of 10 mm; and (b) Fe^{3+} yield per pulse as a function of the frequency estimated from (a).

The time period is longer at a lower frequency, meaning there is more time to yield Fe^{3+} originating in slow reactions. However, at a higher frequency, the time period is too short to generate a sufficient yield in slow reactions, which can explain why the Fe^{3+} yield decreased per pulse with an increase in the frequency. To gain more insights into understanding this observation, I also performed calculations of the Fe^{3+} yield within times equivalent to the time periods and frequencies used in this study. The assumptions and methods of these calculations are presented in Section 4.3. The yield of all reactants

was calculated for half of the time period of each pulse (i.e., for the reaction time before another plasma plume arrived). It is important to note that the plasma ignites at the rising and falling edges of the voltage applied [100]. After solving the differential equations, I plotted evolutions of all the species after the first plasma pulse (Figure 4.8).

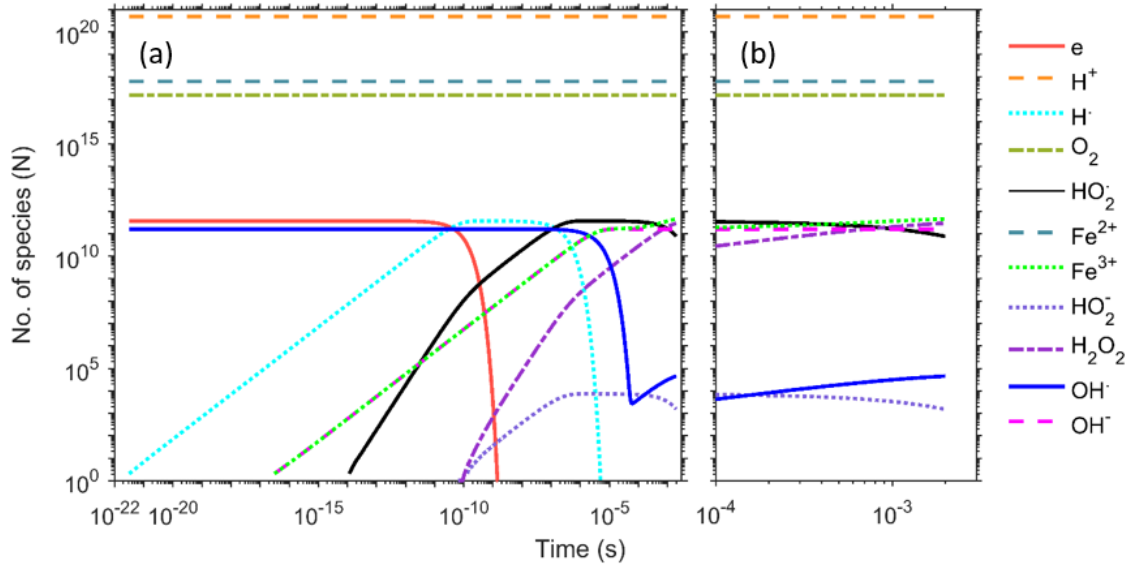


Figure 4.8: (a) Number of species as a function of reaction time obtained by solving the corresponding differential equations for each reactant; (b) enlarged image of (a) in the time range from 1×10^{-4} to 2×10^{-3} s equivalent to the time periods/frequencies used in this study.

In Figure 4.8, I noticed that e^- and H^\bullet were quenched within 10^{-5} s while the number of Fe^{3+} ions increased significantly within that time due to occurrence of reactions (4.3), (4.5), and (4.6) in the solution. Based on the overlapping of normalized Fe^{3+} yields as a function of frequency obtained from the experimental study and calculations (Figure 4.9), in which I assumed that electrons and OH^\bullet are delivered from the APPJ to the solution, I suggest that, among all the reactants, e^- and OH^\bullet came from

the plasma jet whereas the remaining ones were formed in the solution during plasma exposure.

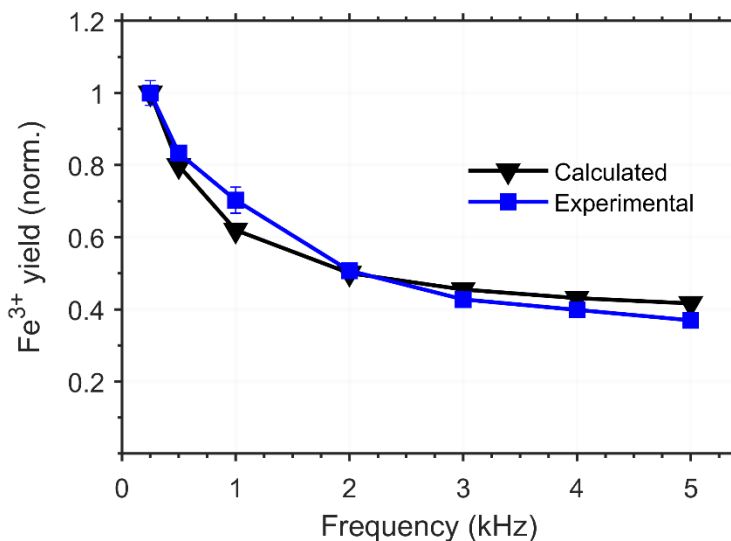


Figure 4.9: Normalized Fe³⁺ yields as a function of frequency used in experimental study and the calculated yield after the first pulse assuming that electrons and OH[•] are delivered from the APPJ to the solution.

The exceptions were H⁺, Fe³⁺, and O₂, which were in the solution already. The excited species (e.g., He^{*}) and electrons in the APPJ contributed to the production of highly reactive OH[•] and H[•] on the surface of the liquid sample [91]. These highly reactive species immediately reacted with O₂ and Fe²⁺ because of the large rate constants of reactions (4.2) and (4.6). I observed that the number of reacting species in reactions (4.2) and (4.6) (e.g., H[•], OH[•]) decreased rapidly and became almost zero within 10⁻⁶ s. Moreover, a significant increase in the Fe³⁺ yield occurred until the H[•], OH[•], and electrons were present in the solution. The rapid increase in the Fe³⁺ yield within 10⁻⁵ s is largely attributable to reaction (4.6). Above 10⁻⁵ s, the Fe³⁺ yield increased gradually

because of reactions (4.3) and (4.5). The reactants in reactions (4.3) and (4.5), HO_2^\bullet and H_2O_2 , formed in the solution due to plasma exposure.

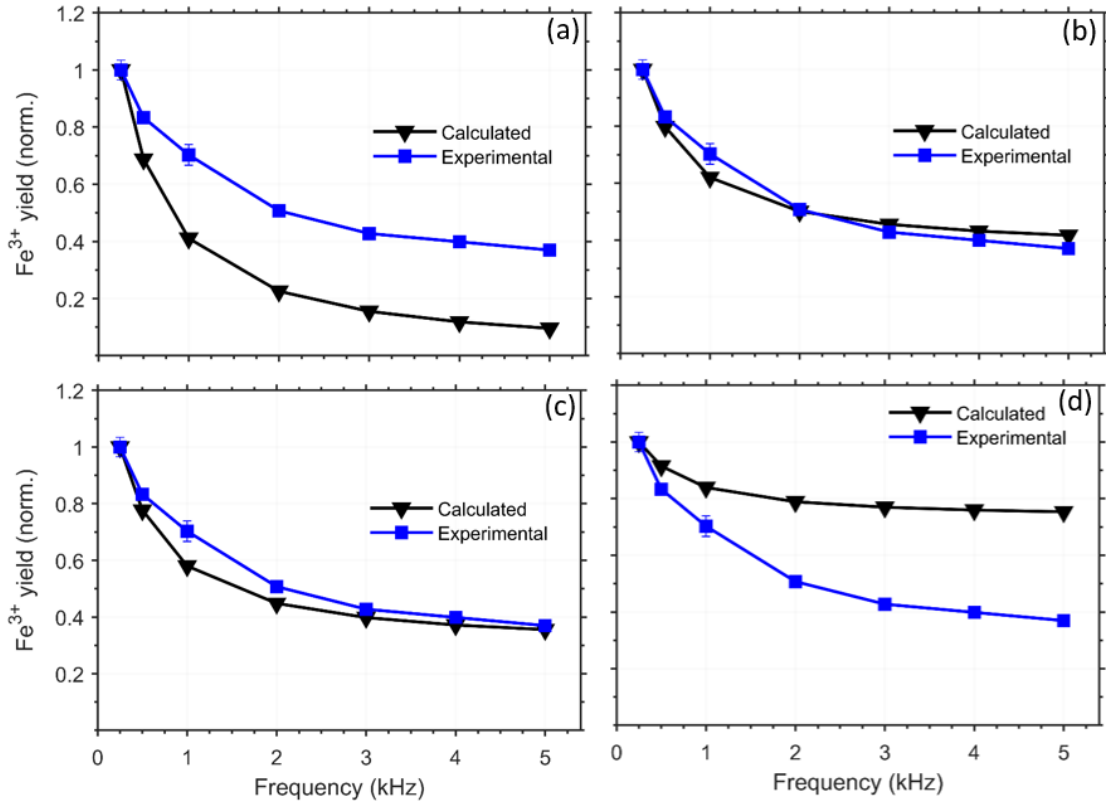


Figure 4.10: Normalized Fe^{3+} yields as a function of frequency used in experimental study and the calculated yield after one pulse assuming that (a) only electrons are delivered from the APPJ to the solution (b) electrons and OH^\bullet with some initial amount of H_2O_2 are delivered from the APPJ to the solution (c) electrons and OH^\bullet with some initial amount of H_2O_2 and HO_2^\bullet are delivered from the APPJ to the solution (d) electrons and OH^\bullet with some initial amount of H_2O_2 and HO_2^\bullet are delivered from the APPJ to the solution and some Fe^{3+} amount present in the solution generated from the previous pulse. All initial values for electrons, OH^\bullet , H_2O_2 , HO_2^\bullet and Fe^{3+} are reported in reference [95].

This indicates that the plasma species delivered to the Fricke solution, as well as the reactive species formed in the solution, contributed to the increased Fe^{3+} yield. The calculated effects on the Fe^{3+} yield are attributable to the several plasma reactive species in the solution for different initial conditions and are shown and compared to the experimental results in Figures 4.10(a) to (d)).

Moreover, as the Fe^{3+} yield can differ significantly because the species formed in or delivered to the Fricke solution can accumulate in each pulse, I calculated the Fe^{3+} yield associated with many consecutive pulses (≈ 10000) at each frequency used in my experimental study. The normalized Fe^{3+} yield is shown in Figure 4.11, where the dotted line represents the yield after the thousandth pulse. To compare the results from the calculation and experiment, I used the average data from calculated yields. From the calculation, I found that the yield per pulse increased with higher pulse numbers (Figure 4.12) and became saturated at approximately the thousandth pulse, before beginning to decrease, as shown in Figure 4.11. Some discrepancies emerged between the calculated and experimental data, largely because of the exclusion of the role of any reactive nitrogen species and my assumption that the plasma delivered only electrons and OH^\bullet . The decrease in the Fe^{3+} yield per pulse in the experimental study, as well as in the data calculated, confirmed that some incomplete reactions occurred (reactions (4.3) and (4.5)) before the next plasma plume reached the sample, and, as demonstrated in Figure 4.8(b), there was a gradual increase in the number of Fe^{3+} ions within the time range of 1×10^{-4} to 2×10^{-3} s. Hence, the Fe^{3+} yield per pulse was higher at lower frequencies (i.e., longer time periods) than at higher frequencies (i.e., shorter time periods).

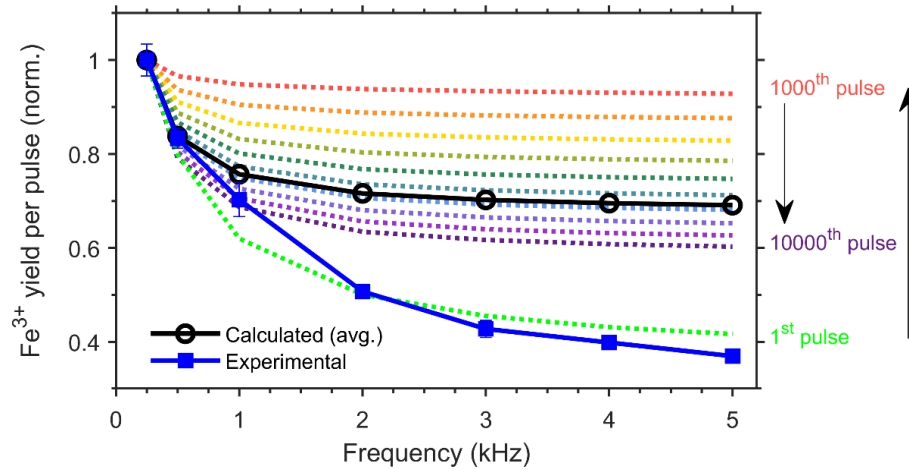


Figure 4.11: Normalized Fe^{3+} yield per pulse for a typical pulse at every 1000th pulse. Dotted curves are the yield per pulse for a particular pulse number while the data points are the average values of 10000 pulses. The arrow indicates the increasing order of pulse number.

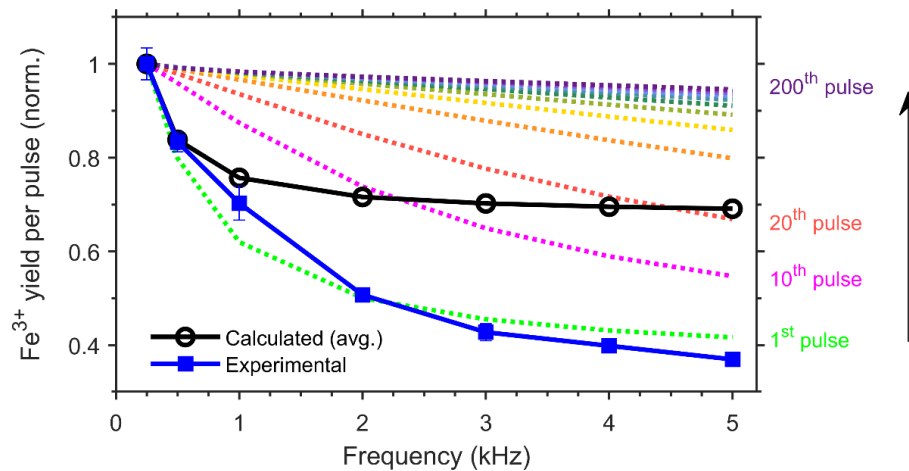


Figure 4.12: Normalized Fe^{3+} yields after different number of pulses as a function of frequency used in experimental study. Dotted curves are the yields for a particular pulse number, while circle data points are the average values of 10000 pulses as in Figure 4.11. The arrow indicates the increasing order of pulse number.

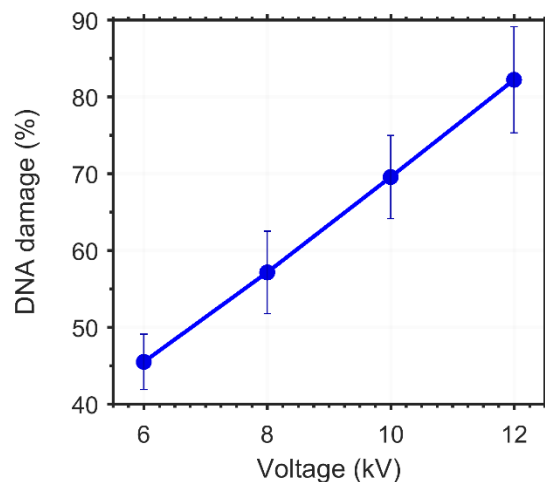


Figure 4.13: Total DNA damage induced within 15 s of plasma irradiation as a function of pulse voltage at a frequency of 1 kHz, flow rate of 2 slm, and treatment distance of 10 mm.

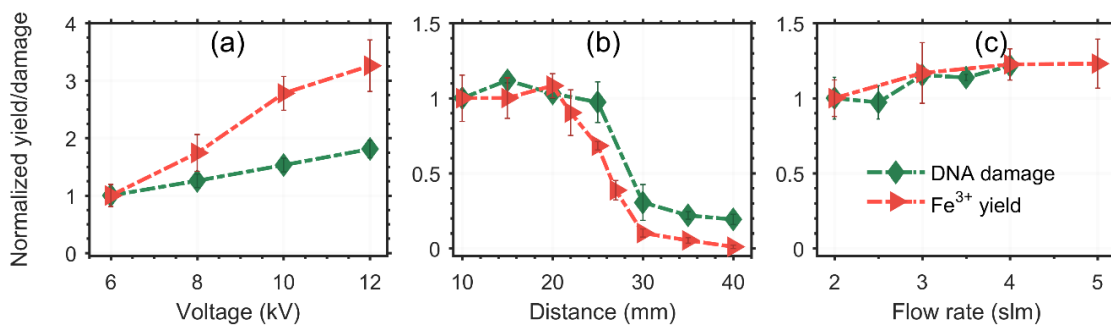


Figure 4.14: Normalized Fe³⁺ yield and DNA damage level within 15 s of plasma exposure as functions of (a) voltage, (b) treatment distance, and (c) flow rate of the feed gas (DNA damage level data in (b) and (c) were taken from Chapter 2 Figures 2.4(d) and (b) respectively).

I also used DNA as a molecular probe [100] to find any correlation between DNA damage and the formation of Fe^{3+} ions due to the plasma reactive species. The detailed procedure of DNA irradiation and the choice of experimental parameters are explained in previous works [34], [79]. I observed that the DNA damage level increased from 45% to 82% within 15 s of plasma exposure when the voltage applied increased from 6 to 12 kV (Figure 4.13). I normalized the DNA damage level and Fe^{3+} yield by dividing each dataset by its first data point. Figure 4.14(a) illustrates that both the DNA damage level and Fe^{3+} yield increased when the applied voltage increased. However, the slope of the Fe^{3+} yield was significantly higher than that of the DNA damage level.

This discrepancy in the slope demonstrates that some additional reactive species are formed in the plasma at higher voltages and react more effectively with Fe^{2+} than with DNA. Furthermore, I compared the Fe^{3+} yield and DNA damage level for different treatment distances and flow rates and observed that the Fe^{3+} yield and DNA damage level were correlated, as shown in Figures. 4.14(b) and (c). The correlation between the DNA damage level and the Fe^{3+} yield as functions of flow rate or treatment distance also shows the potential to use both techniques to quantitatively estimate the effects of APPJ.

4.4 Conclusions

In this work, I estimated the Fe^{3+} yield rate formed in the acidified ferrous sulfate solution during plasma exposure. The increase in the Fe^{3+} yield corresponded to the increase of plasma reactive species delivered from the APPJ and formed in the solution. The reactive species in the solution increased significantly as the pulse voltage and repetition frequency increased, and I recorded a minor change in their total yield when

the flow rate of the feed gas increased within the treatment distance along the jet. By solving the differential equation for each species involved in Fe^{3+} formation, I found agreements with my experimental data and calculations when I assumed that electrons and OH^{\bullet} radicals are the only species delivered to the solution. Moreover, both species interact quickly with the reactants in the solution; thus, both played an important role in initiating further reactions. The overall quantification of reactive species in plasma jets using the Fricke solution in real time can serve as a time-efficient technique for *in situ* characterization of an APPJ. Such characterization can also be helpful in comparing the effects of different APPJ developed in other laboratories. Thus, it may transform APPJs from subjects of laboratory research to instruments with useful clinical applications.

Further studies should be implemented to investigate not only the quantification of all reactive species, but also to quantify and qualify the effects of particular plasma reactive species. Better knowledge on the type and amount of reactive oxygen and nitrogen species formed due to plasma exposure can lead to a more comprehensive understanding of biochemical interactions induced by plasma.

CHAPTER 5:
ROLE OF HYDROGEN PEROXIDE TO GENERATE REACTIVE SPECIES IN AN
APPJ⁴

5.1 Introduction

It is become well-known now that reactive species in the atmospheric pressure plasma jets (APPJs) play a crucial role in the clinical applications such as wound healing, sterilization, blood coagulation, dentistry, and cancer treatment [54], [57], [87]–[89], [104], [105]. But, the optimization of most useful reactive species (e.g., H₂O₂, O₃, OH[•], NO[•], etc.) in clinical trials utilizing all the current achievement in plasma medicine is still challenging [106], [107]. One of the crucial parameters that can influence the amount and type of reactive species in the plasma jet is feed gas. There are several studies using a mixture of gases as the feed gas, and some of them have also used another gas as a shielding gas other than feed gas to have better control in the amount and type of the reactive species in a plasma jet [6], [108]. One of the important and long-lived reactive species in the plasma jet is hydrogen peroxide. In the presence of Fe²⁺, an H₂O₂ molecule split off to form most reactive hydroxyl (OH[•]) radical via “Fenton” reaction [8], [109],

⁴ The results in this Chapter are included in a manuscript, which is ready to submit to Applied Physics Letters. Authors: E. R. Adhikari, V. Samara, E. Wellman and S. Ptasinska.

which takes place in the cells. It also plays a vital role in intracellular signaling and works as microbicidal to infectious pathogens [109]. Ahmad reported that hydrogen peroxide-ultraviolet A (HUVA) therapy is a valuable asset for mankind in controlling leprosy and other skin diseases [110]. H_2O_2 is also used as a bleaching agent in dentistry [111]. Due to the versatile utility of H_2O_2 in medical applications, the possibility to introduce or produce H_2O_2 in APPJs brings potential plasma benefits. It has been already reported that hydrogen peroxide in the feed gas leads to an enhancement in bacterial inactivation [112] and is necessary in the tissue removal process in electrosurgery [113]. Both research works attempted to correlate the formation of other reactive species such as OH^\bullet or O_3 due to H_2O_2 presence in plasma. Therefore, it is essential to gain a deeper understanding of the role of hydrogen peroxide in the feed gas to further increase the chemical reactivity of a plasma jet. In this study, I monitored the total reactive species (e.g., OH^\bullet , HO_2^\bullet) as well as electrons in the plasma jet in real time due to the addition of hydrogen peroxide in the feed gas of the APPJ. In general, the experiment was based on the oxidation of a ferrous (Fe^{2+}) to ferric (Fe^{3+}) ions [94] due to plasma radiation. The concentration of Fe^{3+} ions was measured from UV absorption at 296 nm. The total yield of Fe^{3+} ions from Fe^{2+} ions in acidified solution corresponds to total reactants delivered from the plasma jet or formed in the solution due to plasma irradiation [114]. However, water is inevitable from the feed gas when H_2O_2 is introduced. Therefore I also added a fraction of water vapor in the feed gas and compared the results with those for which only hydrogen peroxide was added. The overall goal of this work is to understand the role of H_2O_2 in the feed gas in increasing the total reactive species in a plasma jet.

5.2 Materials and methods

In this study, I used an APPJ source similar to that used in my previous studies. Details regarding the plasma source and experimental setup are provided in Chapter 4 (Section 4.2). Briefly, plasma was ignited using square pulses of 10 kV with a frequency of 1 kHz and 50% duty cycle which was generated by a home-made HV pulse waveform generator. These parameters were kept constant for the entire experiment. The amplitude along with the shape of waveforms of voltage and current were monitored by a high voltage probe (P6015A, Tektronix, Inc., Beaverton, OR, USA) and induction coil (Pearson Current Monitor Model 2877, Pearson Electronics, Inc., Palo Alto, CA, USA), respectively, and recorded using a digital oscilloscope (NI USB-5133, National Instruments, Austin, TX, USA). The details of sample preparation and absorption measurement are explained in Chapter 4 (Section 4.2). Briefly, a cuvette (inner dimension 10 mm x 10 mm x 10 mm) made up of quartz (1 mm thick) with an acidified ferrous sulfate solution (1 millimolar (mM) iron(II) sulfate heptahydrated from Sigma-Aldrich, St. Louis, MO, USA in 0.4 M H₂SO₄ (Fisher Scientific, Waltham, MA, USA)), also known as Fricke solution, was positioned on a magnetic stirrer (HI190M-1, Hanna Instruments, Woonsocket, RI, USA) beneath the plasma jet, 10 mm from the outlet of the glass capillary, as shown in Figure 5.1. During the plasma treatment of a Fricke solution, Fe²⁺ was oxidized into Fe³⁺. The concentration of the Fe³⁺ was estimated from the absorbance of UV light at 296 nm using Beer-Lambert law:

$$A = \epsilon LC \tag{5.1}$$

Where A is measured absorbance, ϵ is the extinction coefficient, L is the length of the cuvette and C the concentration. The extinction coefficient of Fe^{3+} depends on temperature as follows [95], [101].

$$\epsilon_T = (1 + 0.007 * (T - 22^\circ\text{C})) * \epsilon_{22C} \quad (5.2)$$

Where $\epsilon_{22C} = 2132 \text{ mol L}^{-1} \text{ cm}^{-1}$, extinction coefficient for 296 nm at 22°C [114].

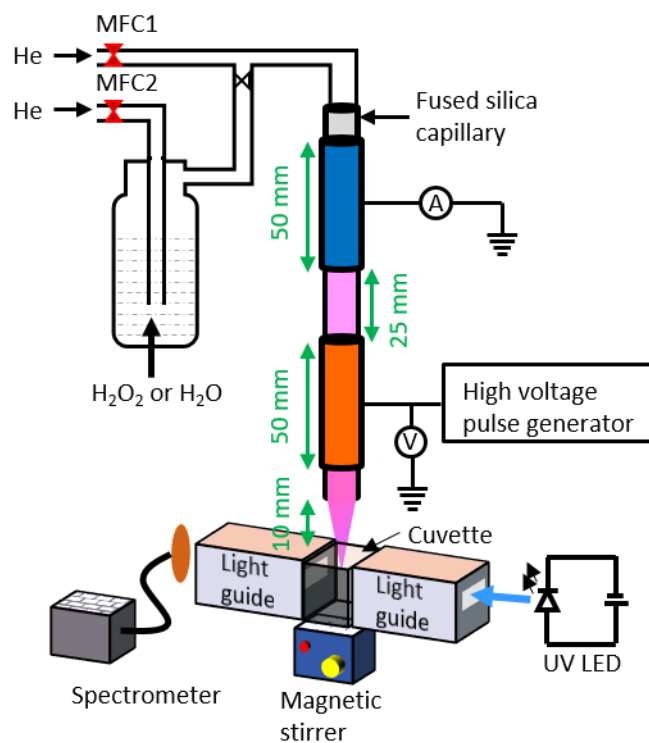


Figure 5.1: Schematic of the experimental setup.

The total flow rate of helium (HE UHP300, Airgas Inc., Radnor, PA, USA) in the capillary was maintained at 2 slm (standard liter per minute) for the entire experiment, as monitored by a mass flow controller, MFC1 (MV-394-He, Bronkhorst High-Tech B.V., Ruurlo, The Netherlands). I also passed helium through H₂O₂ (50 wt.% in H₂O) (Fisher Scientific, Waltham, MA, USA) to carry a fraction of hydrogen peroxide vapor to the feed gas, as shown in Figure 5.1. In this chapter, I refer to this procedure as “hydrogen peroxide with water.” It is important to note that hydrogen peroxide contains water because some water vapor is inevitable when introducing hydrogen peroxide to the feed gas. To understand the effect of the presence of water in the feed gas, in another experiment I introduced only water vapor to the feed gas by passing a fraction of helium through a water bottle, a procedure that I refer to here as “only water”. To maintain the desired amount of hydrogen peroxide or water in the feed gas, I adjusted the flow rate of helium gas through the bottle with hydrogen peroxide with water (or only water). The flow rate of helium (0-400 sccm; standard cubic centimeter per minute) through the bottle was controlled using another flow controller, MFC2 (Mass Flow Controller, MKS Instruments, Andover, MA, USA), which was powered and adjusted by a Type 247 4 channel readout (MKS Instruments, Andover, MA, USA). I used the modified Raoult’s law to estimate the fraction of hydrogen peroxide and water vapor in the feed gas, as described in refs. [115], [116]. To estimate the partial pressure of hydrogen peroxide and water at room temperature, I used a four-parametric activity coefficient model presented by Manatt et al. [117] and adopted all the other coefficients values needed for estimation from ref. [118]. To minimize variations in the experimental conditions (e.g., temperature, evaporation) while collecting the absorption spectra, I used the initial portion of the data

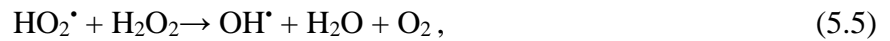
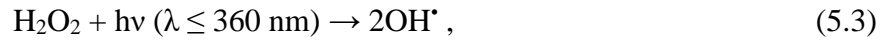
set (acquired within 50–300 s after ignition of plasma) to estimate the rate of generation of Fe^{3+} , for which changes in evaporation and temperature were neglected [114]. Further, I used DNA as a molecular probe to monitor the reactive species in the plasma jet after adding a fraction of either hydrogen peroxide or water to the feed gas. Details of the sample preparation, irradiation, and analysis of the DNA damage level are as described in a previous Chapter (Chapter 2, Section 2.2).

5.3 Results and discussion

As noted above, since the occurrence of water is inevitable upon the introduction of H_2O_2 to the feed gas, I had to deduce the H_2O_2 effect in the feed gas on the oxidization of Fe^{2+} to Fe^{3+} by comparing the yield rate of Fe^{3+} during plasma irradiation where the water vapor was fed in the two ways, i.e., (1) via “only water” (red circles), (2) via “hydrogen peroxide with water” (green triangles) in Figure 5.2(a). Initially, there is a rapid increase in the yield rate of Fe^{3+} (118 to 193 $\mu\text{M}/\text{min}$) when I introduce a very small fraction of water ($< 0.1\%$). Between 0.1–0.25% of water content in the feed gas, there is a minor change in the yield rate of Fe^{3+} (193 to 194 $\mu\text{M}/\text{min}$). Above 0.25% of water content, there is a minor increase in the yield rate of Fe^{3+} (194 to 201 $\mu\text{M}/\text{min}$) when the water vapor is fed via “only water” (red circles) whereas there is a significant increase in the yield rate of Fe^{3+} (194 to 219 $\mu\text{M}/\text{min}$) when the water vapor was fed via “hydrogen peroxide with water” (green triangles). Figure 5.2(b) shows the difference between the yields as a function of the fraction of water vapor in the feed gas when the water vapor was fed via “hydrogen peroxide with water” and “only water.” There is a minor difference in the yield rate of Fe^{3+} with +5 to -15 $\mu\text{M}/\text{min}$ for a small fraction of

water (<0.25%), whereas the difference is increased (up to +30 $\mu\text{M}/\text{min}$) for an increase in the fraction of the water content to 0.32%.

It is important to note here that hydrogen peroxide quickly decomposes into water and oxygen molecules as final products via photolysis in the presence of UV light (< 360 nm) as follows [119]–[121]:



The UV light is provided by the plasma itself, as indicated by the optical emission spectra of the plasma jet, which shows that the significant species in the plasma jet are the 2nd positive system of molecular nitrogen with wavelengths between 315 nm and 365 nm [34]. Therefore, during plasma discharge in the capillary as well as in the APPJ UV light can interact with H_2O_2 and decomposes it. Reactions (5.3) to (5.6) can indicate that the addition of H_2O_2 to the feed gas is equivalent to the addition of water or oxygen molecule to the feed gas. However, the addition of a fraction of oxygen in the feed gas has a minor effect in the yield of Fe^{3+} (Appendix B, Figure: A.4) in comparison with those observed in Figure 5.2(a) and (c). Therefore, the increase in the yield rate of Fe^{3+} may be due to the presence of the inevitable water vapor in the feed gas while adding hydrogen peroxide (Figure 5.2(a)). However, plasma may or may not be able to decompose all H_2O_2 molecules in the feed gas so it is essential to investigate the effect of undecomposed H_2O_2 in the feed gas in increasing the yield rate of Fe^{3+} .

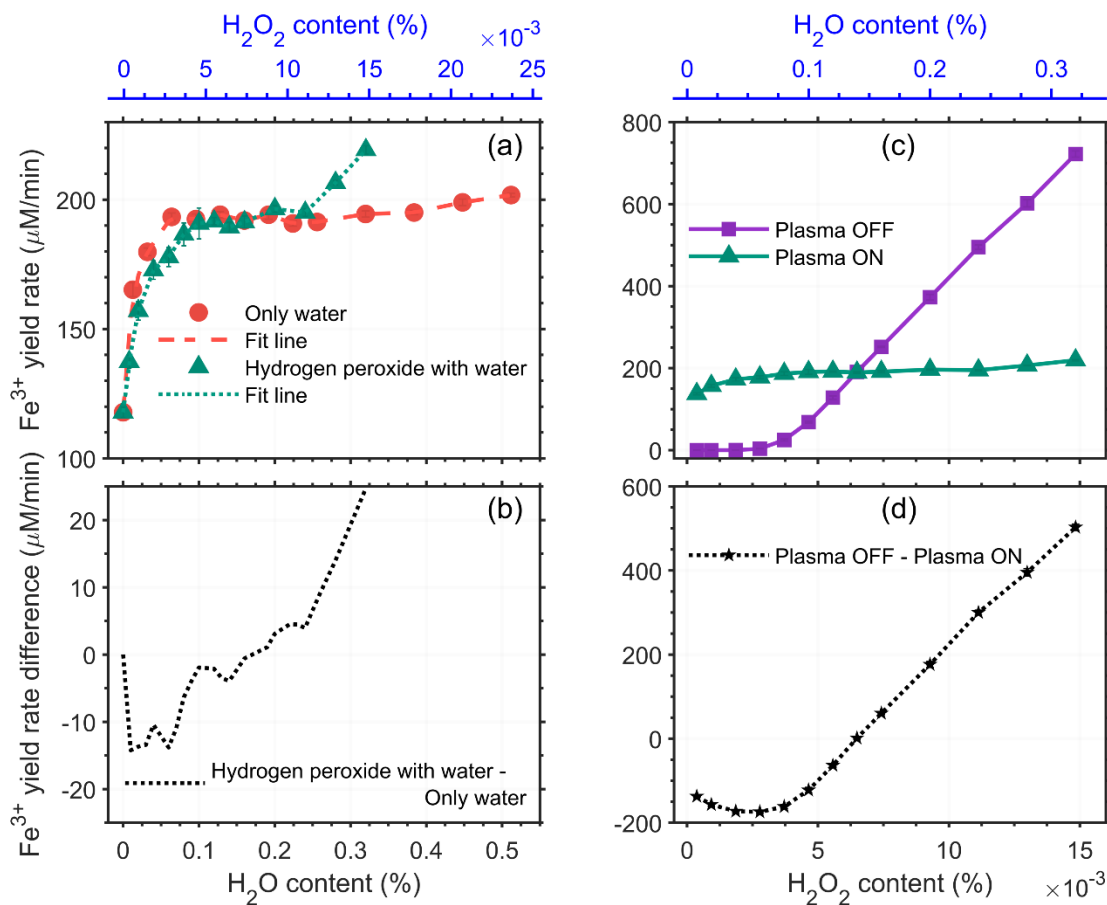


Figure 5.2: (a) The yield rate of Fe^{3+} due to plasma irradiation as a function of the fraction of water vapor in the feed gas. Water vapor was fed into the feed gas with only water (H_2O , red circles) or hydrogen peroxide with water (H_2O_2 , green triangles); (b) difference in the yield rates of Fe^{3+} for conditions in (a) as a function of the fraction of water in the feed gas; (c) yield rate of Fe^{3+} as a function of the fraction of hydrogen peroxide in the feed gas for plasma OFF (purple squares) and plasma ON (green triangles) conditions; (d) difference in the yield rates of Fe^{3+} for conditions in (c) as a function of the fraction of hydrogen peroxide in the feed gas.

To investigate the effect of the presence of undecomposed H_2O_2 in the feed gas during plasma irradiation, I conducted a helium flow control experiment with a fraction of hydrogen peroxide in the feed gas, where the sample was exposed to the feed gas without plasma irradiation (referred as the plasma OFF condition). For this plasma OFF condition, I observed a nominal yield rate of Fe^{3+} ($< 25 \mu\text{M}/\text{min}$) with up to 0.003% hydrogen peroxide in the feed gas. However, there was a significant increase in the yield rate of Fe^{3+} ($25 \mu\text{M}/\text{min}$ to $722 \mu\text{M}/\text{min}$) in response to an increase in the fraction of hydrogen peroxide from 0.003% to 0.015% in the feed gas, as shown in Figure 5.2(c) (purple squares). To compare the results observed in the plasma OFF condition, I also plotted the yield rate of Fe^{3+} as a function of the fraction of hydrogen peroxide in the feed gas (green triangles) with plasma irradiation (referred to as the plasma ON condition) in Figure 5.2(c), where it can be observed that there is a relatively constant yield rate of Fe^{3+} ($\sim 195 \mu\text{M}/\text{min}$) for the plasma ON. Figure 5.2(d) shows the difference in the yield rate of Fe^{3+} for plasma OFF and ON condition for the addition of a fraction of hydrogen peroxide to the feed gas. This significant difference in yield rate of Fe^{3+} (more than $500 \mu\text{M}/\text{min}$) also indicates that plasma decomposes H_2O_2 in the feed gas into the less reactive species to Fe^{2+} . However, if there is a significant amount of water (as well as hydrogen peroxide) in the feed gas, the plasma current intensity will decrease [100] (Appendix B, Figure A.5), and hence the plasma power as shown in Figure 5.3. This means there is less ionization in the plasma, which eventually affects the formation of reactive species. Also, plasma with lower power may not decompose all the H_2O_2 molecules when there is a higher fraction of H_2O_2 in the feed gas.

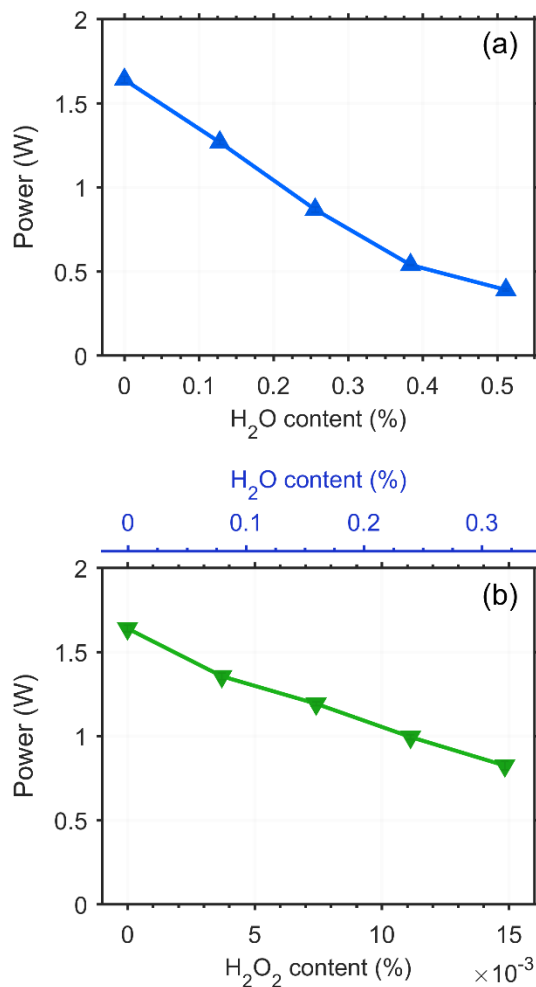


Figure 5.3: The average plasma power for various fractions of (a) water vapor and (b) hydrogen peroxide vapor in the feed gas.

That means the significant increase in the yield rate of Fe³⁺ (194 to 219 μM/min) above 0.25% of water content in the feed gas when the water vapor was fed via “hydrogen peroxide with water” (green triangles) (Figure 2(a)) may be due to the undecomposed H₂O₂ in the feed gas. I also investigated the induction of DNA damage due to plasma irradiation for an addition of a fraction of hydrogen peroxide or water in the feed gas. Figure 5.4 (a) shows the DNA damage level due to the addition of a fraction of water in the feed gas. There is a minor change in DNA damage level (66 to 62%) when

the fraction of water increased from 0 to 0.15% whereas there is a decrease in the DNA damage level (62 to 50%) for an increase in the water in the feed gas from 0.15 to 0.32%. The minor decrease in the DNA damage level for the excessive presence of water can be attributed by the decrease in plasma power for those conditions. In Figure 5.4(b), it can be observed that there is a minor change in the DNA damage level (66 to 61%) for an increase in the fraction of H_2O_2 in the feed gas from 0 to 0.015%.

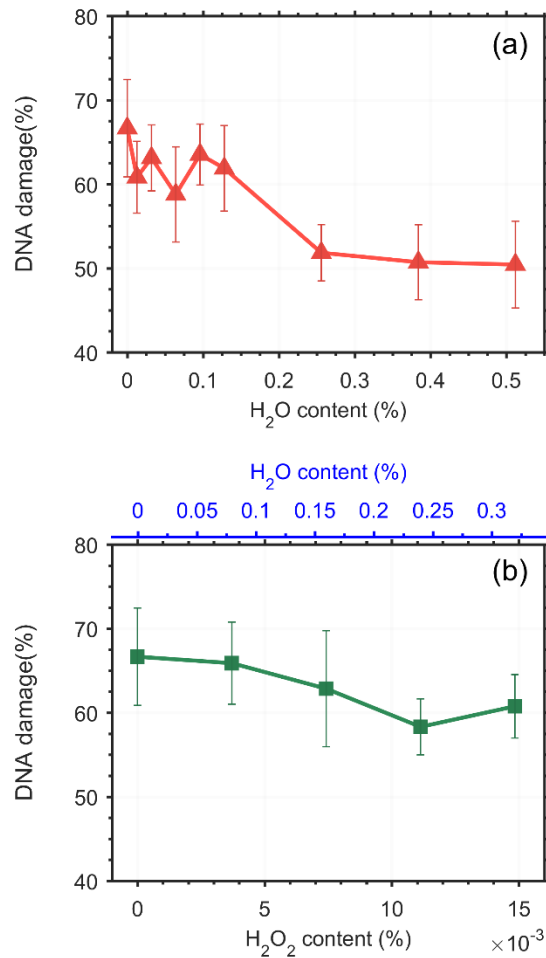


Figure 5.4. Fractions of DNA damage in the sample after 15 s of plasma irradiation as a function of the fraction of (a) water in the feed gas, and (b) hydrogen peroxide in the feed gas.

It is important to note that there is a significant increase in the yield rate of Fe^{3+} for the addition of a small fraction of water in the feed gas. However, there is a minor decrease in the DNA damage level for the addition of a small fraction of water in the feed gas. That means some reactive species are formed in the plasma-liquid interface which are highly reactive to Fe^{2+} but not to the DNA in an open atmosphere. For instance, H_2O_2 is one of the possible candidate because helium flow control experiment with a fraction of H_2O_2 has minor effect on the DNA damage level (Appendix B, Figure A.6, purple squares) whereas similar flow control experiment shows the significant increase in the yield rate of Fe^{3+} (Figure 5.1(c), purple squares). In a previous study, it is reported that H_2O_2 is generated inside the plasma and delivered to the sample [62], however, some other studies are reported that plasma forms H_2O_2 in the liquid sample [63], [122]–[124]. Here, I would stress that some metallic reagent (e.g., Fe^{2+}) must be present to decompose H_2O_2 into a highly reactive OH^\bullet radical (“Fenton” reaction) [8], but there is no such reagent in the aqueous DNA sample to decompose H_2O_2 . Therefore, I see only a minor effect of H_2O_2 on the DNA damage level. It would be interesting future work to investigate the interfacial phenomena in the plasma-liquid interaction that could answer the mystery behind the plasma interaction with the liquid surface in many clinical applications.

5.4 Conclusions

The effectiveness of the addition of a fraction of hydrogen peroxide as well as water in a helium APPJ in increasing the total reactive species in the plasma jet was investigated using *in situ* absorption spectroscopy. There is a significant increase in yield

rate of Fe^{3+} for a small fraction of hydrogen peroxide or water in the feed gas that indicates the increase in reactive species in the plasma jet due to the presence of hydrogen peroxide or water. The effect of hydrogen peroxide in the feed gas is observed as similar as adding water in the feed gas because the hydrogen peroxide decomposes into water and oxygen quickly in the plasma jet. Moreover, the investigation of the damage level of DNA due to the addition of a fraction of hydrogen peroxide or water in the feed gas shows that there is a minor change in the DNA damage level. That means some reactive oxygen species are formed in the plasma jet due to the addition of water, but those species might be very reactive to Fe^{2+} but not to aqueous DNA in an open atmosphere. The flow control experiments with hydrogen peroxide, the irradiation by feed gas only, shows that hydrogen peroxide is one of the reactive species which is very reactive to Fe^{2+} but not with the aqueous DNA. Therefore, H_2O_2 is one of the candidates, which might form near plasma-liquid interface that result into significant increase in the yield rate of Fe^{3+} due to the addition of H_2O as well as H_2O_2 in the feed gas. However, it is essential to investigate more on the interfacial phenomena in the plasma-liquid interaction to answer the mystery behind the plasma interaction with the liquid surface in many clinical applications.

CHAPTER 6: SUMMARY AND FUTURE WORK

6.1 Summary

This thesis focuses on the characterization of a helium APPJ including plasma jet interaction with air components such as oxygen and water vapor. It also introduces a novel technique for *in situ* characterization of an APPJ and that technique was also used to investigate the contribution of H₂O₂ to generate reactive species in the plasma jet.

I started my research work building a helium APPJ source and focused to understand that APPJ. In the very first experiment, I measured the plasma current and power for various flow rates and voltages along with the qualitative study of reactive species for various plasma parameters (flow rate, distance, sample concentration, etc.) using DNA damage level as a marker to monitor reactive species (Chapter 2). The fraction of different types of DNA damage (i.e., double-strand breaks (DSBs), and single-strand breaks (SSBs)) that occurred as the result of plasma irradiation as well as intact (undamaged) DNA were quantified through the analysis of agarose gel electrophoresis images. From these experiments, I observed that the length of the plasma jet is increased linearly with an increase in the flow rate from 1 to 4 slm. Above 4 slm, the jet length continued to increase until attained its maximum value of about 100 mm at the flow rate of 9 slm. Here, the damage in the DNA was significantly higher when the sample was in

contact with the visible plasma region. Moreover, the increase in jet length may have induced changes in the distribution of plasma species in the visible plasma region and increased the number of these species delivered to the sample, which may eventually induce more DNA damage. In another experiment, I observed a higher DNA damage level for a sample with lower DNA concentration (3.3 ng/ μ L) than higher DNA concentration (10 ng/ μ L). In a sample with a lower DNA concentration, the number of available plasma species to interact with DNA molecules was much higher, which led to more significant damage.

In Chapter 3, I reported the interactions of plasma jet with air components such as oxygen, and water vapor. I monitored changes in plasma current and power, as well as in the level of DNA damage attributable to plasma irradiation, by adjusting the fraction of major air components, oxygen, and water vapor, in the plasma jet environment and feed gas. I obtained an optimal amount of oxygen or water vapor in the plasma jet environment, as well as in the feed gas, which increased the level of DNA damage significantly (30% to ~55%). This increase can be attributed primarily to the formation of reactive species caused by water and oxygen decomposition in the APPJ detected with mass spectrometry. Moreover, I observed there is an increase in DNA damage level irrespective of plasma power remained the same or decreased depending on where the mixture of gases was added to the jet environment or the feed gas, respectively. This indicates that the interaction between plasma species and biological matter is superior over the electrical power applied to ignite the plasma in APPJ sources used in medical applications.

In chapter 4, I reported the formation of plasma reactive species in an acidified ferrous sulfate (Fricke) solution interacting with an APPJ. A yield of ferric (Fe^{3+}) ions measured using *in situ* absorption spectroscopy was attributed to the formation of plasma reactive species provided and/or originated in the solution. It is observed that the number of reactive species formed was proportional to the applied voltage and its frequency. However, the Fe^{3+} yield per pulse decreased with an increase in frequency from 0.25 to 5 kHz. To get more insight in the process occurred in a very short interval of time (equivalent to the time period of experimental frequency range), I tracked the evolution of the species involved in the chemical reactions due to plasma exposure using differential equations and calculations. At higher frequencies, there was insufficient time to complete all reactions before the next pulse reached the solution; at lower frequencies, the Fe^{3+} yield was higher because of the relatively longer time available for reactions to occur. Also, the comparison between DNA damage levels and Fe^{3+} yields was investigated under different experimental conditions in order to verify the usefulness of both the Fricke solution and the DNA molecule as a probe to characterize APPJs.

Further, I utilized the technique of *in situ* characterization of an APPJ to study the contribution of hydrogen peroxide as well as water vapor to form the reactive species in the plasma jet which I reported in Chapter 5. I observed that there is a significant increase in the yield rate of Fe^{3+} (118 $\mu\text{M}/\text{min}$ to 200 $\mu\text{M}/\text{min}$) due to the addition of a small fraction of hydrogen peroxide (0 to 0.011%) as well as water (0 to 0.51%) in the feed gas. However, there is a minor decrease in DNA damage level (66 to 50%) due to plasma irradiation for an increase in the fraction of hydrogen peroxide as well as water in the feed gas. These results show that some reactive species (e.g., H_2O_2) are formed in the

plasma-liquid interface which are very reactive to Fe^{2+} but not to aqueous DNA in an open atmosphere.

6.2 Future work

So far, the key role of RONS in clinical medicine has been understood to some extent however, the control of the generation of those species in an open atmosphere is still challenging. Therefore, the reproducibility and detailed understanding of the clinical applications of plasma has yet to be achieved.

The plasma medicine community is facing the following two major challenges at this moment:

1. Understanding the interactions between complex plasma and complex biological fluid: The plasma contains the “cocktail” of many short-lived reactive species, and the biological fluid (e.g., cytoplasm) itself is a very complex fluid [54]. To understand the interactions between these two complex components, some of the investigations have been done on plasma-water and plasma-cell culture medium. However, the cell membrane seems to be a dominating factor in the interaction between the plasma species and the cell, more specifically between the gas phase plasma outside the cells (or tissue) and the cytoplasm inside the cells. Therefore, it is essential to study the plasma-biological fluid interactions through the cell membrane [125]. The field of biophysics can address these interactions, so it is essential for plasma medicine community to have a collaborative study with the biophysics community to understand those interactions and bring the cold plasmas from the research lab to clinical applications.

2. Defining the 'dose' of the plasma treatment: The question of how to define the 'dose' associated with plasma treatment is one of the current important topics in the field. The outcome of the plasma treatment significantly depends on the device and target [125]. The plasma takes different pathways for various applications, for example, the working mechanism of plasma in wound healing and the induction of apoptosis in cancer cell might be different. It is crucial to fully understand the mechanism of plasma interactions with the bulk cellular system to define the plasma 'dose' meaningfully. The experience and knowledge of the radiologist working on biological effects of low doses of ionizing radiation would be helpful for plasma medicine community to address the plasma 'dose' issue.

These are some of the proposed research work to address these issues by broadening my research work that I have done so far.

6.2.1 Modification of experimental setup

In Chapter 3, I reported the qualitative change in the reactive species due to the addition of a fraction of oxygen or water vapor in the feed gas as well as plasma jet environment. I also observed the significant change in the plasma discharge pattern on the basis of current waveforms. The exact quantification of the reactive species and time evolution study of the discharge pattern can be done with some modification in the experimental set up as shown in Figure 6.1. This new experimental set up would be useful to get more insight about the interaction at the plasma-liquid interface with a controlled plasma jet environment. The plasma interaction with biological fluids is essential to understand to get more insight into the clinical applications of plasma.

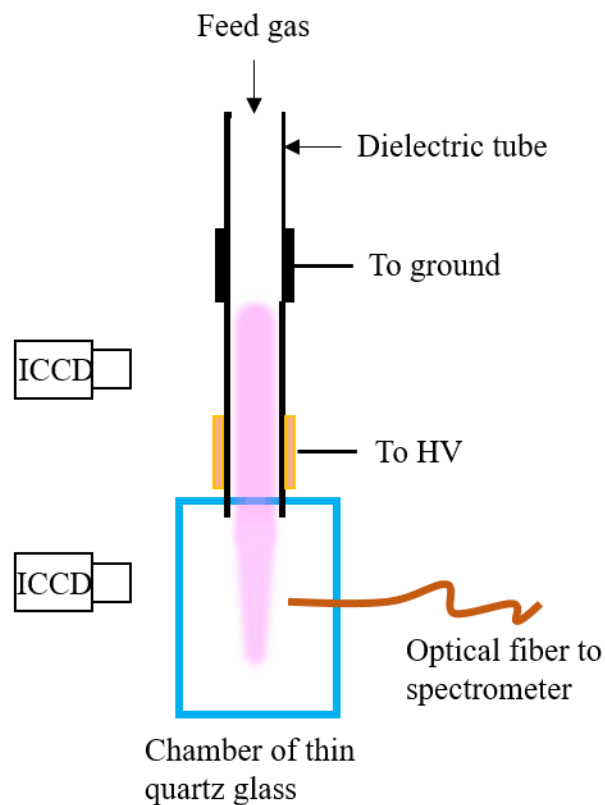


Figure 6.1: Schematic of the experimental set up to monitor the propagation of plasma bullets and reactive species in a controlled environment

This new experimental set up will provide quantitative information of reactive species formed during the plasma treatment of a bulk cellular system. For instance, the time-resolved imaging with an ICCD camera may reveal the interactions of plasma bullets with the liquid surface in a controlled environment.

6.2.2 Target dependence of plasma propagation

In Chapter 4, I employed an acidified ferrous sulfate solution, which is commonly used as a chemical dosimeter to measure the total yield of reactive species formed during plasma exposure. Future work in this project is to fully understand the pathways of

biochemical reactions triggered by plasma irradiation using experimental as well as computational approaches leading to quantification of the plasma species that are useful for clinical applications.

Further, I used a high-speed ultra-fast imaging technique to take the time-resolved images of a plasma jet, and I utilized those data to calculate the speed of plasma bullets for various experimental conditions. The results are summarized in Table 6.1.

TABLE 6.1:
THE SPEED OF PLASMA BULLETS FOR VARIOUS EXPERIMENTAL
CONDITIONS

Experimental Condition	Speed (km/s)
Free jet	103.16
Empty cuvette	128.21
Water in cuvette	160.9
Fricke solution in cuvette	166.07
Fricke solution in cuvette with magnetic stirrer	246.94

From Table 6.1, it can be observed that the propagation of the plasma bullet depends on the target. There is an increase of 24% of the speed of the plasma bullet when an empty cuvette was introduced as a target. There is also an increase in speed when the target is non-conductive (water) or conductive liquid (Fricke solution). It was reported in previous research that plasma propagation is significantly affected by the conductivity of the target [6]. I also observed that the speed of plasma bullet significantly increases after turning on the magnetic stirrer, i.e., applying an external electromagnetic field. In a

previous study coherent anti-Stokes Raman scattering (CARS) was used to measure the electric field of a nanosecond pulse discharge in atmospheric over liquid surface [126]. The understanding of the electric and magnetic field in my *in situ* characterization of a plasma jet experiment would reveal the mystery behind the plasma-biological fluid interactions in the clinical application of plasma.

APPENDIX A:
AGAROSE GEL ELECTROPHORESIS OF DNA

1. Preparation of 0.8% agarose mixture (liquid)

Add 480 mg agarose and 60 mL 1X TBE (Tris-Borate EDTA) buffer into a conical flask of 125 mL.

2. Heating agarose mixture

Microwave the agarose mixture solution for 1 min at high heat. Agarose should be dissolved, and the solution should be boiling when the time is up. Remove the flask from the microwave with heat protective gloves.

3. Cooling down the agarose solution down to 60 °C

Put a thermometer inside the liquid for monitoring the temperature of the agarose solution.

4. Making the gel fluorophore

Add 3 µL SYBR Green I into the flask, and mixed well with the agarose liquid.

5. Shaping the gel to load DNA

Level the tray using a leveling bubble. Pour the gel into the tray slowly and carefully avoiding bubble formation. If there are bubbles, use small pipette tips to remove the bubbles. Place the comb on one side of the tray and wait for around 40 min for the gel to be solidified.

5. Preparation of DNA samples for loading

Add 6X loading dye of 1/5th of the volume of the sample in each DNA sample and mix well.

6. Transferring gel to running apparatus

Remove the comb gently without making any rupture in the gel. Transfer the tray into the running apparatus. Add more 1X TBE running buffer to the gel running apparatus till the buffer covers the gel or maximum mark.

7. Load DNA samples to the gel

Add colored DNA sample into the well of the gel slowly and gently without making any rupture in the gel and avoiding bubbles.

8. Running the gel

Put the lid on the apparatus. Set up voltage (70 V) and time (180 min) and start running the gel. If there are bubbles formed at the electrodes inside the tank, then the apparatus is in operation. When the time is up, the voltage is terminated automatically, and the gel is ready for imaging.

9. Imaging the gel

Turn on Bio-Rad Gel Doc RX and select UV light source. Start Gel Doc RX using Quantity One software. Select the proper exposure time without saturating the images. The previously loaded DNA sample will be divided into mainly three portions (Undamaged, SSB, and DSB) which are visible as a band in the gel images. Make contour around each band of DNA, and the corresponding volume of each contour is proportional to the amount of DNA in that particular band.

APPENDIX B:
SUPPLEMENTARY MATERIALS

I recorded photographs during each experimental trial to confirm direct contact between the plasma jet and sample. Some typical photographs are shown in Figure A.1. Also, I recorded photographs of the plasma jet and discharged between electrodes in a fused silica capillary for various experimental conditions (Figure A.2).

To observe the effect of gas temperature on the current waveform, a fused silica capillary together with electrodes was wrapped with heating tape. I adjusted the feed helium gas temperature using the voltage power supply that consisted of a variable transformer (Ohmite Manufacturing Co., Skokie, IL, USA). At a voltage of 70 V, the gas temperature, which was measured using a fiber optic temperature sensor (Optocon AG, Germany), was 149 °C. Pure helium (HE UHP300, Airgas Inc.) gas with a flow rate of 2 slm was used as a feed gas, and the plasma was ignited using a DC pulsed voltage of 10.6 kV and a frequency of 1.5 kHz (Figure A.3(a)). The current waveforms for the feed gas at room temperature (21 °C) and 149 °C are shown in Figure A.3(b).

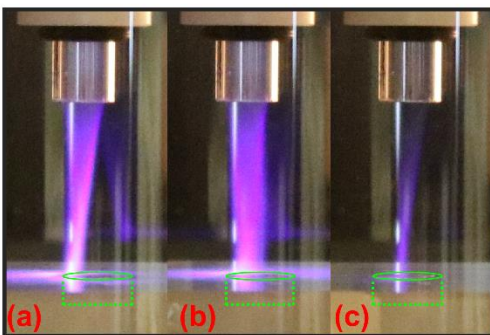


Figure A.1: Typical photographs taken for the various experimental conditions using a D3100 Nikon camera (exposure time 0.5 s, $f/5.6$, iso6400) (a) Jet striking the edge of the glass well; (b) and (c) Jet striking the center of the sample in two different trials. The green part represents the sample well.

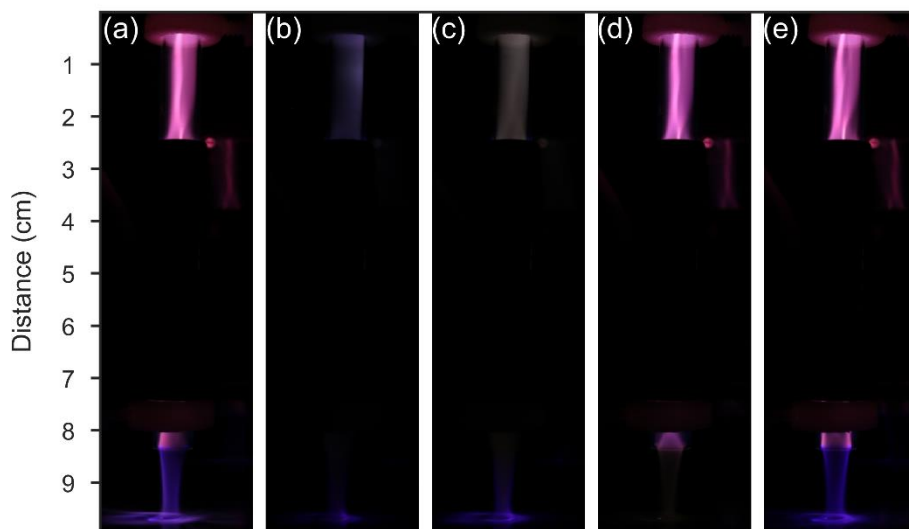


Figure A.2: Photographs of the plasma jet and plasma discharged between the electrodes obtained under different experimental conditions using a Canon EOS Rebel T6i (exposure time: 2 s, $f/5.6$, ISO: 100, focal length: 18 mm). (a) 4 slm helium feed gas and 5 slm nitrogen in the chamber, (b) 16% humidity in the feed gas, (c) 0.25% oxygen in the feed gas, (d) 56% oxygen in the chamber, and (e) 62% humidity in the chamber.

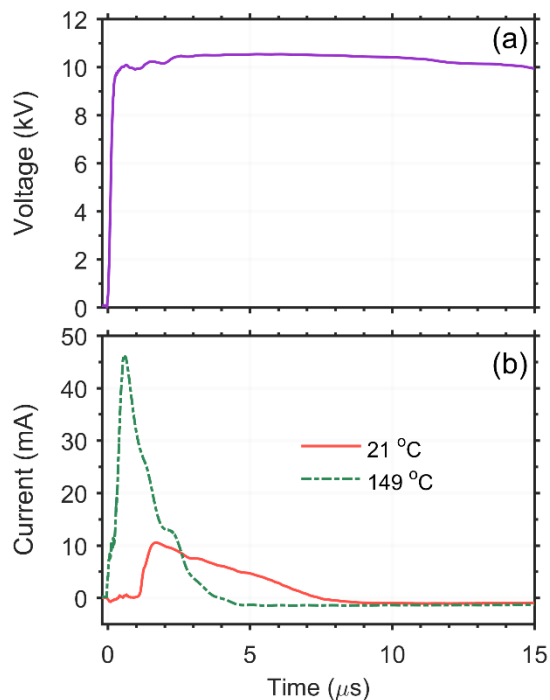


Figure A.3: (a) Voltage waveform at a voltage of 10.6 kV; (b) Current waveforms for the feed gas at room temperature and heated gas at temperature of 149 °C.

Further, I did some experiment to investigate the effect of oxygen in the feed to form the Fe^{3+} ions in the sample. Figure A.4 shows the yield rate of Fe^{3+} as a function of oxygen content in the feed gas. The current intensity and waveforms are also recorded for the various fractions of hydrogen peroxide and water vapor in the feed gas, which is shown in Figure A.5. The DNA damage level induced for various types of feed gas and experimental conditions as a function of plasma irradiation time is shown in Figure A.6.

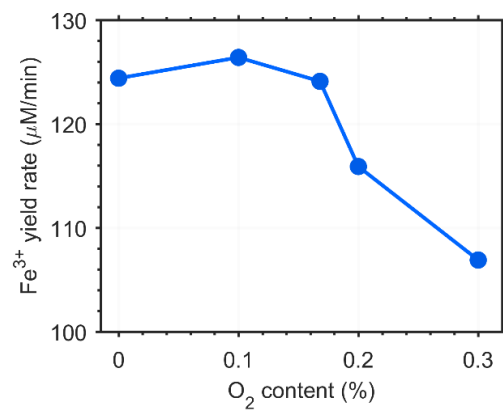


Figure A.4: Fe³⁺ yield rate during plasma exposure at a voltage of 10 kV, frequency of 1 kHz, and a flow rate of 2 slm as a function oxygen content in the feed gas.

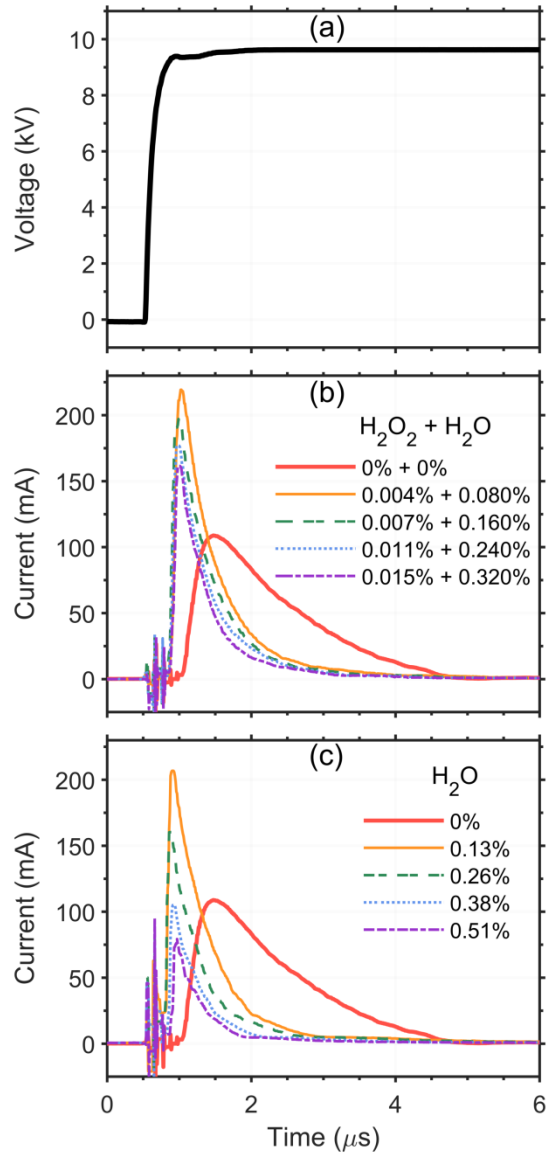


Figure A.5: (a) Applied voltage waveform. Plasma current waveforms for various fractions for (a) hydrogen peroxide with water (b) only water for the voltage applied in (a).

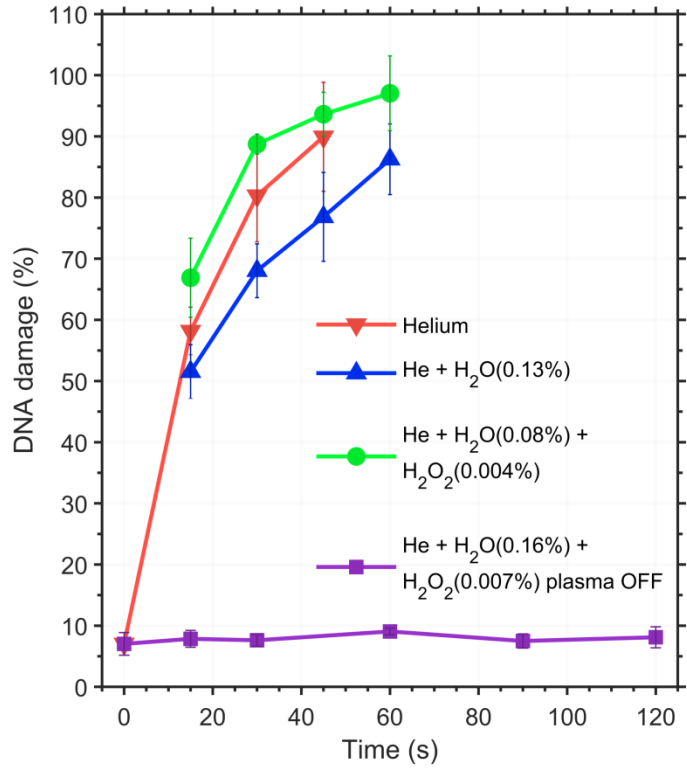


Figure A.6: Total DNA damage fractions due to the plasma irradiation as a function of irradiation time for the pure helium, and the mixture of water vapor or hydrogen peroxide vapor in helium, note that the time “0” indicates the control sample.

BIBLIOGRAPHY

- [1] D. P. Dowling and C. P. Stallard, "Achieving enhanced material finishing using cold plasma treatments," *Trans. IMF*, vol. 93, no. 3, pp. 119–125, 2015.
- [2] C. Tendero, C. Tixier, P. Tristant, J. Desmaison, and P. Leprince, "Atmospheric pressure plasmas: A review," *Spectrochim. Acta Part B At. Spectrosc.*, vol. 61, no. 1, pp. 2–30, 2006.
- [3] J. Winter, R. Brandenburg, and K.-D. Weltmann, "Atmospheric pressure plasma jets: an overview of devices and new directions," *Plasma Sources Sci. Technol.*, vol. 24, no. 6, p. 064001, 2015.
- [4] R. Wang, K. Zhang, Y. Shen, C. Zhang, W. Zhu, and T. Shao, "Effect of pulse polarity on the temporal and spatial emission of an atmospheric pressure helium plasma jet," *Plasma Sources Sci. Technol.*, vol. 25, no. 1, p. 015020 2016.
- [5] K. Arjunan, V. Sharma, and S. Ptasinska, "Effects of Atmospheric Pressure Plasmas on Isolated and Cellular DNA—A Review," *Int. J. Mol. Sci.*, vol. 16, no. 2, pp. 2971–3016, 2015.
- [6] X. Lu, G. V. Naidis, M. Laroussi, S. Reuter, D. B. Graves, and K. Ostrikov, "Reactive species in non-equilibrium atmospheric-pressure plasmas: Generation, transport, and biological effects," *Phys. Rep.*, vol. 630, pp. 1–84, 2016.
- [7] T. von Woedtke, S. Reuter, K. Masur, and K.-D. Weltmann, "Plasmas for medicine," *Phys. Rep.*, vol. 530, no. 4, pp. 291–320, 2013.
- [8] D. B. Graves, "Low temperature plasma biomedicine: A tutorial review," *Phys. Plasmas*, vol. 21, no. 8, p. 080901, 2014.
- [9] E. Stoffels, I. E. Kieft, and R. E. J. Sladek, "Superficial treatment of mammalian cells using plasma needle," *J. Phys. D. Appl. Phys.*, vol. 36, no. 23, pp. 2908–2913, 2003.
- [10] K. R. Stalder and J. Woloszko, "Some Physics and Chemistry of Electrosurgical Plasma Discharges," *Contrib. to Plasma Phys.*, vol. 47, no. 1–2, pp. 64–71, 2007.

- [11] X. Zhang, M. Li, R. Zhou, K. Feng, and S. Yang, "Ablation of liver cancer cells in vitro by a plasma needle," *Appl. Phys. Lett.*, vol. 93, no. 2, p. 021502, 2008.
- [12] M. Laroussi, "Low temperature plasma-based sterilization: Overview and state-of-the-art," *Plasma Process. Polym.*, vol. 2, no. 5, pp. 391–400, 2005.
- [13] T. Sato, O. Furuya, K. Ikeda, and T. Nakatani, "Generation and transportation mechanisms of chemically active species by dielectric barrier discharge in a tube for catheter sterilization," *Plasma Process. Polym.*, vol. 5, no. 6, pp. 606–614, 2008.
- [14] T. Sato, T. Miyahara, A. Doi, S. Ochiai, T. Urayama, and T. Nakatani, "Sterilization mechanism for Escherichia coli by plasma flow at atmospheric pressure," *Appl. Phys. Lett.*, vol. 89, no. 7, pp. 88–90, 2006.
- [15] E. Dolezalova and P. Lukes, "Membrane damage and active but nonculturable state in liquid cultures of Escherichia coli treated with an atmospheric pressure plasma jet," *Bioelectrochemistry*, vol. 103, pp. 7–14, 2015.
- [16] G. Fridman *et al.*, "Blood Coagulation and Living Tissue Sterilization by Floating-Electrode Dielectric Barrier Discharge in Air," *Plasma Chem. Plasma Process.*, vol. 26, no. 4, pp. 425–442, 2006.
- [17] T. Von Woedtke *et al.*, "Clinical Plasma Medicine: State and Perspectives of in Vivo Application of Cold Atmospheric Plasma," *Contrib. to Plasma Phys.*, vol. 54, no. 2, pp. 104–117, 2014.
- [18] G. Isbary *et al.*, "A first prospective randomized controlled trial to decrease bacterial load using cold atmospheric argon plasma on chronic wounds in patients," *Br. J. Dermatol.*, vol. 163, no. 1, pp. 78–82, 2010.
- [19] I. E. Kieft, J. L. V Broers, V. Caubet-Hilloutou, D. W. Slaaf, F. C. S. Ramaekers, and E. Stoffels, "Electric discharge plasmas influence attachment of cultured CHO K1 cells," *Bioelectromagnetics*, vol. 25, no. 5, pp. 362–368, 2004.
- [20] M. Vandamme *et al.*, "ROS implication in a new antitumor strategy based on non-thermal plasma," *Int. J. Cancer*, vol. 130, no. 9, pp. 2185–2194, 2012.
- [21] G. J. Kim, W. Kim, K. T. Kim, and J. K. Lee, "DNA damage and mitochondria dysfunction in cell apoptosis induced by nonthermal air plasma," *Appl. Phys. Lett.*, vol. 96, no. 2, p. 021502, 2010.
- [22] X. Han, M. Klas, Y. Liu, M. Sharon Stack, and S. Ptasinska, "DNA damage in oral cancer cells induced by nitrogen atmospheric pressure plasma jets," *Appl. Phys. Lett.*, vol. 102, no. 23, p. 233703, 2013.
- [23] E. A. Ratovitski *et al.*, "Anti-cancer therapies of 21st century: Novel approach to

- treat human cancers using cold atmospheric plasma,” *Plasma Process. Polym.*, vol. 11, no. 12, pp. 1128–1137, 2014.
- [24] S. Mohades, M. Laroussi, J. Sears, N. Barekzi, and H. Razavi, “Evaluation of the effects of a plasma activated medium on cancer cells,” *Phys. Plasmas*, vol. 22, no. 12, 2015.
- [25] S. Arndt *et al.*, “Effects of Cold Atmospheric Plasma (CAP) on β -Defensins, Inflammatory Cytokines, and Apoptosis-Related Molecules in Keratinocytes In Vitro and In Vivo,” *PLoS One*, vol. 10, no. 3, p. e0120041, 2015.
- [26] G. Fridman *et al.*, “Floating Electrode Dielectric Barrier Discharge Plasma in Air Promoting Apoptotic Behavior in Melanoma Skin Cancer Cell Lines,” *Plasma Chem. Plasma Process.*, vol. 27, no. 2, pp. 163–176, 2007.
- [27] J. Heinlin *et al.*, “Plasma applications in medicine with a special focus on dermatology,” *J. Eur. Acad. Dermatology Venereol.*, vol. 25, no. 1, pp. 1–11, 2011.
- [28] G. Fridman, G. Friedman, A. Gutsol, A. B. Shekhter, V. N. Vasilets, and A. Fridman, “Applied plasma medicine,” *Plasma Process. Polym.*, vol. 5, no. 6, pp. 503–533, 2008.
- [29] H. J. W. J. Lee, G. Y. Park, Y. S. Seo, Y. H. Im, S. B. Shim, and H. J. W. J. Lee, “Modelling of atmospheric pressure plasmas for biomedical applications,” *J. Phys. D. Appl. Phys.*, vol. 44, no. 5, p. 053001, 2011.
- [30] G. Y. Park *et al.*, “Atmospheric-pressure plasma sources for biomedical applications,” *Plasma Sources Sci. Technol.*, vol. 21, no. 4, p. 043001, 2012.
- [31] M. G. Kong *et al.*, “Plasma medicine: an introductory review,” *New J. Phys.*, vol. 11, no. 11, p. 115012, 2009.
- [32] G. Lloyd, G. Friedman, S. Jafri, G. Schultz, A. Fridman, and K. Harding, “Gas Plasma: Medical Uses and Developments in Wound Care,” *Plasma Process. Polym.*, vol. 7, no. 3–4, pp. 194–211, 2010.
- [33] M. Keidar, “Plasma for cancer treatment,” *Plasma Sources Sci. Technol.*, vol. 24, no. 3, p. 033001, 2015.
- [34] X. Han, W. A. Cantrell, E. E. Escobar, and S. Ptasinska, “Plasmid DNA damage induced by helium atmospheric pressure plasma jet,” *Eur. Phys. J. D*, vol. 68, no. 3, p. 46, 2014.
- [35] D. O’Connell *et al.*, “Cold atmospheric pressure plasma jet interactions with plasmid DNA,” *Appl. Phys. Lett.*, vol. 98, no. 4, p. 043701, 2011.

- [36] M. Y. Alkawareek *et al.*, “Plasmid DNA Damage Following Exposure to Atmospheric Pressure Nonthermal Plasma : Kinetics and Influence of Oxygen Admixture,” *Plasma Med.*, vol. 4, no. 1–4, pp. 211–219, 2014.
- [37] K. Niemi *et al.*, “Cold atmospheric pressure plasma jets: Interaction with plasmid DNA and tailored electron heating using dual-frequency excitation,” in *AIP Conference Proceedings*, 2012, vol. 1438, pp. 23–28.
- [38] S. Ptasińska, B. Bahnev, A. Styczyńska, M. Bowden, N. J. Mason, and N. S. J. Braithwaite, “DNA strand scission induced by a non-thermal atmospheric pressure plasma jet,” *Phys. Chem. Chem. Phys.*, vol. 12, no. 28, pp. 7779–7781, 2010.
- [39] X. Yan *et al.*, “Effect of the atmospheric pressure nonequilibrium plasmas on the conformational changes of plasmid DNA,” *Appl. Phys. Lett.*, vol. 95, no. 8, p. 083702, 2009.
- [40] A. Styczyńska, S. Ptasińska, B. Bahnev, M. Bowden, N. S. J. Braithwaite, and N. J. Mason, “The influence of amino acids on DNA damage induced by cold plasma radiation,” *Chem. Phys. Lett.*, vol. 500, no. 4–6, pp. 313–317, 2010.
- [41] J. Young Kim, D. Lee, J. Ballato, W. Cao, and S. Kim, “Reactive oxygen species controllable non-thermal helium plasmas for evaluation of plasmid DNA strand breaks,” *Appl. Phys. Lett.*, vol. 101, no. 22, p. 224101, 2012.
- [42] B. Bahnev, M. D. Bowden, A. Styczyńska, S. Ptasińska, N. J. Mason, and N. S. J. Braithwaite, “A novel method for the detection of plasma jet boundaries by exploring DNA damage,” *Eur. Phys. J. D*, vol. 68, no. 6, p. 140, 2014.
- [43] H. Kurita, S. Miyachika, H. Yasuda, K. Takashima, and A. Mizuno, “Use of molecular beacons for the rapid analysis of DNA damage induced by exposure to an atmospheric pressure plasma jet,” *Appl. Phys. Lett.*, vol. 107, no. 26, p. 263702, 2015.
- [44] H. Kurita *et al.*, “Single-molecule measurement of strand breaks on large DNA induced by atmospheric pressure plasma jet,” *Appl. Phys. Lett.*, vol. 99, no. 19, p. 191504, 2011.
- [45] X. Zhang and S. Ptasińska, “Growth of silicon oxynitride films by atmospheric pressure plasma jet,” *J. Phys. D: Appl. Phys.*, vol. 47, no. 14, p. 145202, 2014.
- [46] W.-C. Zhu, Q. Li, X.-M. Zhu, and Y.-K. Pu, “Characteristics of atmospheric pressure plasma jets emerging into ambient air and helium,” *J. Phys. D: Appl. Phys.*, vol. 42, no. 20, p. 202002, 2009.
- [47] A. Schmidt-Bleker *et al.*, “Propagation mechanisms of guided streamers in plasma jets: the influence of electronegativity of the surrounding gas,” *Plasma Sources Sci. Technol.*, vol. 24, no. 3, p. 035022, 2015.

- [48] M. Klas and S. Ptasinska, "Characteristics of N₂ and N₂/O₂ atmospheric pressure glow discharges," *Plasma Sources Sci. Technol.*, vol. 22, no. 2, p. 025013, 2013.
- [49] N. Mericam-Bourdet, M. Laroussi, a Begum, and E. Karakas, "Experimental investigations of plasma bullets," *J. Phys. D. Appl. Phys.*, vol. 42, no. 5, p. 055207, 2009.
- [50] S. Lehnert, *Biomolecular Action of Ionizing Radiation*, First. Taylor & Francis Group, New York, London, 2008.
- [51] Q. Xiong *et al.*, "Pulsed dc- and sine-wave-excited cold atmospheric plasma plumes: A comparative analysis," *Phys. Plasmas*, vol. 17, no. 4, p. 043506, 2010.
- [52] C. Giustranti, C. Perez, S. Rousset, E. Balanzat, and E. Sage, "Radiosensitivity of plasmid DNA : Role of topology and concentration," *J. Chim. Phys.*, vol. 96, pp. 132–137, 1999.
- [53] J. Jarrige, M. Laroussi, and E. Karakas, "Formation and dynamics of plasma bullets in a non-thermal plasma jet: influence of the high-voltage parameters on the plume characteristics," *Plasma Sources Sci. Technol.*, vol. 19, no. 6, p. 065005, 2010.
- [54] K.-D. Weltmann and T. von Woedtke, "Plasma medicine—current state of research and medical application," *Plasma Phys. Control. Fusion*, vol. 59, no. 1, p. 014031, 2017.
- [55] J. Gay-Mimbrera, M. C. García, B. Isla-Tejera, A. Rodero-Serrano, A. V. García-Nieto, and J. Ruano, "Clinical and Biological Principles of Cold Atmospheric Plasma Application in Skin Cancer," *Adv. Ther.*, vol. 33, pp. 894–909, 2016.
- [56] M. Ishaq, M. Evans, and K. Ostrikov, "Effect of atmospheric gas plasmas on cancer cell signaling," *Int. J. Cancer*, vol. 134, no. 7, pp. 1517–1528, 2014.
- [57] L. Gan *et al.*, "Medical applications of nonthermal atmospheric pressure plasma in dermatology," *J. Ger. Soc. Dermatology*, vol. 16, no. 1, pp. 7–13, 2018.
- [58] M. Schuster *et al.*, "Visible tumor surface response to physical plasma and apoptotic cell kill in head and neck cancer," *J. Cranio-Maxillofacial Surg.*, vol. 44, no. 9, pp. 1445–1452, 2016.
- [59] A. Sarani, C. Nicula, X. F. Gonzales, and M. Thiyagarajan, "Characterization of Kilohertz-Ignited Nonthermal He and He/O₂ Plasma Pencil for Biomedical Applications," *IEEE Trans. Plasma Sci.*, vol. 42, no. 10, pp. 3148–3160, 2014.
- [60] A. Sarani, A. Y. Nikiforov, and C. Leys, "Atmospheric pressure plasma jet in Ar and Ar/H₂O mixtures: Optical emission spectroscopy and temperature measurements," *Phys. Plasmas*, vol. 17, no. 6, p. 063504, 2010.

- [61] A. Y. Nikiforov, A. Sarani, and C. Leys, “The influence of water vapor content on electrical and spectral properties of an atmospheric pressure plasma jet,” *Plasma Sources Sci. Technol.*, vol. 20, no. 1, p. 015014, 2011.
- [62] Y. Gorbanev, D. O’Connell, and V. Chechik, “Non-Thermal Plasma in Contact with Water: The Origin of Species,” *Chem. Eur. J.*, vol. 22, no. 10, pp. 3496–3505, 2016.
- [63] J. Winter *et al.*, “Tracking plasma generated H₂O₂ from gas into liquid phase and revealing its dominant impact on human skin cells,” *J. Phys. D. Appl. Phys.*, vol. 47, no. 28, p. 285401, 2014.
- [64] J. Benedikt *et al.*, “Absolute OH and O radical densities in effluent of a He/H₂O micro-scaled atmospheric pressure plasma jet,” *Plasma Sources Sci. Technol.*, vol. 25, no. 4, p. 045013, 2016.
- [65] C. Cheng *et al.*, “Atmospheric pressure plasma jet utilizing Ar and Ar/H₂O mixtures and its applications to bacteria inactivation,” *Chinese Phys. B*, vol. 23, no. 7, p. 075204, 2014.
- [66] K. P. Arjunan, A. Obrušník, B. T. Jones, L. Zajíčková, and S. Ptasinska, “Effect of Additive Oxygen on the Reactive Species Profile and Microbicidal Property of a Helium Atmospheric Pressure Plasma Jet,” *Plasma Process. Polym.*, vol. 13, no. 11, pp. 1087–1103, 2016.
- [67] N. Hayashi, S. Tsutsui, T. Tomari, and W. Guan, “Sterilization of Medical Equipment Using Oxygen Radicals Produced by Water Vapor RF Plasma,” *IEEE Trans. Plasma Sci.*, vol. 36, no. 4, pp. 1302–1303, 2008.
- [68] F. Rossi, O. Kylián, H. Rauscher, M. Hasiwa, and D. Gilliland, “Low pressure plasma discharges for the sterilization and decontamination of surfaces,” *New J. Phys.*, vol. 11, p. 115017, 2009.
- [69] X. Yan *et al.*, “Plasma-induced death of HepG2 cancer cells: Intracellular effects of reactive species,” *Plasma Process. Polym.*, vol. 9, no. 1, pp. 59–66, 2012.
- [70] A. Schmidt-Bleker, J. Winter, S. Iseni, M. Dünnbier, K.-D. Weltmann, and S. Reuter, “Reactive species output of a plasma jet with a shielding gas device—combination of FTIR absorption spectroscopy and gas phase modelling,” *J. Phys. D. Appl. Phys.*, vol. 47, no. 14, p. 145201, 2014.
- [71] T. Ito, G. Uchida, A. Nakajima, K. Takenaka, and Y. Setsuhara, “Control of reactive oxygen and nitrogen species production in liquid by nonthermal plasma jet with controlled surrounding gas,” *Jpn. J. Appl. Phys.*, vol. 56, no. 1S, p. 01AC06, 2017.
- [72] A. Schmidt-Bleker, J. Winter, A. Bösel, S. Reuter, and K.-D. Weltmann, “On the

- plasma chemistry of a cold atmospheric argon plasma jet with shielding gas device,” *Plasma Sources Sci. Technol.*, vol. 25, no. 1, p. 015005, 2016.
- [73] Y. Yue, Y. Xian, X. Pei, and X. Lu, “The effect of three different methods of adding O₂ additive on O concentration of atmospheric pressure plasma jets (APPJs),” *Phys. Plasmas*, vol. 23, no. 12, p. 123503, 2016.
- [74] A. Mizuno, “Destruction of biological particles using non-thermal plasma,” *J Clin Biochem Nutr*, vol. 60, no. 1, pp. 12–24, 2016.
- [75] W. H. Chung, “Mechanisms of a novel anticancer therapeutic strategy involving atmospheric pressure plasma-mediated apoptosis and DNA strand break formation,” *Arch. Pharm. Res.*, vol. 39, no. 1, pp. 1–9, 2016.
- [76] D. F. Regulla, “ESR spectrometry: A future-oriented tool for dosimetry and dating,” *Appl. Radiat. Isot.*, vol. 62, no. 2 SPEC. ISS., pp. 117–127, 2005.
- [77] O. Baffa and A. Kinoshita, “Clinical applications of alanine/electron spin resonance dosimetry,” *Radiat. Environ. Biophys.*, vol. 53, no. 2, pp. 233–240, 2014.
- [78] M. F. Desrosiers, J. M. Publ, and S. L. Cooper, “An absorbed-dose/dose-rate dependence for the alanine-EPR dosimetry system and its implications in high-dose ionizing radiation metrology,” *J. Res. Natl. Inst. Stand. Technol.*, vol. 113, no. 2, p. 79, 2008.
- [79] E. R. Adhikari and S. Ptasinska, “Correlation between helium atmospheric pressure plasma jet (APPJ) variables and plasma induced DNA damage,” *Eur. Phys. J. D*, vol. 70, no. 9, p. 180, 2016.
- [80] K. McKay, J.-S. Oh, J. L. Walsh, and J. W. Bradley, “Mass spectrometric diagnosis of an atmospheric pressure helium microplasma jet,” *J. Phys. D. Appl. Phys.*, vol. 46, no. 46, p. 464018, 2013.
- [81] Z. Abd-Allah, D. A. G. Sawtell, K. McKay, G. T. West, P. J. Kelly, and J. W. Bradley, “Mass spectrometric investigation of the ionic species in a dielectric barrier discharge operating in helium-water vapour mixtures,” *J. Phys. D. Appl. Phys.*, vol. 48, no. 8, p. 085202, 2015.
- [82] S. Große-Kreul *et al.*, “Mass spectrometry of atmospheric pressure plasmas,” *Plasma Sources Sci. Technol.*, vol. 24, no. 4, p. 044008, 2015.
- [83] P. J. Linstrom and W. G. Mallard, “NIST Chemistry WebBook, NIST Standard Reference Database Number 69,” *National Institute of Standards and Technology, Gaithersburg MD, 20899*, 2017. [Online]. Available: <http://webbook.nist.gov/chemistry/>. (Accessed: November 30, 2017)

- [84] K. Anzai *et al.*, “Cross section data sets for electron collisions with H₂, O₂, CO, CO₂, N₂O and H₂O,” *Eur. Phys. J. D*, vol. 66, no. 2, p. 36, 2012.
- [85] X. Lu, G. V. Naidis, M. Laroussi, and K. Ostrikov, “Guided ionization waves: Theory and experiments,” *Phys. Rep.*, vol. 540, no. 3, pp. 123–166, 2014.
- [86] D. Yan *et al.*, “The Specific Vulnerabilities of Cancer Cells to the Cold Atmospheric Plasma-Stimulated Solutions,” *Sci. Rep.*, vol. 7, no. 1, pp. 1–12, 2017.
- [87] X. Liao *et al.*, “Inactivation mechanisms of non-thermal plasma on microbes: A review,” *Food Control*, vol. 75, pp. 83–91, 2017.
- [88] H.-P. Li *et al.*, “Translational plasma stomatology: applications of cold atmospheric plasmas in dentistry and their extension,” *High Volt.*, vol. 2, no. 3, pp. 188–199, 2017.
- [89] T. Shimizu and Y. Ikehara, “Benefits of applying low-temperature plasma treatment to wound care and hemostasis from the viewpoints of physics and pathology,” *J. Phys. D. Appl. Phys.*, vol. 50, no. 50, p. 503001, 2017.
- [90] M. U. Rehman, P. Jawaaid, H. Uchiyama, and T. Kondo, “Comparison of free radicals formation induced by cold atmospheric plasma, ultrasound, and ionizing radiation,” *Arch. Biochem. Biophys.*, vol. 605, pp. 19–25, 2016.
- [91] K. Seiji, F. Takashi, N. Takeshi, A. Shuichi, and I. Ryuta, “Measurement of OH Radicals in Aqueous Solution Produced by Atmospheric plasma pressure jet,” *Int. J. Plasma Environ. Sci. Technol.*, vol. 6, no. 2, pp. 166–171, 2012.
- [92] L. Chandana, P. Manoj Kumar Reddy, and C. Subrahmanyam, “Atmospheric pressure non-thermal plasma jet for the degradation of methylene blue in aqueous medium,” *Chem. Eng. J.*, vol. 282, pp. 116–122, 2015.
- [93] B. T. J. van Ham, S. Hofmann, R. Brandenburg, and P. J. Bruggeman, “In situ absolute air, O₃ and NO densities in the effluent of a cold RF argon atmospheric pressure plasma jet obtained by molecular beam mass spectrometry,” *J. Phys. D. Appl. Phys.*, vol. 47, no. 22, p. 224013, 2014.
- [94] J. W. T. Spinks and R. J. Woods, *Introduction to Radiation Chemistry*, First. New York: John Wiley & Sons, Inc., 1964.
- [95] X. Han, “Characterization and Interactions of Atmospheric Pressure Plasma Jets (APPJ) with DNA and Human Cells,” University of Notre Dame, 2017.
- [96] R. Meesat, S. Sanguanmith, J. Meesungnoen, M. Lepage, A. Khalil, and J.-P. Jay-Gerin, “Utilization of the Ferrous Sulfate (Fricke) Dosimeter for Evaluating the Radioprotective Potential of Cystamine: Experiment and Monte Carlo

- Simulation,” *Radiat. Res.*, vol. 177, no. 6, pp. 813–826, 2012.
- [97] T. N. Andersen, N. Vanorden, and W. J. Schlitt, “Effects of nitrogen oxides, sulfur dioxide, and ferric ions on the corrosion of mild steel in concentrated sulfuric acid,” *Metall. Trans. A*, vol. 11, no. 8, pp. 1421–1428, 1980.
- [98] P. J. Bruggeman *et al.*, “Plasma–liquid interactions: a review and roadmap,” *Plasma Sources Sci. Technol.*, vol. 25, no. 5, p. 053002, 2016.
- [99] V. Samara and S. Ptasinska, “Interferometry of plasma bursts in helium atmospheric-pressure plasma jets,” *J. Vac. Sci. Technol. A*, vol. 36, no. 4, p. 04F402, 2018.
- [100] E. R. Adhikari, V. Samara, and S. Ptasinska, “Influence of O₂ or H₂O in a plasma jet and its environment on plasma electrical and biochemical performances,” *J. Phys. D: Appl. Phys.*, vol. 51, no. 18, p. 185202, 2018.
- [101] C. Austerlitz, V. L. B. De Souza, D. M. T. Campos, C. Karachi, V. Bagnato, and C. Sibata, “Enhanced response of the fricke solution doped with hematoporphyrin under x-rays irradiation,” *Brazilian Arch. Biol. Technol.*, vol. 51, no. 2, pp. 271–279, 2008.
- [102] D. J. Higham, “Modeling and Simulating Chemical Reactions,” *SIAM Rev.*, vol. 50, no. 2, pp. 347–368, 2008.
- [103] V. V Kovačević, G. B. Sretenović, E. Slikboer, O. Guaitella, A. Sobota, and M. M. Kuraica, “The effect of liquid target on a nonthermal plasma jet—imaging, electric fields, visualization of gas flow and optical emission spectroscopy,” *J. Phys. D: Appl. Phys.*, vol. 51, no. 6, p. 065202, 2018.
- [104] A. Dubuc *et al.*, “Use of cold-atmospheric plasma in oncology: a concise systematic review,” *Ther. Adv. Med. Oncol.*, vol. 10, pp. 1–12, 2018.
- [105] M. Keidar, D. Yan, I. I. Beilis, B. Trink, and J. H. Sherman, “Plasmas for Treating Cancer: Opportunities for Adaptive and Self-Adaptive Approaches,” *Trends Biotechnol.*, vol. 36, no. 6, pp. 586–593, 2018.
- [106] M. Laroussi, X. Lu, and M. Keidar, “Perspective: The physics, diagnostics, and applications of atmospheric pressure low temperature plasma sources used in plasma medicine,” *J. Appl. Phys.*, vol. 122, no. 2, p. 020901, 2017.
- [107] X. Dai, K. Bazaka, D. J. Richard, E. (Rik) W. Thompson, and K. (Ken) Ostrikov, “The Emerging Role of Gas Plasma in Oncotherapy,” *Trends Biotechnol.*, vol. 36, no. 11, pp. 1183–1198, 2018.
- [108] S. Reuter, T. von Woedtke, and K.-D. Weltmann, “The kINPen—a review on physics and chemistry of the atmospheric pressure plasma jet and its applications,”

- J. Phys. D. Appl. Phys.*, vol. 51, no. 23, p. 233001, 2018.
- [109] D. B. Graves, “The emerging role of reactive oxygen and nitrogen species in redox biology and some implications for plasma applications to medicine and biology,” *J. Phys. D. Appl. Phys.*, vol. 45, no. 26, 2012.
- [110] S. I. Ahmad, “Control of skin infections by a combined action of ultraviolet A (from sun or UVA lamp) and hydrogen peroxide (HUVA therapy), with special emphasis on leprosy,” *Med. Hypotheses*, vol. 57, no. 4, pp. 484–486, 2001.
- [111] M. V. Marshall, L. P. Cancro, and S. L. Fischman, “Hydrogen Peroxide: A Review of Its Use in Dentistry,” *J. Periodontol.*, vol. 66, no. 9, pp. 786–796, 1995.
- [112] S. K. Kang *et al.*, “Reactive hydroxyl radical-driven oral bacterial inactivation by radio frequency atmospheric plasma,” *Appl. Phys. Lett.*, vol. 98, p. 143702, 2011.
- [113] M. Y. Choi *et al.*, “Helium/H₂O₂ Atmospheric Pressure Plasma-Assisted Electrosurgery,” *Plasma Process. Polym.*, vol. 9, no. 10, pp. 1015–1019, 2012.
- [114] E. R. Adhikari, V. Samara, and S. Ptasinska, “Total yield of reactive species originating from an atmospheric pressure plasma jet in real time,” *Biol. Chem.*, vol. 400, no. 1, pp. 93–100, 2019.
- [115] H. A. Khorami, P. Wild, and N. Djilali, “Fiber Optic Sensors for Hydrogen Peroxide Vapor Measurement,” *Int. J. Chem. Mol. Nucl. Mater. Metall. Eng.*, vol. 9, no. 10, pp. 1149–1153, 2015.
- [116] S. Radl, S. Ortner, R. Sungkorn, and J. G. Khinast, “The engineering of hydrogen peroxide decontamination systems,” *J. Pharm. Innov.*, vol. 4, no. 2, pp. 51–62, 2009.
- [117] S. L. Manatt and M. R. R. Manatt, “On the analyses of mixture vapor pressure data: The hydrogen peroxide/water system and its excess thermodynamic functions,” *Chem. - A Eur. J.*, vol. 10, no. 24, pp. 6540–6557, 2004.
- [118] J. F. Botero-cadavid, “Fiber-optic sensor for detection of hydrogen peroxide in PEM fuel cells,” University of Victoria, 2014.
- [119] W. Tian and M. J. Kushner, “Atmospheric pressure dielectric barrier discharges interacting with liquid covered tissue,” *J. Phys. D. Appl. Phys.*, vol. 47, no. 16, p. 165201, 2014.
- [120] J. H. Baxendale and J. A. Wilson, “The photolysis of hydrogen peroxide at high light intensities,” *Trans. Faraday Soc.*, vol. 53, p. 344, 1957.
- [121] K. J. Gill and R. A. Hites, “Rate Constants for the Gas-Phase Reactions of the Hydroxyl Radical with Isoprene, α - and β -Pinene, and Limonene as a Function of

- Temperature,” *J. Phys. Chem. A*, vol. 106, no. 11, pp. 2538–2544, 2002.
- [122] B. Ghimire, J. Sornsakdanuphap, Y. J. Hong, H. S. Uhm, K. D. Weltmann, and E. H. Choi, “The effect of the gap distance between an atmospheric-pressure plasma jet nozzle and liquid surface on OH and N₂ species concentrations,” *Phys. Plasmas*, vol. 24, no. 7, p. 073502, 2017.
- [123] Y. F. Yue, S. Mohades, M. Laroussi, and X. Lu, “Measurements of Plasma-Generated Hydroxyl and Hydrogen Peroxide Concentrations for Plasma Medicine Applications,” *IEEE Trans. Plasma Sci.*, vol. 44, no. 11, pp. 2754–2758, 2016.
- [124] J. Chauvin, F. Judée, M. Yousfi, P. Vicendo, and N. Merbahi, “Analysis of reactive oxygen and nitrogen species generated in three liquid media by low temperature helium plasma jet,” *Sci. Rep.*, vol. 7, no. 1, pp. 1–15, 2017.
- [125] I. Adamovich *et al.*, “The 2017 Plasma Roadmap: Low temperature plasma science and technology,” *J. Phys. D. Appl. Phys.*, vol. 50, no. 32, p. 323001, 2017.
- [126] M. S. Simeni, E. Baratte, C. Zhang, K. Frederickson, and I. V. Adamovich, “Electric field measurements in nanosecond pulse discharges in air over liquid water surface,” *Plasma Sources Sci. Technol.*, vol. 27, no. 1, p. 015011, 2018.